2012

A 77 GHz Reconfigurable Micromachined Microstrip Antenna Array

Ismail Hamieh
University of Windsor

A 77 GHz Reconfigurable Micromachined Microstrip Antenna Array

by

Ismail Ali Hamieh

A Thesis
Submitted to the Faculty of Graduate Studies
through Electrical and Computer Engineering
in Partial Fulfillment of the Requirements for
the Degree of Master of Applied Science at the
University of Windsor

Windsor, Ontario, Canada

2012

A 77 GHz Reconfigurable Micromachined Microstrip

Antenna Array

by

Ismail Ali Hamieh

APPROVED BY:

_____

Dr. Afsaneh Edrisy, Outside Department Reader
Mechanical Automotive & Manufacturing Engineering

_____

Dr. Kemal Tepe, Department Reader
Department of Electrical & Computer Engineering

_____

Dr. Sazzadur Chowdhury, Advisor
Department of Electrical and Computer Engineering

_____

Dr. J. Wu , Chair of Defense
Department of Electrical and Computer Engineering

DECLARATION OF ORIGINALITY

I hereby certify that I am the sole author of this thesis and that no part of this thesis has been published or submitted for publication.

I certify that, to the best of my knowledge, my thesis does not infringe upon anyone's copyright nor violate any proprietary rights and that any ideas, techniques, quotations, or any other material from the work of other people included in my thesis, published or otherwise, are fully acknowledged in accordance with the standard referencing practices. Furthermore, to the extent that I have included copyrighted material that surpasses the bounds of fair dealing within the meaning of the Canada Copyright Act, I certify that I have obtained a written permission from the copyright owner(s) to include such material(s) in my thesis and have included copies of such copyright clearances to my appendix.

I declare that this is a true copy of my thesis, including any final revisions, as approved by my thesis committee and the Graduate Studies office, and that this thesis has not been submitted for a higher degree to any other University or Institution.

ABSTRACT

A micromachined silicon based MEMS single-pole-Single-Throw (SPST) switches embedded reconfigurable microstrip antenna array for use in a 77 GHz tri-mode automotive collision avoidance radar is presented. The emphasis is put on compact 77 GHz micromachined microstrip antenna array, capable of being integrated with silicon base Rotman lens that provides an intrinsic beamforming capability without any microelectronic signal processing.

The first part of this thesis deals with the theory behind microstrip antennas and a deep explanation of antenna arrays. The second part of the thesis is concerned with design procedures and considerations. It provides a detailed study of how to design and fabricate an inset fed rectangular micromachined microstrip patch antenna array using XFDTD™ 3-D software and study the effect of antenna dimensions.

At last, this thesis shows the simulation results that by incorporating a micromachined technology into microstrip antenna array we are able to achieve higher radiation efficiency and bandwidth than conventional antenna array.

DEDICATION

This thesis is dedicated to my parents who have supported me all the way since the beginning of my studies. Also, it is dedicated to my wife and my daughter, Wadad and Aya, who have been a great source of motivation and inspiration.

ACKNOWLEDGEMENTS

I would like to express my appreciation to my advisory committee: Dr. Sazzadur Chowdhury, Dr. Kemal Tepe, and Dr. Afsaneh Edrisy. Thanks for giving me the opportunity to be part of the University of Windsor research MEMS group. Special thanks to Dr. Chowdhury for his time, patience, and understanding. Also, thanks to the Auto21 and CMC, Canadian research and development community, for making this study possible by providing its funding to the University of Windsor.

The most special thanks go to my best partner and friend, my wife. Wadad, you gave me your unconditional support and love through all this long process. I express my thanks and appreciation to my family for their understanding, motivation and patience. Lastly, but in no sense the least, I am thankful to all colleagues and friends who made my stay at the university a memorable and valuable experience.

TABLE OF CONTENTS

DECLARATION OF ORIGINALITY iii

ABSTRACT iv

DEDICATION v

ACKNOWLEDGEMENTS vi

LIST OF TABLES x

LIST OF FIGURES xi

LIST OF ABBREVIATIONS xv

NOMENCLATURE xvii

CHAPTER

I. INTRODUCTION

1.1 Problem Statement 1
1.2 Automotive radar 5
1.2.1 Electronically scanned radar 5
1.2.2 The MEMS radar 7
1.2.3 MEMS radar principle of operation 10
1.3 Research hypothesis 11
1.4 Motivation 12
1.5 Principal Results 13
1.6 Thesis Organization 14

II. REVIEW OF LITERATURE

2.1 Literature Review 15
2.1.1 MEMS technology 17
2.1.2 Radar type 18
2.2 Microelectronic beamforming with phased array antenna 19
2.2.1 Microelectronic beamforming types 20
2.2.2 Rotman lens beamforming 23
2.2.2.1 Antenna array 25
2.3 State-of-the-art automotive radar 27
2.4 State-of-the-art antenna array 29

III. MICROSTRIP PATCH ANTENNA

3.1 Microstrip patch antenna 31
3.2 basic Principle of Operation 34
3.2.1 Transmission line model....34
3.2.2 Cavity model....37
3.2.3 Full wave solutions-method of moment 39
3.2.4 Radiating conductance 40
3.2.5 Input resistance....40
3.2.6 Fringing affect....42
3.3 Overview of the rectangular patch parameters 43
3.3.1 Return loss....43
3.3.2 Radiation patterns 45
3.3.3 Gain & directivity 48
3.3.4 Bandwidth 49
3.3.5 Input impedance 50
3.3.6 Polarization 52
3.4 Antenna array 53
3.4.1 Linear antenna array 54
3.4.2 Planar antenna array 55
3.5 Microstrip antenna feed techniques....57
3.6 Summary 59

IV. MICROMACHINED MICROSTRIP ANTENNA

4.1 Micromachining....60
4.2 Bulk micromachining 62
4.3 Synthesized permittivity....65
4.3.1 How micromachined substrates work 66

V. ANTENNA ARRAY DESIGN, SIMULATION AND FABRICATION

5.1 Microstrip antenna design specifications 69
5.2 Design procedure 72
5.3 Single patch design calculation....74
5.4 Antenna array 76
5.4.1 Short range antenna array....79
5.4.2 Mid-range antenna array....86
5.4.3 Long range antenna array 93
5.5 Fabrication 100
5.6 Summary 104

VI. CONCLUSION AND FUTURE WORK

6.1 Conclusion 107

6.2 Future work.....109

MATLAB CODE 110

FABRICATED MICROSTRIP ANTENNA ARRAY.....115

REFERENCES.....125

VITA AUCTORIS ……..……. 133

LIST OF TABLES

TABLE 1.1. WORLD REPORT ON ROAD TRAFFIC INJURY 3

TABLE 1.2. RADAR SIMULATION RESULTS 13

TABLE 2.1. APPLICATION THAT ENPLOY BEAMFORMING 20

TABLE 2.2. CLASSIFICATIONS OF AUTOMOTIVE RADAR SYSTEMS 28

TABLE 2.3. NEW GENERATION OF AUTOMOTIVE RADAR SYSTEMS 28

TABLE 2.4. DIFFERENT ANTENNA ARRAY DESIGNS 30

TABLE 3.1. MICROSTRIP ANTENNA FEEDING TECHNIQUES COMPARISON [9] 59

TABLE 4.1. COMPARISON BETWEEN HIGH AND LOW INDEX MATERIALS 61

TABLE 4.2. MICROMACHINED SOLUTION ON A GAAS WITH AIR CAVITY [10] 65

TABLE 5.1. SINGLE PATCH CALCULATION 75

TABLE 5.2. SINGLE PATCH MATHEMATICAL AND OPTIMIZED PARAMETERS 76

TABLE 5.3. DIFFERENT RADARS AND ANTENNA ARRAYS 77

TABLE 5.4. SHORT RANGE ANTENNA ARRAY PARAMETERS 79

TABLE 5.5. SRR SUMMARY TABLE 86

TABLE 5.6. MID-RANGE ANTENNA ARRAY PARAMETERS 86

TABLE 5.7. MRR SUMMARY 93

TABLE 5.8. LONG RANGE ANTENNA ARRAY PARAMETERS 93

TABLE 5.9. LRR SUMMARY 100

LIST OF FIGURES

FIGURE 1.1. PHASED ANTENNA ARRAY 6

FIGURE 1.2. AUTOMOTIVE RADAR SYSTEM BLOCK DIAGRAM 9

FIGURE 1.3. TRI-MODE AUTOMOTIVE RADAR..... 10

FIGURE 2.1. ANALOG BEAMFORMER OF THE ANTENNA PATTERN..... 21

FIGURE 2.2. DIGITAL BEAMFORMER 22

FIGURE 2.3. ROTMAN LENS GEOMETRY AND DESIGN PARAMETERS 24

FIGURE 2.4. DIRECTION OF THE OUTGOING BEAM FROM INPUTS AT DIFFERENT FEED POINT…….. 25

FIGURE 2.5. ROTMAN LENS AND ANTENNA ARRAY..... 26

FIGURE 3.1. MICROSTRIP RECTANGULAR PATCH ANTENNA; (A) TOP VIEW; (B) SIDE VIEW. . ……..32

FIGURE 3.2. MICROSTRIP RECTANGULAR PATCH ANTENNA; (C) 3D VIEW 33

FIGURE 3.3. MICROSTRIP PATCH ANTENNA GEOMETRY 33

FIGURE 3.4. EFFECTIVE DIELECTRIC CONSTANT AND FRINGING AFFECT 35

FIGURE 3.5. RECTANGULAR MICROSTRIP PATCH ANTENNA 36

FIGURE 3.6. FUNDAMENTAL TM10 OF RECTANGULAR ANTENNA WITH TWO RADIATING SLOTS…….. 36

FIGURE 3.7. CAVITY MODEL CHARGE DISTRIBUTION [10] 37

FIGURE 3.8. EQUIVALENT CIRCUIT TRANSMISSION LINE MODEL 40

FIGURE 3.9. TRANSMISSION LINE MODEL 41

FIGURE 3.10. FUNDAMENTAL TM10 MODE 42

FIGURE 3.11. (A) ELECTRICAL CURRENT FOR (1, 0) PATCH;(B) MAGNETIC CURRENT FOR (1,0) PATCH 46

FIGURE 3.12. RADIATION PATTERN OF A GENERIC DIRECTIONAL ANTENNA 47

FIGURE 3.13. INSET FED PATCH ANTENNA 51

FIGURE 3.14. LINEAR POLARIZED WAVE 52

FIGURE 3.15. GENERAL POLARIZATION SCHEMES 53

FIGURE 3.16. LINEAR ANTENNA ARRAY 55

FIGURE 3.17. PLANAR ANTENNA ARRAY 57

FIGURE 3.18. (A) MICROSTRIP INSET FED; (B) COAXIAL PROBE; (C) APERTURE FEED LINE ……...……58

FIGURE 4.1. (A) ISOTROPIC ETCHING WITH AGITATION; (B) ISOTROPIC ETCHING WITHOUT AGITATION 62

FIGURE 4.2. (A) ANISOTROPIC ETCHING ON (100) SURFACE; (B) ANISOTROPIC ETCHING ON (110) SURFACE 63

FIGURE 4.3. ILLUSTRATION OF A SURFACE MICROMACHINING PROCESS 64

FIGURE 4.4. MICROMACHINED PATCH ANTENNA; (A) SIDE VIEW; (B) TOP VIEW 67

FIGURE 5.1. DRIE PROCESS OR BOSCH PROCESS; (A) TOP WAFER DRIE ETCH PART OF THE SILICON SUBSTRATE; (B) BOTTOM WAFER TOPPED WITH A GROUND PLANE; (C) THERMOCOMPRESSIVELY BON OF THE TWO WAFERS 71

FIGURE 5.2. SYSTEM CONCEPT OF ROTMAN LENS, ANTENNA ARRAY AND SWITCHES 78

FIGURE 5.3. (3 BEAM PORTS, 5 ARRAY PORTS AND 16 DUMMY PORTS) ROTMAN LENS 80

FIGURE 5.4. 3D VIEW OF THE SRR DESIGN FROM XFDTD™ (A) TOP VIEW (B) 3D VIEW…… 81

FIGURE 5.5. SRR MAXIMUM RADIATION OCCURS AT GAIN OF 8.8DBI; (A) AZIMUTH ANGLE, (B) ELEVATION ANGLE 82
FIGURE 5.6. SRR S22 PARAMETER IS -25 DB 83
FIGURE 5.7. SRR S11 VSWR IS 1.2 84
FIGURE 5.8. XFDTD™ SRR RADIATION PATTERN 85
FIGURE 5.9. 3D VIEW OF THE MRR DESIGN FROM XFDTD™ (A) TOP VIEW (B) 3D VIEW……. 87
FIGURE 5.10. MRR MAXIMUM RADIATION OCCURS AT GAIN OF 12 DBI; (A) AZIMUTH ANGLE, (B) ELEVATION ANGLE 89
FIGURE 5.11. MRR S11 PARAMETER IS -25.3 DB 90
FIGURE 5.12. MRR VSWR IS 1.2 91
FIGURE 5.13. XFDTD™ MRR RADIATION PATTERN 92
FIGURE 5.14. 3D VIEW OF THE LRR DESIGN FROM XFDTD™ (A) TOP VIEW (B) 3D VIEW.. …….....95
Figure 5.15. LRR maximum radiation occurs at gain of 20.5 dBi, (a) Azimuth angle, (b) Elevation angle....……96
FIGURE 5.16. LRR S11 PARAMETER IS -23 DB 97
FIGURE 5.17. LRR VSWR IS 1.1 98
FIGURE 5.18. XFDTD™ LRR RADIATION PATTERN 99
FIGURE 5.19. PREPARATION OF SILICON WAFER 101
FIGURE 5.20. ALTERATION AND LITHOGRAPHY 101
FIGURE 5.21. ALTERATION AND LITHOGRAPHY 102
FIGURE 5.22. STRIP PHOTORESIST 102

FIGURE 5.23. STRIP PHOTORESIST 103
FIGURE 5.24. PREPARATION OF BOTTOM WAFER 103
FIGURE 5.25. DEPOSITIONS OF CR AND AU 103
FIGURE 5.26. WAFER BONDING 104
FIGURE 5.26. WAFER BONDING 104
FIGURE 5.27. THIS PHOTOGRAPH IS A CROSS-SECTION OF THE ANTENNA ARRAY THAT SHOWS THE TOP LAYER WITH THE MICOMACHINED AIR CAVITIES 105
FIGURE 5.28. THIS PHOTOGRAPH SHOWS THE TOP LAYER OF THE ANTENNA ARRAY 106
FIGURE 6.1. RECONFIGURABLE ANTENNA ARRAY 109

LIST OF ABBREVIATIONS

MEMS - Microelectromechanical Systems

Radar - Radio Detection and Ranging

RF - Radio Frequency

SP3T - Single Pole Triple Throw

SP3T – Single Pole Single Throw

DSP - Digital Signal Processing

FPGA- Field Programmable Gate Array

EC - The European Commission

DAC - Digital to Analog Converter

ADC - Analog to Digital Converter

LFMCW - Linear Frequency Modulated Continuous Wave

TLC - Top Level Control

LRR - Long Range Radar

MRR - Medium Range Radar

SRR-Short Range Radar

IF - Intermediate Frequency

FF-Flip-Flop

VSWR - Voltage Standing Wave Ratio

NHTSA - National Highway Traffic Safety Administration

FMCSA Federal Motor Carrier Safety Administration

LTVs - pickup trucks, sport utility vehicles and vans

SARA - Strategic Automotive Radar frequency Allocation

BMBF - German Government

DBF - Digital Beamforming

ACC - Adaptive Cruise Control

FDTD - Finite Difference Time Domain

TEM - Transverse Electromagnetic

TX - Transmit signal

RX - Receive Signal

GaAs - Gallium arsenide

Si - Silicon

Au - Gold

Cu - Copper

DRIE - Deep Reactive Ion Etching

3D - Three Dimensions

HPBW - Half Power Beamwidth

HDL- Hardware Description Language

ECCM - Electronic Counter-Countermeasures

FFT- Fast Fourier Transform

DFT- Discrete Fourier Transform

DIT- Decimation In Time

DIF - Decimation In Frequency

LIST OF NOMENCLATURE

L_{eff} = effective length of the patch

ε_r = dielectric constant of substrate

f = operating frequency

ε_{reff} = effective dielectric constant

c = free space velocity of light, which is $3x10^8$ m/s.

h = height of dielectric substrate

W = width of the patch

L = length of the patch

ΔL = patch length extension

λ = lambda

$\lambda/2$ = half lambda

y_0 = position of the feed from the edge along the direction of the patch length

δ_{eff} = effective loss tangent

Q_T = total antenna quality factor

Q_d = dielectric quality factor

ω_r = angular resonant frequency

W_T = total energy stored in the patch at resonance

P_d = dialectic loss

$\tan\delta$ = loss tangent of the dielectric

Q_c = conductor quality factor

Δ = skin depth of the conductor

Pc = conductor loss

Q_r = radiation quality factor

P_r = power radiated from the patch

λ_0 = free-space wavelength

$|\Gamma|$ = reflection coefficient

V_0^+ = incident voltage

V_0^- = reflected voltage

Z_L = load impedance

Z_0 = characteristic impedance

$\vec{M}_s$ = magnetic current

$\hat{\boldsymbol{n}}$ = outward pointing unit-normal vector at the patch boundary

$\vec{E}$ = electric field of the cavity mode at the edge of the patch

G = gain

$\boldsymbol{\eta}$ = radiation efficiency

D = directivity of the patch antenna

AF = array factor

N = number of elements

BW = bandwidth

fH = frequency high

fL = frequency low

fC = frequency center

AF_{planar} = planar antenna array factor

k = wave vector

β = phase difference

ε_{synth} = synthesized permittivity

h_{eq} = equivalent height

$h_{material}$ = material height

h_{air} = air height

CHAPTER I

INTRODUCTION

In this thesis, a micromachined silicon based MEMS single-pole-Single-Throw (SPST) switch embedded reconfigurable microstrip antenna array for use in a 77 GHz tri-mode automotive collision avoidance radar is presented. An FPGA / ASIC implemented algorithm controls the operation of the MEMS SPST switches to dynamically alter the beamwidth of the antenna array to cycle the radar constantly from short-range (SRR) to mid-range (MRR) to long range (LRR) mode.

In this chapter, the background of this project has been discussed, providing the objective and scope of this work in addition to the application of automobile radar antenna and the antenna array. It highlights the importance of the work and its outcomes to the present day. It starts with the problem statement, followed by the facts about road safety and accident records around the globe.

The potential benefits of automotive radar systems in road safety, and the radar being developed at the University of Windsor, along with a concise operating principle are presented. After defining the aim of this thesis, this chapter closes with an overview, listing a brief summary of the topics discussed in latter chapters.

1.1 Problem Statement

Automotive safety is the study of vehicle design, construction, and equipment to minimize the occurrence and consequences of accidents. It has progressed from using only seatbelts and airbags to involve telematics systems that provide automatic crash notifications and road support if an accident occurs. Currently, automakers offer safety

technology that intervenes during a collision to help reduce the occupant injury and damage to vehicles. Existing safety technologies such as parking assist, blind spot detection, backup cameras and sensors, adaptive cruise control, and pre-crash radar detection systems fall short of establishing a real-time dynamic safety shell around a vehicle due to their high latency time associated with microelectronic signal processing, and the need for a scanning system for the targeted area in case of radars. In addition, the expense of implementing these technologies prevents automakers from incorporating such devices into vehicles. Consequently, road safety situation remains short considering the above reasons.

Despite automotive infotainment and telematics technological progress, about 40,000 people die every year in the U.S [1]. Although the fatality rates per vehicle registered and per vehicle distance travelled have steadily decreased since the advent of significant vehicle and driver regulations, the raw number of fatalities generally increases as a function of rising population and more vehicles on the road. However, sharp rises in the price of fuel and related driver behavioural changes are reducing 2007 - 2008 highway fatalities in the U.S. to below the 1961 fatality count [2]. Litigation has been central in the struggle to mandate safer cars [3].

The following table, Table 1.1, is from the World Health Organization on road traffic injury [4]. It predicts the road traffic fatalities by region (in thousands), and the data is displayed according to the regional classifications of the World Bank. In this table, high income countries include North America (USA and Canada), Western and Central Europe; whereas, the rest regions are listed independently.

Table 1.1. World report on road traffic injury

Different Regions	Number of Countries	Yearly fatalities in thousands				Change (%) 2000 - 2020	Fatality rate (death/100000 persons)	
		1990	2000	2010	2020		2000	2020
East Asia and Pacific	15	112	188	278	337	79	10.9	16.8
East Europe and Central Asia	9	30	32	36	38	19	19.0	21.2
Latin America and Caribbean	31	90	122	154	180	48	26.1	31.0
Middle East and North Africa	13	41	56	73	94	68	19.2	22.3
South Asia	7	87	135	212	330	144	10.2	18.9
Sub-Saharan Africa	46	59	80	109	144	80	12.3	14.9
Sub-total	121	419	613	862	1124	83	13.3	19.0
High-income countries	35	123	110	95	80	-27	11.8	7.8
Total	156	542	723	957	1204	67	13.0	17.4

Market research firm Strategy Analytics predicts that over the period 2006 to 2011, the use of long-range distance warning systems in cars could increase by more than 65 percent annually, with demand reaching 3 million units in 2011, with 2.3 million of them using radar sensors. By 2014, 7 percent of all new cars will include a distance warning system, primarily in Europe and in Japan [5].

"Radar technology is the key to building innovative driver assistance systems to help avoid automobile accidents," says Hans Adlkofer, Vice President and General Manager of Infineon Technologies Sense and Control business unit.

Despite the fact that the technology first appeared on luxury cars, crash prevention systems have started to trickle down to more reasonably priced vehicles. This will increase the market for telematics and create a positive competition between the automakers. Global auto industries and governments are extensively pursuing radar based proximity detection systems such as:

1. ACC support with Stop & Go functionality
2. Pre-crash warning using tri-mode radar system
3. Blind spot detection
4. Self-parking aid
5. Side sensors for parking aid
6. Lane change assistant for the driver
7. Backup camera and sensor for impact warning
8. Car to computer communication devises which utilize GPS tracking feature
9. Geofencing car capability for vehicle tracking
10. Remote speed sensing

The European Commission (EC) had set an ambitious target to reduce road deaths by 50% by the end of 2010. It has been concluded that the use of Forward Collision Warning long range radar and Lane Departure Warning camera-based sensor, among other security features, will become very effective to reduce road fatality rates. In [6], it has been mentioned that with the proposed crash prevention technologies equipped in

vehicles, the number of crashes can be reduced by 3.8 million in North America alone, and the number of human lives saved from that amounts close to 17,000 per year. This warrants the use of multi-range radar as an indispensable feature to improve highway safety and minimize loss of lives and property damage.

1.2 Automotive radar

The first patent of radar application on car was claimed by Christian Huelsmeyer in a German Patent on 30, April 1904 [7]. Since this time many different radar systems have been developed for various industries. The general requirement for automotive radars is to detect any targets in the field of view with high probability, high accuracy and low false alarm rate. Automotive sensors usually operate in the dedicated frequency band of 77 GHz. Beside this technology, SRR sensors are under development today in the 24 GHz ISM band.

High performance automotive radars measure target range, azimuth and radial velocity simultaneously in a short time and have the ability to resolve reflectors in multiple target situations. The main technical challenge lies in the waveform, antenna and signal processing design.

1.2.1 Electronically scanned radar

Electronically scanned antenna arrays propose great benefits that facilitate radar sensors and broadband communications for different military and commercial applications. The most advanced function of electronically scanned antenna is the phased antenna array. It implements a large number of individual antenna elements that are phased in union to create a single beam that is electronically steerable. This beam is

steered by adjusting the amplitude and phase of the RF signal at each of the individual antenna elements. In other words traditional phased array antennas are constructed with active electronics behind every radiating element. A linear phased array with equal spaced elements is easiest to analyze and forms the basis for most array designs. Figure 1.1 schematically illustrates a corporate feed linear array with element spacing *d*. By controlling the phase and amplitude of excitation to each element, as depicted, we can control the direction and shape of the beam radiated by the array. The phase excitation, $\Phi_{(n)}$, controls the beam pointing angle, θ_0, in a phased array. To produce a broadside beam, $\theta_0 = 0$, requires phase excitation, $\Phi_{<(n)>} = 0$. Other scan angles require an excitation, $\Phi_{(n)} = nkd\ sin(\theta_0)$, for the nth element where k is the wave number ($2\pi/\lambda$).

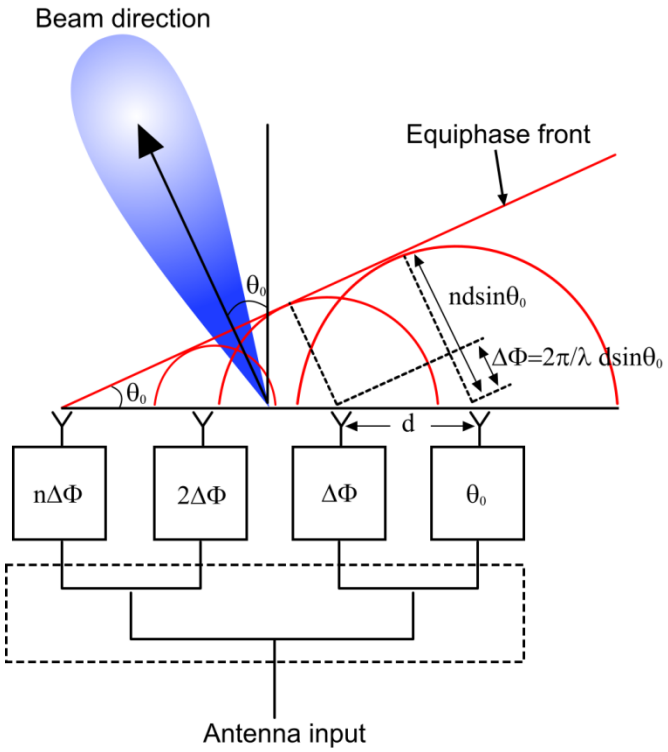

Figure 1.1. Phased antenna array

The electronics typically includes a phase shifter for setting the beam position and amplification to overcome the losses of the phase shifter and establish output power or noise figure of the system. The cost of this microwave electronics circuitry is typically quite expensive, on the order of $1K - $2K for each antenna element, making electronically scanned antennas very expensive to build [8] [9].

A way to lower the cost of these radars is to utilize microelectromechanical systems, or *MEMS*, approach where we can fabricate our design on low cost material and eliminate any electronic devices for phase shifting. The Rotman lens offers a cheap and compact means to extend the single beam systems generally used, to fully functional beamsteering arrangements. Furthermore the antennae array presented herein radiates the signal to a specific controlled direction.

The use of MEMS technology to reduce the number of electronics modules greatly reduces the hardware costs of the radar. In addition, the use of innovative manufacturing methods allows not only the Rotman lens phase shifter replacement, but whole antenna arrays to be integrated onto a single substrate. This greatly reducing the packaging and interconnect complexity, and lowers costs. These two factors make an inexpensive development of the antenna arrays for both space-based and ground-based microwave systems. A block diagram for this radar architecture is shown in the next section.

1.2.2 The MEMS radar

Depending on the range coverage, the radar antenna's radiation pattern must have narrow beamwidth of a few degrees, low side lobe levels and high radiation efficiency to achieve high accuracy. For these requirements, design of highly directive planar

automotive radar antennas on a low cost micromachined silicon substrate is under development. A MEMS single-pole-Single-Throw (SPST) switch is implemented on the microstrip antenna array for use in 77 GHz tri-mode automotive collision avoidance radar. The advantage of such design is that it enables simple integration of the antenna arrays in the vehicle. Extensive work has been published in the design of planar patch antenna arrays for automotive radar applications at 77 GHz and serves as a starting point for this thesis. However, to be able to accomplish higher precision and accuracy, the usage of a micromachined technology is desirable.

In order to produce a complete sensor or communication device the implementation of the antenna is a critical aspect. While long distance radar needs large high gain antennas, the targeted application for this thesis will be tri-mode automotive collision avoidance radar. At millimetre wave frequency, the use of mechanical scanning antenna experiences slow response and suffers reliability problem due to shock and vibration. As for antennas with phase shifters, they are expensive to fabricate and initiate considerable RF losses. By avoiding those disadvantages, Rotman lens antenna could open new applications for millimetre wave radar.

The automotive radar module is prepared according to the desired coverage. Long range radar (LRR), medium range radar (MRR) and short range radar (SRR) are used in cruise control and collision avoidance applications. Generally, the requirement for automotive radars is to detect any targets in the field of view with high probability, high accuracy and low false alarm rate. Automotive radars usually operate in the dedicated frequency band of 76 – 77 GHz. Beside this technology, today MRR and SRR automotive radars are under development. They are supposed to be less expensive than

laser sensors and video cameras but still provide the advantages of microwave based sensing with respect to

High performance automotive radars cover different target ranges, measure azimuth and radial velocity simultaneously in a short time and have the capability to resolve reflectors in multiple target situations. The main technical challenge lies in the waveform, antenna and signal processing design.

Having established that automotive radar can be very helpful in reducing the number of fatal accidents, it is essential that low cost and reliable radar systems be made to improve road safety globally. Lower cost (compared to $2000-$3000 approx. for current systems) will enable lower-end vehicles to be equipped with safety options.

The principle of operation is explained thoroughly in the coming section. The following block diagram, Figure 1.2, presents the major components of the automotive radar system.

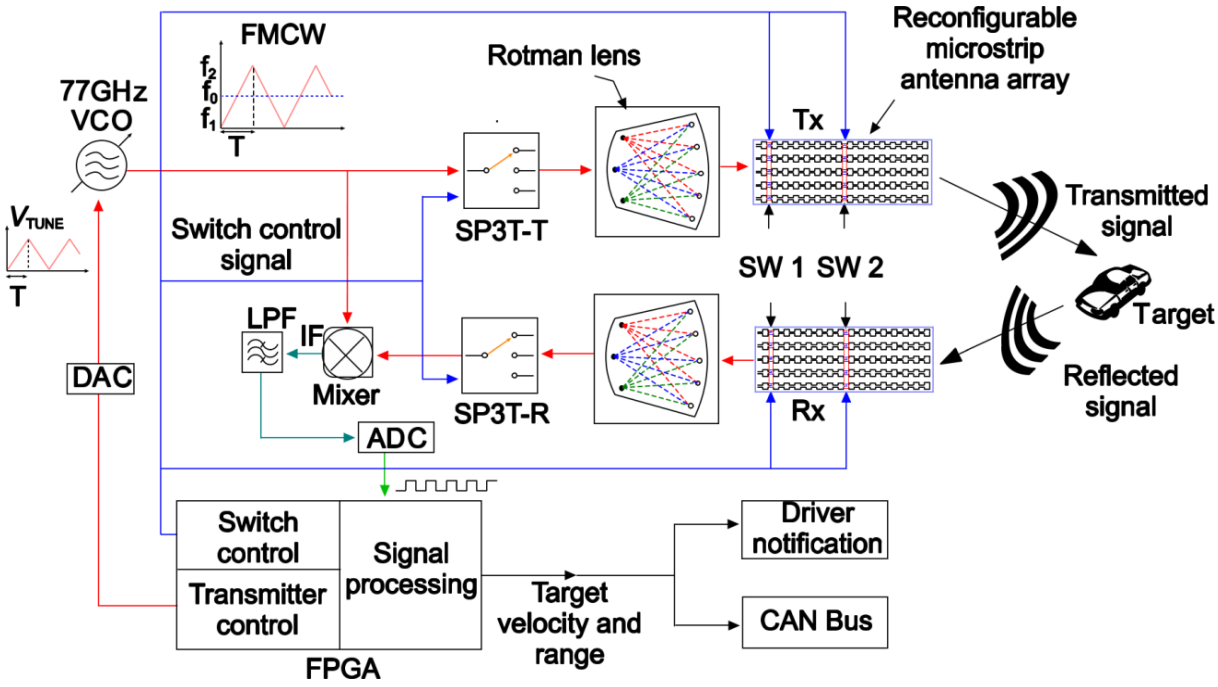

Figure 1.2. Automotive radar system block diagram

The major components of the MEMS based tri-mode radar:

- Microfabricated Rotman lens
- MEMS SP3T RF switches
- TLC MINT77TR GaAs transceiver
- MEMS reconfigurable microstrip antenna array
- MEMS SPST RF switches
- FPGA/ASIC implemented controller

The following figure, Figure 1.3, demonstrates the tri-mode radar coverage currently under development.

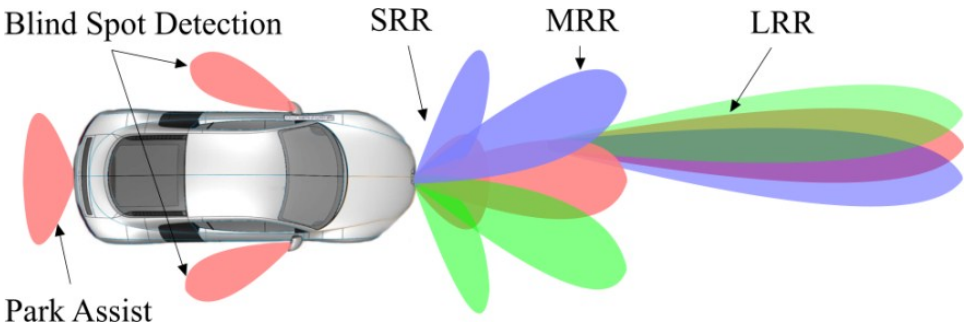

Figure 1.3. Tri-mode automotive radar

1.2.3 MEMS radar principle of operation

Transmitting side:

1. AN FPGA/ASIC implemented control algorithm will generate a linear frequency modulated continuous wave (LFMCW) signal that will be fed to a MEMS SP3T switch.
2. The FPGA/ASIC implemented control algorithm controls the MEMS switch to sequentially trigger the LFMCW signals among the three beamports of Rotman lens.

4. The signal will travel through the Rotman lens, and the time delayed in-phase signals are fed to a microstrip antenna array that radiates the signal in a specific direction.
5. The steering of the radiated signal is guided by the switching of the input signal among the beamports of the Rotman lens.
6. An FPGA/ASIC implemented algorithm controls the operation of the MEMS SPST switches to dynamically adjust the microstrip antenna array from one mode to another.

Receiving side:

7. The microstrip antenna array receives the radiated signal reflected off a vehicle or an obstacle and feeds the signal to SP3T switch through Rotman lens.
8. The receiver SP3T switch passes the signal coming to the mixer in order to generate an IF signal in the range of 0-200 KHz.
9. The analog signal converts to digital through ADC.
10. The received digital signal will be processed by the FPGA/ASIC implemented algorithm to determine the position of the detected object.

1.3 Research hypothesis

The objective of this research is to develop a 77 GHz reconfigurable micromachined microstrip antenna array for the aforementioned MEMS based radar system. The system complexity will be greatly reduced by introducing the MEMS technology to realize a directional scanning beam without any microelectronic signal processing for beamforming. Such a system could be batch fabricated using standard

micro-fabrication technology to lower production costs. As a result, the highway safety situation will drastically improve resulting in less collision, less loss of lives and less property damage, and will have a significant impact on car insurance premiums.

The micromachined silicon based microstrip antenna array outperforms conventional Duroid 5880 substrate based microstrip antenna system operating in 77 GHz in terms of low loss, very high efficiency, bandwidth, and low cost batch fabrication capability for similar design specifications [10]. As the frequency modulated continuous wave (FMCW) radar requires a high chirp bandwidth to improve the range and velocity accuracy and resolution, the high bandwidth and high efficiency feature of the designed antenna array enable to realize high performance tri-mode radar for automotive collision avoidance applications.

1.4 Motivation

Automotive radar systems in the 77 GHz domain were introduced in the 90's into the passenger car market as a security and safety system for the driver [11]. For collision avoidance applications different ranges are used, having limited potential to extend the functionality to other applications like stop & go support of narrow beam long range radar.

For this reason radar systems in the 77 GHz frequency domain, which have good performance in range and azimuth angle coverage, are of interest and can therefore be applied in different automotive applications as follows:

- Parking Assist with higher precision, longer range and higher update rates than conventional ultrasonic systems
- Blind Spot Detection with a low cost sensor technology

- It provides support to Adaptive Cruise Control systems (ACC) in Cut-in and Stop & Go-situations due to the fact that the short range sensors can have a wider beamwidth than the directive long range sensor
- Pre-Crash Detection with very high detection update rates

This thesis aims to develop the 77 GHz reconfigurable micromachined microstrip antenna array for a MEMS based radar system to detect the distance and velocity of target vehicle(s) in a pre-specified range to meet the requirements of long range radar.

1.5 Principal Results

A micromachined silicon based MEMS single-pole-Single-Throw (SPST) switch embedded reconfigurable microstrip antenna array for use in a 77 GHz tri-mode automotive collision avoidance radar is presented. An FPGA / ASIC implemented algorithm controls the operation of the MEMS SPST switches to dynamically alter the beamwidth of the antenna array to cycle the radar constantly from short-range (SRR) to mid-range (MRR) to long range (LRR) mode. Major achieved designed simulation results of the developed system are listed below:

Table 1.2. Radar simulation results

Parameters	**SRR**	**MRR**	**LRR**
Gain	8.8 dBi	12 dBi	20.5 dBi
Azimuth angle	0°	0°	0°
Elevation angle	10°	10°	10°
-3dB Beamwidth (HPBW)	40°	26°	11°
S11 Parameter (return loss)	-25.5 dB	-25.3 dB	-23 dB
Bandwidth	1.2 GHz	1.2 GHz	1.8 GHz
Radiation Efficiency	97 %	94 %	90 %
VSWR	1.2	1.2	1.1

Wet etching and wafer bonding based fabrication techniques have been developed to fabricate the antenna array. The antenna is now in fabrication stage and a working unit ready for testing will be obtained soon.

1.6 Thesis Organization

Chapter 1 highlights the importance of the work and its outcomes to the present day. It reviews the significance of radar technology and studies their purpose in the automotive industry. This chapter recaps the statistics of the World Health Organization and the vehicle fatality rate in different regions.

Chapter 2 briefly summarizes the existing literature of radar antenna array technologies and studies their applications in the automotive industry. This chapter provides a good background and targeted specifications for the MEMS base radar.

Chapter 3 presents all the necessary characteristics and the mathematical concept of the microstrip antenna array. It includes all the essential parameters needed to design a microstrip antenna. Also, this chapter details the theory behind antenna arrays and the difference between linear and planar antenna arrays.

Chapter 4 follows Chapter 3 in introducing and explaining the micromachining technology and its affect on microstrip antennas. As well, a deep description of various types of micromachining and how can it manipulate our design in a positive way.

Chapter 5 provides simulation and measurement results of our short range radar (SRR), mid-range radar (MRR), and long range radar (LRR). In this chapter, an explanation of the fabrication process is been offered for our antenna.

Chapter 6 concludes this thesis with a summary of our work and what can be done in the future to enhance and prepare our product for the automotive industry.

CHAPTER II

REVIEW OF LITERATURE

This chapter reviews the state-of-the-art in the automotive radar systems and the antenna arrays used in the automotive radars. The development of MEMS base tri-mode radar is also discussed. MEMS base radars are then compared to existing radar technology.

2.1 Literature Review

Worldwide, about 1.2 million people are killed and 50 million people are injured in road crashes each year [4]. Developing countries are experiencing high rates of increase in car ownership, population and in demands for enhanced mobility. The resultant increase in the number of people killed or injured in road crashes poses a great challenge for those responsible for the road transport system in the developing world. To enhance road safety system and reduce automobile collisions, automakers and governments are extensively pursuing radar based proximity detection systems in all on-road vehicles. As mentioned in the previous chapter that study of crash avoidance technologies shows a promising potential for reducing road crashes. This technology will provide safety benefits for motor carriers and all road users.

More than one-quarter of the nearly 400,000 police-reported crashes each year are potentially relevant to at least one of four crash avoidance technologies: side view assist, forward collision warning/mitigation, lane departure warning/prevention, or vehicle stability control. Side view assist has the greatest potential to prevent or mitigate crashes of any severity, potentially preventing or mitigating up to 39,000 crashes, or 10 percent,

of the 384,000 police-reported crashes each year. These crashes involve vehicles traveling in the same direction, and relatively few involve moderate-to-serious injury or fatality. Vehicle stability control is another promising technology, with the potential to prevent or mitigate up to 31,000 crashes each year including more serious crashes — up to 7,000 moderate-to serious injury crashes and 439 fatal crashes per year. Vehicle stability control could prevent or mitigate up to 20 and 11 percent of moderate-to-serious injury crashes and fatal crashes, respectively [12].

Accordingly, the National Highway Traffic Safety Administration (NHTSA) evaluated its Federal Motor Carrier Safety Administration (FMCSA) and computed the benefits and costs specific to both small and large motor carriers. The evaluation covered the life-saving benefits as well as the consumer cost for a substantial "core" group of safety technologies for passenger cars and LTVs (pickup trucks, sport utility vehicles and vans). In 2002, these technologies added an estimated $11,353,000,000 to the cost of new cars and LTVs of that model year. They saved an estimated 20,851 lives in the cars and LTVs on the road during that calendar year. That amounts to $544,482 per life saved in 2002. These technologies added a total of $189,842,000,000 to the consumer cost of new cars and LTVs over model years 1968-2002. They saved 252,989 lives in model year 1968 and later vehicles during calendar years 1968-2002. That amounts to $750,782 (in 2002 Dollars) per life saved in 1968-2002 [13].

As a solution, the strategic Automotive Radar frequency Allocation (SARA) consortium allocated 77-79 GHz frequency range for automotive to reduce size and improve performance of automotive radars [14]. Despite the benefits of the crash

avoidance technologies, automakers and suppliers are being pursued vigorously to minimize the cost and size while improving the performance of automotive radars. They are looking into ways to reduce application cost and batch fabrication capability of the MEMS technology to implement better sophisticated radar system that can provide improved performance over the microelectronic conventional based radars.

2.1.1 MEMS technology

MEMS field progressed rapidly from the integrated circuit industry. The most fundamental characteristics are miniaturization, microelectronics integration and precise mass production. MEMS technology makes it possible to fabricate electromechanical and microelectronics component in a single small device ranging from 1 μm ~ 1 cm. The reduction in dimension of electromechanical systems offers advantages such as soft spring, high resonance frequency and low thermal mass, and leads to dramatic decrease in power consumption [15]. In MEMS, while the electronics are fabricated adopting integrated circuit (IC) process sequences, the micromechanical components are fabricated using compatible "micromachining" processes that selectively etch away parts of the silicon wafer or add new structural layers to form the mechanical and electromechanical devices. The mechanical sensor and actuators with electronic processors and controllers can be fabricated in a single substrate in an unbroken, wafer-level process flow and integrated in chip level. The accurate dimension and placement precision is guaranteed by lithography. The batch-based fabrication process has the potential to scale up in large volume and reduce the cost and improve the yield and reliability significantly [16].

2.1.2 Radar type

Car manufacturers and suppliers main objective is to develop a comfort and safety systems to the driver. Driver assistance and active safety systems are becoming very important topics in this industry. They help recognize dangerous situations at early stages and thus facilitate to avoid accidents or at least reduce the accident severity.

Earlier automotive radar systems used pulsed-echo technology that requires high power pulses and false target detection was a crucial problem for those radars. The German government (BMBF) funded joint project "Automotive High Frequency Electronics KOKON" [17] [18] was initiated mainly due to the short range radar (SRR) frequency regulation in Europe. It has been established that phased array based frequency modulated continuous wave (FMCW) radars with beamforming and beamsteering capability is the technology of choice for forward ranging applications. The key advantages of FMCW based phased array radars are:

1. Low power rating
2. beamsteering capabilities without any mechanically rotating mounting base
3. Low effects of phase noise
4. Decreases the effect of clutter and atmospheric noise
5. High precision target range
6. More resistance to interference from other similar radars in the vicinity
7. Determine velocity of the selected target
8. No theoretical blind spot

Various radars have been designed using different technologies; however, MEMS based radar uses microfabricated technology that can be used to batch fabricate several

Rotman lenses at a time with high precision and low cost while maintaining a tight tolerance. Rotman lenses can pave the way to realize high performance low cost radar sensors for automotive collision avoidance application. Moreover, the lens can be fabricated with silicon based antenna array, FMCW routing MEMS based RF switches, and it would be possible to realize complete radar in a chip using low cost silicon technology. The antenna array in this thesis transmits and receives the signals travel through the Rotman lens that radiates the signal in a specific direction.

2.2 Microelectronic beamforming with phased array antenna

A beamformer is a signal processing technique used in conjunction with an array of sensors to provide a versatile form of spatial filtering. The sensor array collects spatial samples of propagating wave fields, which are processed by the beamformer [19]. In another word, it can direct the transmitted or received signal from an antennae array to a chosen angular direction to realize spatial selectivity. When transmitting, a beamformer controls the phase and relative amplitude of the signal at each transmitter, in order to create a pattern of constructive and destructive interference in the wavefront. When receiving, information from different sensors is combined in a way where the expected pattern of radiation is preferentially observed.

In communications, high directivity is desired in the direction of the signal source for a low-noise high-fidelity link to be established. In radar systems, beamforming allows a means of electronic steering of a narrow scanning beam to detect targets with higher angular resolution.

Beamformers provide an effective and versatile means of spatial filtering. The following table, Table 2.1, lists number of applications of spatial filtering, gives examples of arrays and beamformers, and provides a few key references.

Table 2.1. Applications that employ beamforming

Application	Description and References
Radar	Phased array radar [20]; air traffic control [21]; synthetic aperture radar [22]
SONAR	Source localization and classification [23] [24]
Communications	Directional transmission and reception [25] [26]; sector broadcast in satellite communications [27]
Imaging	Ultrasonic [28]; optical [29]; tomography [30]
Geophysical Exploration	Earth crust mapping; oil exploration [31]
Astrophysical Exploration	High resolution imaging of the universe[32] [33]
Biomedical	Fatal heart monitoring [34]; tissue hyperthermia [35]; hearing aids [36]

2.2.1 Microelectronic beamforming types

Beamforming involves both the generation of a directional pattern as well as steering of the main lobe over the azimuth and also the elevation angles and it can be categorized into two main types:

a) Analog beamforming

Analog beamforming means that the received signals from each element for the phased array antenna are combined at the carrier frequency level. Both the amplitude and phase of each antenna element are controlled in beamforming. Combined amplitude and phase

control can be used to adjust side lobe levels and steer nulls better than can be achieved by phase control alone [37]. The following figure, Figure 2.1, represents an analog beamformer using analog RF circuit components:

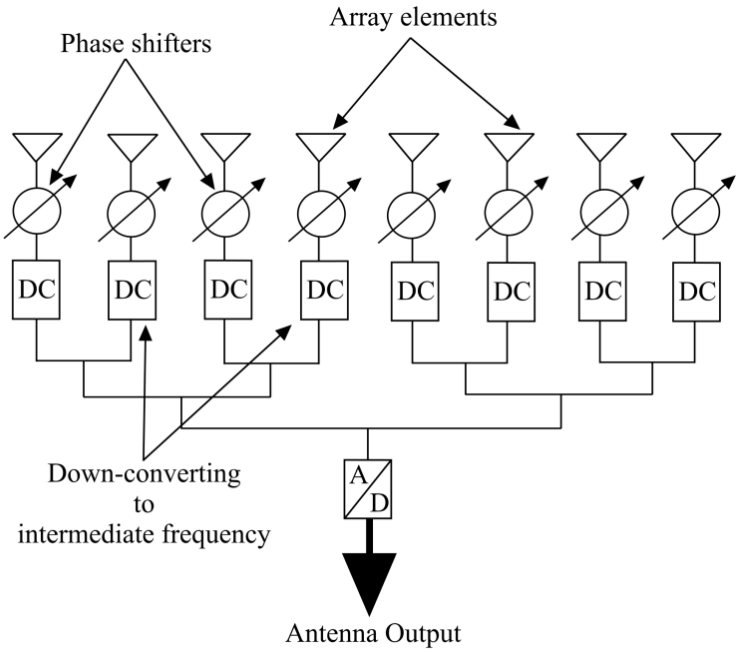

Figure 2.1. Analog beamformer of the antenna pattern

In a beamforming network typically the signals incident at the individual elements are combined intelligently to form a single desired beamformed output. Before the incoming signals are formed, they are brought down to baseband or intermediate frequencies (IF's). The receivers provided at the output of each element perform the necessary frequency down conversion. Therefore it is required that the down-converted signal be converted into digital format before they are processed. Analog-to-digital converters (ADC's) are provided for this purpose. For accurate performance, they are required to provide accurate translation of the RF signal from the analog to the digital domain.

Various manufacturers used the analog beamforming technology on 77 GHz frequency for long range radars (LRR) such as Bosch, Delphi, Denso, TRW, Fujitsu Ten,

and Hitachi. Other companies (Delphi, Fujitsu Ten, Mitsubishi electric, Celsius Tech) used mechanical mechanisms in conjunction with ADC to steer the beam in azimuth [11].

b) Digital beamforming

In digital Beamforming, the operations of phase-shifting and amplitude scaling for each antenna element, and summation for receiving, are done digitally. Multiple independent beams steered in all directions can be formed in the digital beamforming processor. The benefits of this type include:

- Improved dynamic range
- Controlling of multiple beams
- Better and faster control of amplitude and phase

Although the digital beamformer will require memory blocks, adders and multipliers as system building blocks to function, it is still more flexible and efficient than the analog beamformer [38]. The following figure, Figure 2.2, illustrate a digital beamformer:

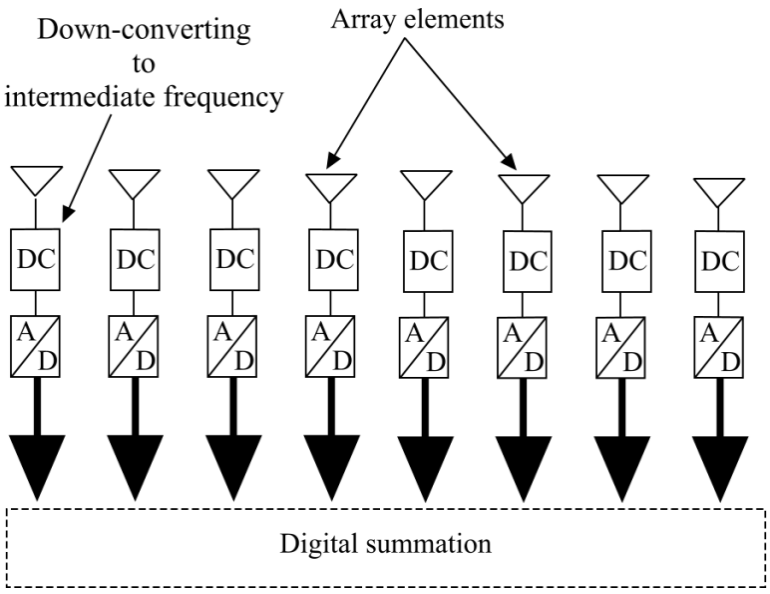

Figure 2.2. Digital beamformer

In digital beamforming there are many digital receivers that can be used. Converting to an intermediate frequency and digitizing the signal is realized at each individual antenna element.

In 2003, 77 GHz radar sensors with digital beamforming (DBF) front ends were introduced into the market by Japanese companies. Denso built a bistatic LRR with planar patch antennas with a range capability up to 150m and a field of view of approx. ±10 degrees [39].

2.2.2 Rotman lens beamforming

Rotman lens offers an inexpensive and compact solution to extend the single beam systems to fully functional beam staring arrangements. The flexibility of microstrip transmission lines and the advent of fast accurate simulation packages allow practical Rotman lenses to be designed at mm-wavelengths. It offers beamforming and beamsteering capabilities without any microelectronic signal processing as needed in analog and digital beamformers [40].

It consists of three major components: A semi-circular shaped focal arc that traces the contour of the beam ports, a curved line called the inner contour that traces the contour of the array ports, and a straight line known as the outer contour that depicts the position of the radiating elements. The semi-circular focal arc is sometimes modified slightly to be elliptical to reduce the aberration [41]. Figure 2.3 shows the general geometry of Rotman lens.

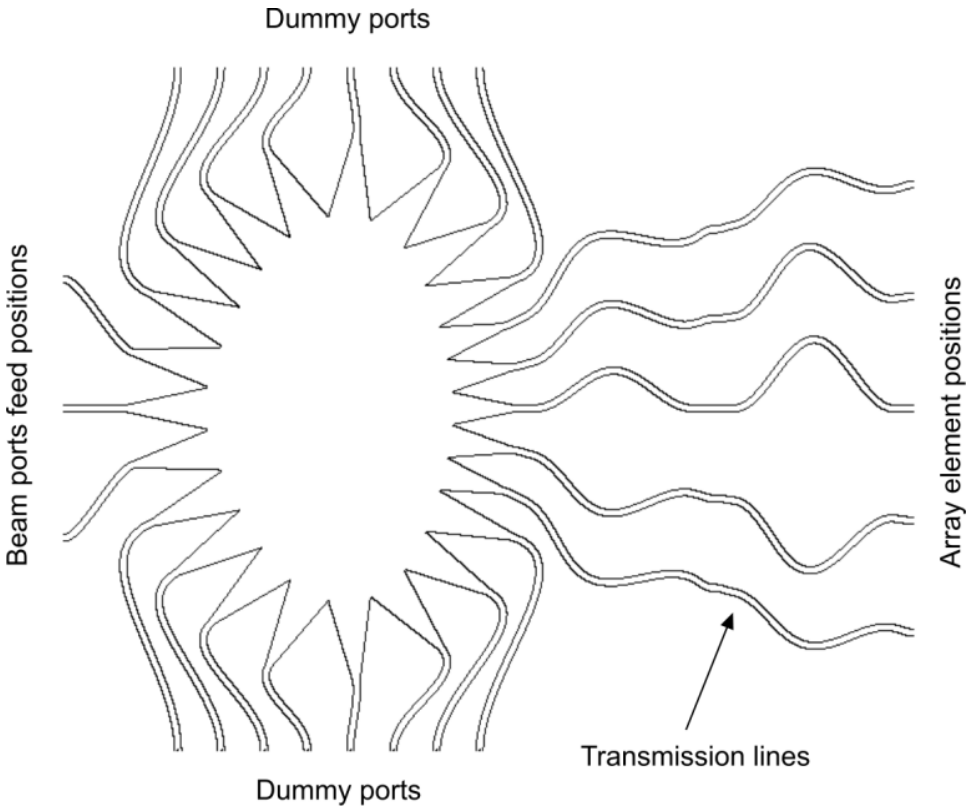

Figure 2.3. Rotman lens geometry and design parameters

Typical Rotman lenses are realized using microstrip substrates like Duroid 5880. The above Rotman lens figure, illustrates the schematic representation of the Rotman lens designed at the University of Windsor. It was made on a high resistivity Silicon wafer and it incorporates three input signals and 5 output ports. The central beam guides the input signal through channels of equal length to the array elements, creating a forward-facing beam.

On beam ports 1 and 3 the input signal travels through different path lengths to the antenna patches, thus undergoing phase shift leading to the beam being steered as shown in the following figure.

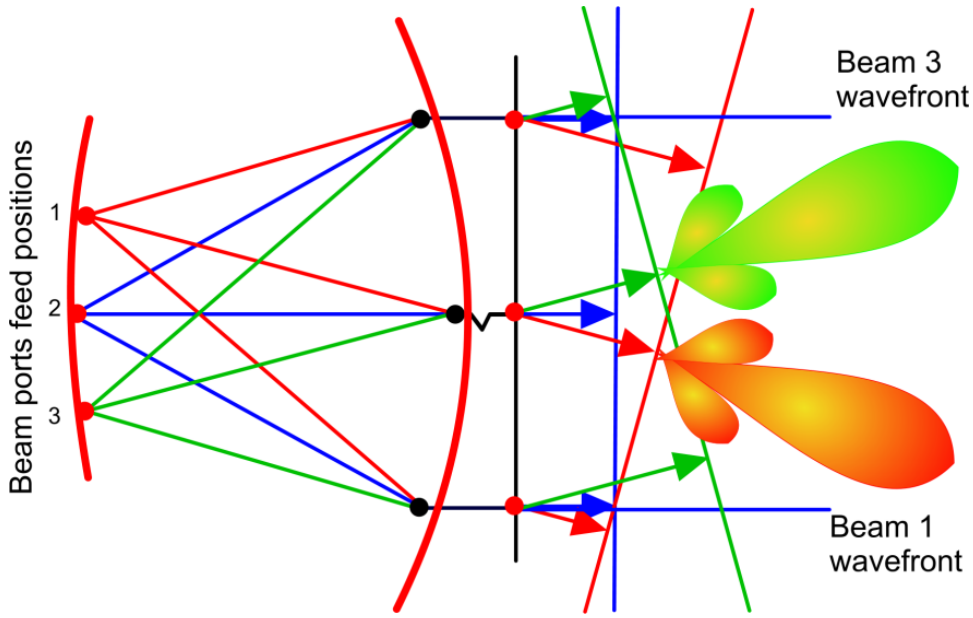

Figure 2.4. Direction of the outgoing beam for input at different feed ports

2.2.2.1 Antenna array

Antenna arrays with reconfigurable capabilities are of tremendous importance in many applications, such as satellite communications, radar systems, point to point communication links and imaging. Planar antenna arrays can satisfy stringent requirements in terms of low-profile, low-weight and fast beam steering capability. Such antennas can be controlled in several manners: the use of electronic phase-shifters and/or amplitude tuners allows one to fully reconfigure the radiation pattern, steer and shape the beam, introduce nulls and control the side-lobe level. Another method of making a reconfigurable antenna arrays can be controlled with switches. Modern approach to a conventional technique is introduced for the electronic control of microstrip patch antenna arrays. The control is achieved by placing microelectromechanical switches (MEMS) at appropriate locations in a patch antenna array. The microwave MEMS are used to switch between open and short circuit conditions that allow reconfiguration of the

modal fields. Changing the number of the patches, changes the radiated field and the area of coverage. This can be achieved without changing the frequency of operation, input impedance or radiation pattern of the patch antenna array.

Rotman lens and microstrip antenna array combine the advantages of the low cost fabrication in printed technology and the low loss characteristics typical of waveguide devices. This is especially true when low permittivity and high thickness substrates are employed.

Figure 2.5, presents Rotman lens along with the micromachined microstrip antenna array:

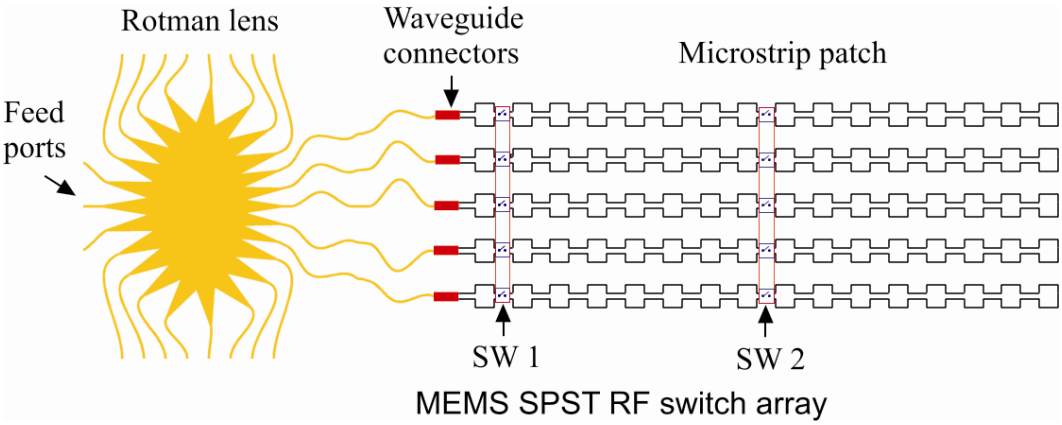

Figure 2.5. Rotman lens and antenna array

The above figure illustrates the antenna arrays designed to work with Rotman lens along with the MEMS RF switches implemented to change the angular coverage of the radiation pattern. Whether the MEMS RF switched “on” (short circuit) or “off” (open circuit), the radiation of the antenna arrays changes accordingly.

The reconfigurable antenna arrays and the MEMS RF switches combination central to this thesis can be used in conjunction with the Rotman lens in order to

accomplish SRR, MRR and LRR beamforming using the same hardware. The control of such a system would be easily realizable digitally by means of the FPGA control algorithm.

2.3 State-of-the-art automotive radar

Automotive radar was first experimented in the late 50's and intensively in the 70's started at microwave frequencies. The activities of the last decades were concentrated mainly on developments at 17 GHz, 24 GHz, 35 GHz, 49 GHz, 60 GHz, and 77 GHz. Even from the early beginning in automotive radar the key driver of all these investigations has been the idea of collision avoidance; this idea has spent enormous motivation for many engineers all over the world to develop smart vehicular radar units [11].

Parking assist, collision warning, and Adaptive Cruise Control (ACC) were the first applications with surround sensing technologies. In the 90's, the collision warning systems were successfully introduced in the US. Greyhound installed more than 1600 radar systems (24 GHz) in their bus lines yielding a reduction of accidents of 21 percent in 1993 compared to the year before. In 1999, Mercedes introduced the 77 GHz "Distronic" into the S class, followed by other premium models equipped optionally with an ACC, such as BMW 7 series, Jaguar (XKR, XK6), Cadillac (STS, XLR), Audi A8, and VW Phaeton. ACC is also available in Mercedes E, CL, CLK, SL class, BMW 5 and 6 series, Audi A6, Nissan (Cima, Primera), Toyota (Harrier, Celsior), Lexus (LS, GS), and Honda (Accord, Inspire, Odyssey). Furthermore, ACC will become an option in the new BMW 3 series and in the new VW Passat, both with start of production in 2005 [11].

Quite a few standards have been established for different applications. For example, short-range (m) radars are adopted to provide parking assistance or to prevent side crash. Because of the short distance, it must provide a wide angular coverage and a good resolution [42]. The mid-range radars usually operate at 24 GHz band to cover a distance of 10 – 40 meters with an angle of 30 – 60 degrees [43] [44]. As for long range radars, the use of 77 GHz band has been dedicated for such coverage, which basically detects the distance and the relative speed of the vehicles in front so as to perform a real-time response by means of the braking system or other protective mechanism. It must cover a range up to 100 – 150 meters [11]. Table 2.2 represents the general standard of automotive radar.

Table 2.2. Classifications of automotive radar systems

Radar type	Frequency	BW	Angle	Range	Resolution	Application
SRR	24 GHz	7 GHz	70°	10m	<10cm	Side crash parking
MRR	24 GHz	250 MHz	30~60°	40m	~ 1m	Stop & go
LRR	77 GHz	1 GHz	16°	150m	~ 1m	ACC

Various car manufacturers and suppliers are developing optimized sensor configurations for comfort and safety functions with respect to functionality, robustness, reliability. Last but not least the total system costs have to meet the marketing targets to be attractive for the end users. The following table, Table 2.3, provides one of the biggest automotive suppliers competing for this technology.

Table 2.3. New generation of automotive radar systems [11]

Company	Frequency	Radar type	Range of coverage	Relative velocity $(km/h)^2$	Field of view
TRW	77 GHz	LRR	1 – 250 m	±220	±8°
Delphi	76.5 GHz	LRR	1 – 174 m	-360 to +90	±10°
Denso	77 GHz	LRR	2 – 250 m	±200	±20°
Chrysler	76 ~ 77 GHz	LRR	1 – 200 m	-100 to +260	±20°
Bosch	77 GHz	LRR	0.5 – 250 m	-500 to +250	±30°

From the above table, Bosch radar system is one of the most recent released applications. It was launched in 2009 on the Porsche Panamera 2010 model. Bosch claims to have the world's smallest radar sensor package at 74mm x 77mm x 58mm. Another radar system The MEMS radar system being developed at the University of Windsor has close to half the dimensions at 30mm x 40mm x 10mm owing to the compact MEMS Rotman lens beamformer and antenna design.

2.4 State-of-the-art antenna array

This section provides an overview of the state of the art of smart antennas, and is particular focused on the reconfigurable antennas as the most quickly developing devices in recent years.

Considering all aspects of the designing process of antenna arrays it can be quite demanding, but it also provides an excellent opportunity to combine state-of-the-art technologies with the antenna theory in an attempt to provide additional degrees of freedom in system performance [10]. Antenna array comes in large variety of different shapes and forms. These types of antennas are typically described by some categories, including reconfigurable radiation pattern and/or polarization and reconfigurable

frequency and/or bandwidth. The following table, Table 2.4, provides different antenna array designs close to our design requirement:

Table 2.4. Different antenna array designs

Year	Frequency	Radar	Antenna	Azimuth	Gain	BW
2005 [45]	76.5 GHz	SRR	Rectangular Microstrip (4x12)	±25.5°	17.8 dBi	1.0 GHz
2005 [45]	76.5 GHz	SRR	Rectangular Microstrip (2x12)	±39.3°	15.5 dBi	1.0 GHz
2010 [46]	34.5 GHz	SRR	Rectangular Microstrip (1x1)	60°	9.0 dBi	1.2 GHz
2005 [47]	122 GHz	SRR	Rectangular Microstrip (1x1)	90°	3.2 dBi	2.0 GHz
2004 [48]	24 GHz	MRR	Rectangular Microstrip (4x6)	±12°	N/P	500 MHz
2008 [49]	140 GHz	LRR	Rectangular Microstrip (2x4)	20°	12 dBi	2.0 GHz
2010 [50]	77 GHz	LRR	Rectangular Microstrip (8x8)	±9°	20 dBi	1.0 GHz

The state-of-the-art of the automotive radar systems and the antenna arrays provide the objective for this thesis and help set the goal for efficiency and performance of the reconfigurable antenna array as designed in this thesis.

CHAPTER III

MICROSTRIP PATCH ANTENNA

This chapter presents the state-of-the-art literature reviews on microstrip antenna, including basic theory, analysis, and feeding methods that are essential for the target antenna array design. As the target microstrip antenna array will have a planar configuration for use in conjunction with the Rotman lens, a review of planar antenna theory is also presented.

3.1 Microstrip patch antenna

Microstrip Patch antenna has been a common choice for integrated antennas not only for automotive but also for various other industries. Government, military, and medical sectors are leading the majority of research initiatives for the development and deployment of wearable communication systems. As populations grow and age, the demand on health care resources increases and many governments are looking for remote healthcare solutions. Military applications are focused on integrating these devices into military clothing in an attempt to enhance soldier performance, awareness and survivability on the battle field. Due to their simple design, planar configuration, high gain, and low fabrication cost [52], microstrip patch antennas are becoming the technology of choice for such applications.

A microstrip patch operates like a resonant cavity, where the patch forms the top of the cavity, the ground plane is the bottom of the cavity, and the edges of the patch form the sides of the cavity. The edges of the patch act as an open-circuit boundary condition. Hence, the patch acts approximately as a cavity with perfect electric conductor on the top and bottom surfaces, and a perfect “magnetic conductor” on the sides. For

good antenna performance, a thick dielectric substrate having a low dielectric constant is desirable since this provides better efficiency, larger bandwidth and better radiation [15]. However, such a configuration leads to a larger antenna size.

The metallic patch may be of various geometries, with rectangular and circular being the most common used shapes. The patch is generally made of conducting materials such as gold or copper. The radiating patch and the feed lines are usually etched out of a metal deposited on the top of a dielectric substrate. Figures 3.1 and 3.2, shows the standard microstrip structure in three different views:

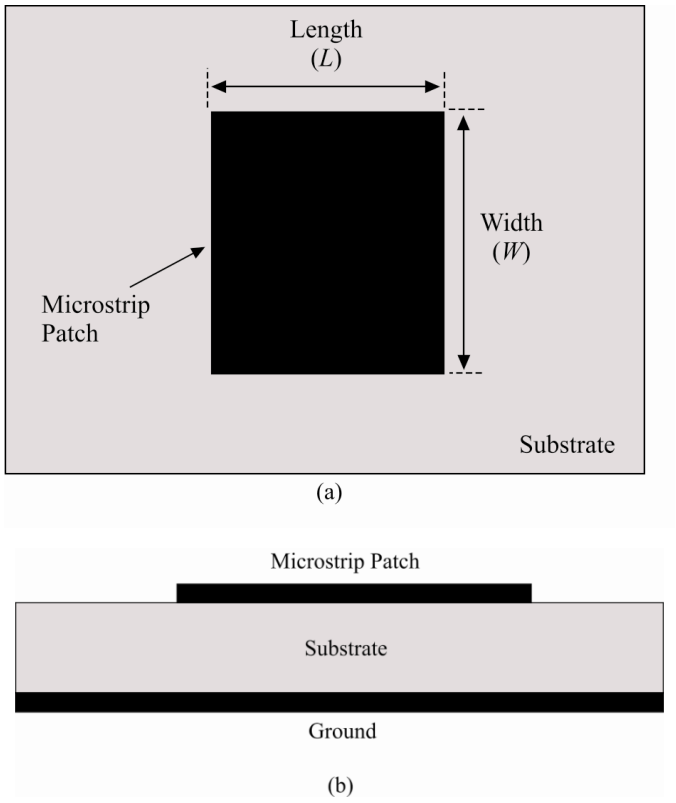

Figure 3.1. Microstrip rectangular patch antenna; (a) top view; (b) side view

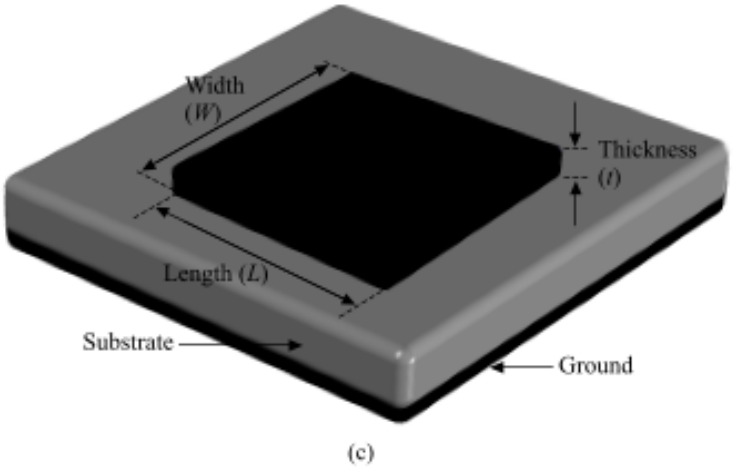

Figure 3.2. Microstrip rectangular patch antenna; (c) 3D view

The microstrip patch geometry is commonly square, rectangular, circular, triangular, and elliptical or some other common shapes as shown in the Figure 3.3. For the target application we have chosen to work with rectangular patches since it has the largest impedance bandwidth compared to other types of geometries.

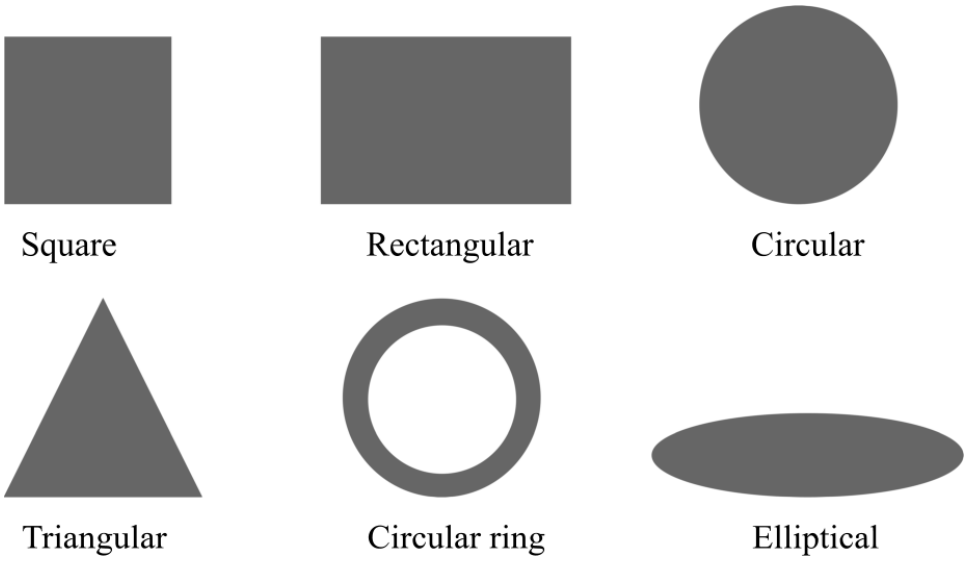

Figure 3.3. Microstrip patch antenna geometry

3.2 basic Principle of Operation

Microstrip patch antennas radiate because of the fringing fields between the patch edge and the ground plane. There are many methods to analyze a microstrip patch antenna and the most popular models are the transmission line model, cavity model, and full wave model. The transmission line model is the simplest and it gives good physical insight but it is less accurate [53]. The cavity model is more accurate and gives good physical insight but is complex in nature. As for the full wave model, it is extremely accurate, versatile, and can treat single elements, finite and infinite arrays, stacked elements, arbitrary shaped elements, and element coupling. These give better insight as compared to the two models mentioned above and are far more complex in nature [10]. In this thesis, the transmission line model has been used to determine initial design specifications which are then optimized using a full wave analysis using a finite difference time domain (FDTD) method.

3.2.1 Transmission line model

The transmission line model represents the microstrip antenna by two slots of width (W) and height (h), separated by a transmission line of length (L). The microstrip is essentially a non-homogeneous line of two dielectrics, typically the substrate and air. Hence, as seen from Figure 3.4, most of the electric field lines reside in the substrate and parts of some lines in air. As a result, this transmission line cannot support pure transverse-electromagnetic (TEM) mode of transmission, since the phase velocities would be different in the air and the substrate. Instead, the dominant mode of propagation would be the quasi-TEM mode. Hence, an effective dielectric constant (ε_{reff}) must be obtained in order to account for the fringing and the wave propagation in the line. The

value of ε_{reff} is slightly less than ε_r because the fringing fields around the periphery of the patch are not confined in the dielectric substrate but are also spread in the air as shown in Figure 3.4. The expression for ε_{reff} is given by Balanis [10] as:

$$\varepsilon_{reff} = \frac{\varepsilon_r + 1}{2} + \frac{\varepsilon_r - 1}{2}\left[1 + 12\frac{h}{W}\right]^{-1/2} \qquad W/h > 1 \qquad \textbf{3.1}$$

where; ε_{reff} is the effective dielectric constant

ε_r is the dielectric constant of substrate

h is the height of dielectric substrate

W is the width of the patch

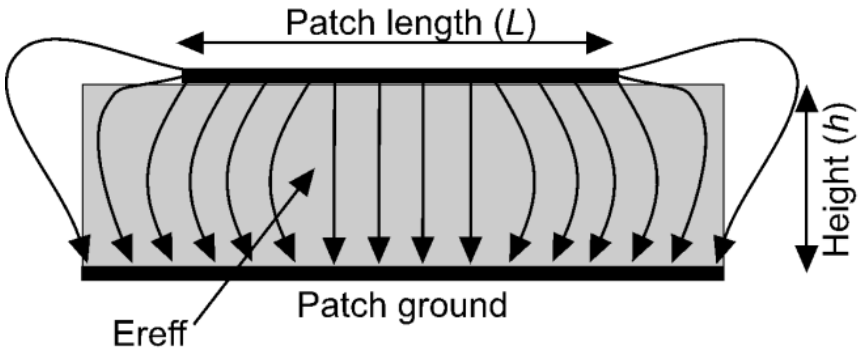

Figure 3.4. Effective dielectric constant and fringing affect

Figure 3.5 shows a rectangular microstrip patch antenna of length (L), width (W) resting on a substrate of height (h). The co-ordinate axis is selected such that the length is along the x-axis direction, width is along the y-axis direction and the height is along the z-axis direction.

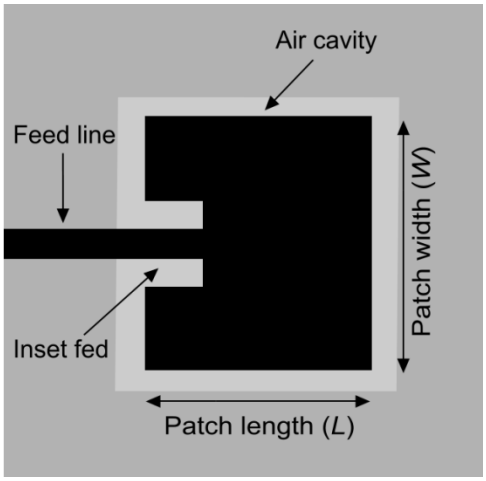

Figure 3.5. Rectangular microstrip patch antenna

In order to operate in the fundamental TM_{10} mode, the length of the patch must be slightly less than λ/2 where λ is the wavelength in the dielectric medium and is equal to $\lambda_o/\sqrt{\varepsilon_{reff}}$ *where* λ_o is the free space wavelength. The TM_{10} mode implies that the field varies one λ/2 cycle along the length, and there is no variation along the width of the patch. In the Figure 3.6 shown below, the microstrip patch antenna is represented by two slots, separated by a transmission line of length *L* and open circuited at both the ends. Along the width of the patch, the voltage is maximized and the current is minimized due to the open ends. The fields at the edges can be resolved into normal and tangential components with respect to the ground plane.

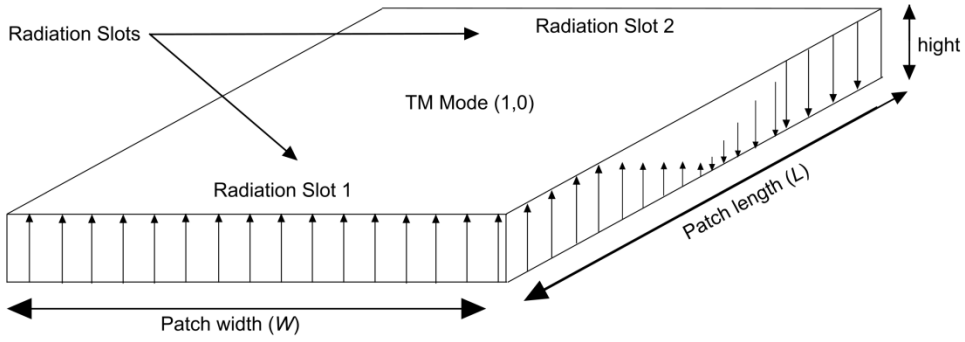

Figure 3.6. Fundamental TM_{10} of rectangular antenna with two radiating slots

3.2.2 Cavity model

This model was introduced in the 1970's by Lo [54]. It is more complex than the transmission line model but it provides better accuracy. In cavity model, the inside region of the patch is filled as a cavity, bounded by the electric walls on both ways; it has a magnetic wall thorough the periphery.

In Figure 3.7, the operation of the cavity model is presented. We can see the charge distribution on the upper and the lower surfaces of the patch and even at the bottom of the ground plane, this happens when there is a power given to the Microstrip patch.

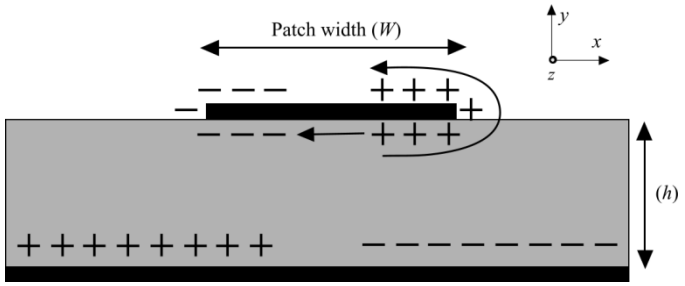

Figure 3.7. Cavity model charge distribution [10]

As shown above, a charge distribution is seen on the upper and lower surfaces of the patch and at also the bottom ground. This occurs when the microstrip patch is powered. As discussed by Richards and Lo, two mechanisms control this charge distribution; an attractive mechanism and a repulsive mechanism. The attractive mechanism is between the opposite charges on the bottom side of the patch and the ground plane, which helps in keeping the charge concentration intact at the bottom of the patch. The repulsive mechanism is between the like charges on the bottom surface of the patch, which causes pushing of some charges from the bottom, to the top of the patch. As a result of this charge movement, currents flow at the top and bottom surface of the patch

[54]. The basis for this assumption is the following observations for thin substrates ($h << \lambda$):

1) Since the substrate is thin, the fields in the interior region do not vary much in the z direction, i.e. normal to the patch.

2) The electric field is z directed only, and the magnetic field has only the transverse components H_x and H_y in the region bounded by the patch metallization and the ground plane. This observation provides for the electric walls at the top and the bottom.

Since the walls of the cavity, as well as the material within it are lossless, the cavity would not radiate and its input impedance would be purely reactive. Hence, in order to account for radiation and a loss mechanism, one must introduce a radiation resistance R_R and a loss resistance R_L. A cavity would now represent an antenna and the loss is taken into account by the effective loss tangent δ_{eff} which is given as:

$$\delta_{\text{eff}} = 1/Q_T \qquad \textbf{3.2}$$

where; Q_T is the total antenna quality factor and it can be expressed as [54]:

$$1/Q_T = 1/Q_d + 1/Q_c + 1/Q_r \qquad \textbf{3.3}$$

where; Q_d represents the dielectric quality factor:

$$Q_d = \omega_r W_T / P_d = 1/\tan\delta \qquad \textbf{3.4}$$

here; ω_r is the angular resonant frequency

W_T is the total energy stored in the patch at resonance.

P_d is the dialectic loss.

$\tan\delta$ is the loss tangent of the dielectric.

where; Q_c represents the conductor quality factor:

$$Q_c = \omega_r W_T / P_c = h / \Delta \quad \textbf{3.5}$$

here; h is the substrate height

Δ is the skin depth of the conductor.

Pc is the conductor loss.

As for Q_r, it represents the radiation quality factor:

$$Q_r = \omega_r W_T / P_r \quad \textbf{3.6}$$

where; P_r represents the power radiated from the patch.

After substituting all the equations in the effective loss tangent equation:

$$\delta_{\text{eff}} = 1/Q_T = \tan\delta + \Delta/h + P_r/\omega_r W_T \quad \textbf{3.7}$$

Therefore, the above equation describes the total effective loss tangent for the microstrip patch antenna using cavity model.

3.2.3 Full wave solutions-method of moment

One of the other methods and much complex in nature that provides the full wave analysis for the microstrip patch antenna is the Method of Moments. In this method, the surface currents are used to model the microstrip patch and the volume polarization currents are used to model the fields in the dielectric slab. It has been shown by Newman and Tulyathan [53] how an integral equation is obtained for these unknown currents and using the Method of Moments, these electric field integral equations are converted into matrix equations which can then be solved by various techniques of algebra to provide the result.

3.2.4 Radiating conductance

Rectangular microstrip antenna can be expressed in an equivalent circuit transmission line model as shown in Figure 3.8. The equivalent circuit representing the whole antenna that includes two radiating slots as parallel R-C circuits and the patch connecting them as a transmission line whose characteristics are computed in the same way as those of a microstrip transmission line.

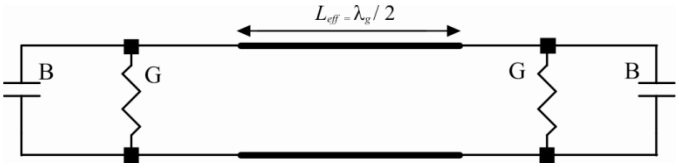

Figure 3.8. Equivalent circuit transmission line model

The equivalent circuit of a slot is constructed as a parallel *R*-*C* circuit. $G = 1/R$ represents the radiation loss, while $B = j\omega C$ is the equivalent susceptance, which represents the capacitance of the slot. Since both edges are identical, the value of the edge conductance is the same as follows:

$$G_1 = \begin{cases} \dfrac{1}{90}\left(\dfrac{W}{\lambda_0}\right)^2 & W << \lambda_0 \\ \dfrac{1}{120}\left(\dfrac{W}{\lambda_0}\right)^2 & W >> \lambda_0 \end{cases} \qquad \textbf{3.8}$$

where; λ_0 is the free-space wavelength.

3.2.5 Input resistance

The total admittance at one radiating slot is determined by transforming the admittance at the other radiating slot using admittance transformation equations of

transmission line. The following figure, Figure 3.9, shows the circuit model after $\lambda/2$ transformation:

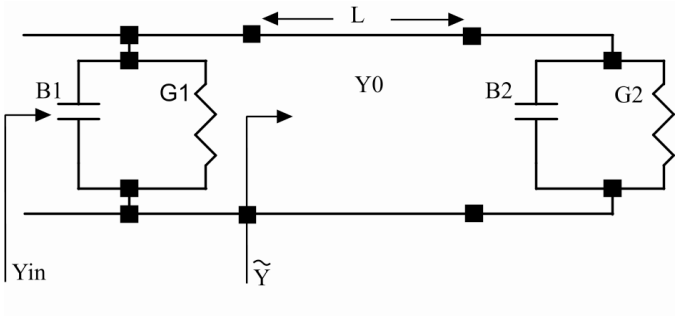

Figure 3.9. Transmission line model

The admittance at the each of the slots is identical

$$Y_1 = G_1 + jB_1 \qquad \textbf{3.9}$$

The total resonant input admittance is real and is giver by:

$$Y_{in}\left(L_{eff} \approx \lambda/2\right) = Y_1 + \widetilde{Y} = B_1 + G_1 + \widetilde{B} + \widetilde{G} = B_1 + G_1 - B_1 + G_1 = 2G_1 \qquad \textbf{3.10}$$

Where the total input impedance at resonance:

$$Z_{in} = 1/Y_{in} = R_{in} = 1/2G_1 \qquad \textbf{3.11}$$

Taking into consideration the mutual conductance [56] [57]:

$$R_{in} = 1/2(G_1 + G_{12}) \qquad \textbf{3.12}$$

where;

$$G_{12} = \frac{1}{120\pi^2}\int_0^x \left[\frac{\sin\left(\frac{k_0 W}{2}\cos\theta\right)}{\cos\theta}\right]^2 J_0\left(k_0 L\sin\theta\right)\sin^3\theta d\theta \qquad \textbf{3.13}$$

3.2.6 Fringing affect

Just like a capacitor, the fringing field of the microstrip patch forms an electric field that does not end up abruptly at the edge of the plates. There is some field outside that plates that curves from one to the other. This caused the microstrip patch to be larger.

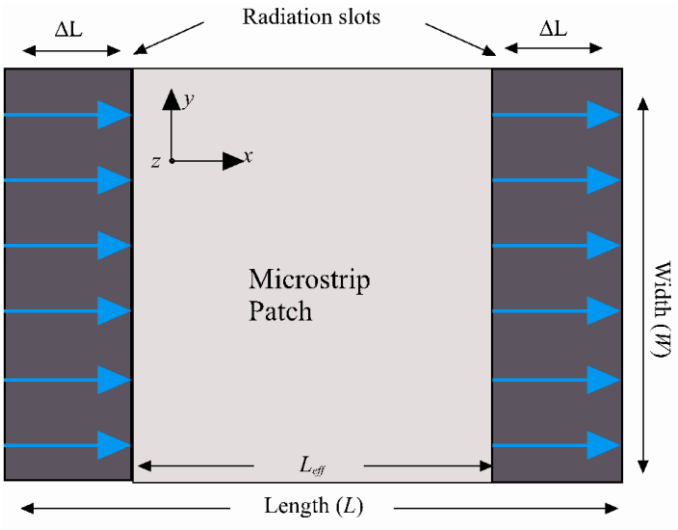

Figure 3.10. Fundamental TM_{10} mode

From Figure 3.10, the normal components of the electric field at the two edges along the width are in opposite directions and thus out of phase since the patch is λ/2 long and hence they cancel each other in the broadside direction. The tangential components, which are in phase, mean that the resulting fields combine to give maximum radiated field normal to the surface of the structure. Hence the edges along the width can be represented as two radiating slots, which are λ/2 apart and excited in phase and radiating in the half space above the ground plane. The fringing fields along the width can be modeled as radiating slots and electrically the patch of the microstrip antenna looks greater than its physical dimensions. The dimensions of the patch along its length have

now been extended on each end by a distance ΔL, which is given empirically by Hammerstad [58] as:

$$\Delta L = 0.412h \frac{\left(\varepsilon_{reff} + 0.3\right)\left(\frac{W}{h} + 0.264\right)}{\left(\varepsilon_{reff} - 0.258\right)\left(\frac{W}{h} + 0.8\right)} \quad \textbf{3.14}$$

As shown in following figure, Figure 3.9, the effective length L_{eff} of the patch:

$$L_{eff} = L + 2\Delta L \quad \textbf{3.15}$$

3.3 Overview of the rectangular patch parameters

In this section, we will discuss the overview of the patch antenna design parameters of the rectangular patch antenna. For designing a perfect antenna there are certain parameters that are to be considered that define the configuration of the antenna.

3.3.1 Return loss

In telecommunications, return loss is the loss of signal power resulting from the reflection caused at a discontinuity in a transmission line. This discontinuity can be a mismatch with the terminating load or with a device inserted in the line. The return loss is related to both standing wave ratio (VSWR) and reflection coefficient (Γ). The increase of return loss corresponds to lower VSWR. An ideal transmission line would have a VSWR of 1:1, with all the power reaching the destination and no reflected power. As for the reflection coefficient (Γ), it is the ratio of the amplitude of the reflected wave (V_0^-) to the amplitude of the incident wave (V_0^+).

In another word, return loss is the measurement of how well devices or lines are matched and a match is good if the return loss is high. A high return loss is desirable and results in a lower insertion loss. Using return loss we can provide the best and most convenient method to calculate the input and output of the signal sources. The Return Loss is determined in dB as follows [59]:

$$RL(dB) = -20\log|\Gamma| \qquad \textbf{3.16}$$

where;

$$|\Gamma| = \frac{V_0^-}{V_0^+} = \frac{Z_L - Z_0}{Z_L + Z_0} \qquad \textbf{3.17}$$

here; $|\Gamma|$ is the reflection coefficient

V_0^+ is the incident wave

V_0^- is the reflected wave

Z_L & Z_0 are the load and characteristic impedances

During the development of designing the rectangular patch antenna there is a response taken from the magnitude of S11 parameter versus frequency. This is known as the return loss. To have a perfect matching between the antenna and the transmitter, Γ= 0 and RL = ∞, this indicates that there is no power that is returned or reflected but when Γ= 0 and RL = 0 dB, this indicated that the power that is sent is all reflected back. It is said that for the practical applications *VSWR* = 2 is acceptable as the return loss would be -9.54dB [8].

3.3.2 Radiation patterns

The radiation pattern is the mathematical representation of the antenna as a function of space coordinates. It is determined in the far field region and is represented as a function of the directional coordinates. Using the "electric current model" or a "magnetic current model", we can resolve the radiation field of the microstrip antenna. Usually, the current is used directly to find the far-field radiation pattern.

Figure 3.11(a) shows the electric current for the (1, 0) patch mode. If the substrate is neglected (replaced by air) for the calculation of the radiation pattern, the pattern may be found directly from image theory. If the substrate is accounted for, and is assumed infinite, the reciprocity method may be used to determine the far-field pattern [9]. In the magnetic current model, the equivalence principle is used to replace the patch by a magnetic surface current that flows on the perimeter of the patch. Figure 3.11(b) shows the magnetic current for the (1, 0) patch mode. The magnetic surface current is given by the following:

$$\vec{M}_s = -\hat{n} \times \vec{E} \qquad \textbf{3.18}$$

Where, $\hat{n}$ is the outward pointing unit-normal vector at the patch boundary, and $\vec{E}$ is the electric field of the cavity mode at the edge of the patch.

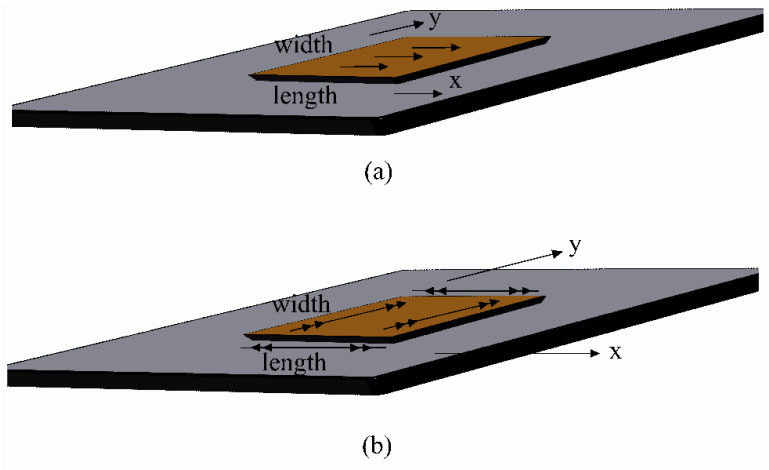

Figure 3.11. (a) Electrical current for (1, 0) patch;

(b) Magnetic current for (1, 0) patch

The far-field pattern can be determined by image theory or reciprocity, depending on whether the substrate is neglected or not. The dominant part of the radiation field comes from the "radiating edges" at $x = 0$ and $x = L$. The two non-radiating edges do not affect the pattern in the principle planes (the E plane at $\varphi = 0$ and the H plane at $\varphi = \pi/2$), and have a small effect for other planes. It can be shown that the electric and magnetic current models yield exactly the same result for the far-field pattern, provided the pattern of each current is calculated in the presence of the substrate at the resonant frequency of the patch [9].

In another word, radiation pattern is defined as the power radiated or received by an antenna in a function of the angular position and radial distance from the antenna. It describes how an antenna directs the energy it radiates. The following is a radiation pattern, Figure 3.12, of a generic dimensional antenna, which consist of main lobe, side

lobes, and black lobes. Side and back lobes are undesirable as they represent the energy that is wasted for transmitting antennas and noise sources at the receiving end.

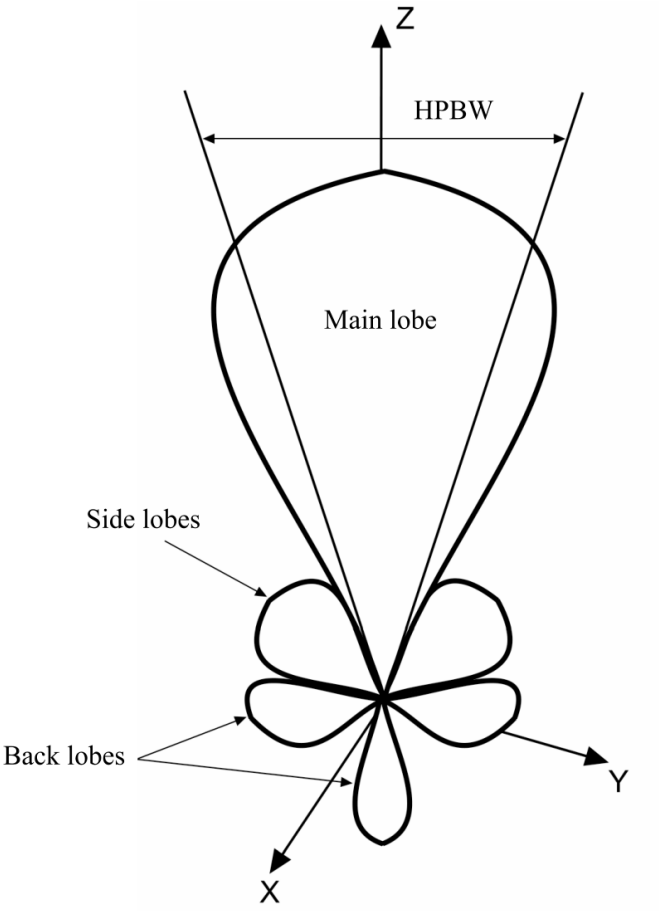

Figure 3.12. Radiation pattern of a generic directional antenna

i. Main lobe

This is the main radiation lobe that represents the maximum and direction of the antenna radiation

ii. Side and back lobes

Basically, all the lobes other than the main lobe called minor lobes. Those lobes are undesirable and the level of minor lobes is usually expressed as a ratio of the power density in the lobe in question to that of the major lobe. In detailed, the side lobes are the

largest in the minor lobes and they have a big affect on the antenna main radiation. Whereas the back lobe, it is generally one of the minor lobes diametrically opposite to the main lobe.

iii. HPBW

HPBW is the half power beamwidth of the main lobe radiation of the antenna. It can be defined as the angle subtended by the half power points of the main lobe. In plane containing the direction of the maximum of a beam, the angle between the directions in which the radiation intensity is one half the maximum value of the beam.

3.3.3 Gain & directivity

The gain of an antenna is a measure of the capability to deliberate power into a constricted angular region of space. It describes the performance of the antenna to concentrate energy through a direction to give a better picture of the radiation performance. This is expressed in dB, in a simple way we can say that this refers to the direction of the maximum radiation [60]. Gain of the rectangular patch antenna can be expressed as following:

$$G = \eta \times D \qquad \textbf{3.19}$$

where η is the radiation efficiency and D is the directivity of the patch antenna.

The directivity of an antenna is defined as the ratio of the radiation intensity in a given direction from the antenna to the radiation intensity averaged over all directions. The ratio between the amounts of energy propagated in these directions compared to the energy that would be propagated if the antenna were omni-directional is known as its gain.

In Figure 3.12, the directivity of the antenna depends on the shape of the radiation pattern. The measurement is done taking a reference of isotropic point source from the response. The quantitative measure of this response is known as the directive gain for the antenna on a given direction. It is determined by the array factor described as [4]:

$$AF = \sum_{n=1}^{N} e^{j(n-1)\Psi} \quad \textbf{3.20}$$

where;

$$\Psi = kd\cos\theta + \beta \quad \textbf{3.21}$$

N is the number of elements. As the number of elements *N* increases, the beam becomes narrower and more directional.

3.3.4 Bandwidth

An antenna's bandwidth specifies the range of frequencies over which its performance does not suffer due a poor impedance match. Primarily, the term bandwidth refers to the frequency span from the lowest to highest frequency of an allocated service area. As a general rule, the higher the frequency, the broader the bandwidth will be for a given antenna design. Likewise, the lower the frequency, the more difficult it is to design antennas with sufficient bandwidth [61].

$$BW_{broadband} = \frac{f_H}{f_L} \quad \textbf{3.22}$$

$$BW_{narrowband}(\%) = \left[\frac{f_H - f_L}{f_C}\right] \times 100 \quad \textbf{3.23}$$

A good method of evaluating how efficiently an antenna is operating is by measuring its VSWR. A VSWR ≤ 2 (RL $\geq$ -9.5dB) ensures good performance.

3.3.5 Input impedance

There are several and different models to calculate input impedance for inset fed patch antenna, as we mentioned in the previous chapter, the most popular methods are transmission line and cavity models. The mentioned models are compatible with very thin substrates, typically giving reliable results for $h / \lambda_0 < 0.02$. Microstrip patch antennas represent one type of antenna family that provides integration capabilities for a given communication application. Using the transmission line model, it is possible to model and analyze inset fed patch antenna designs. It is also possible to locate the accurate inset length needed for given 50 Ω input impedance.

There are various techniques to feed microstrip patch antenna. Coaxial probe feeding is the most popular method in these types of antennas but for our application we were looking for a feeding technique that goes on the same level as the patch antenna. For that reason, we decided to go with microstrip line feed and in particularly the inset fed. It is suitable for developing high-gain microstrip array antennas and it goes along the same level of the patch antenna. In both cases, the probe position or the inset length determines the input impedance.

The input impedance behavior for the inset fed patch antenna has been studied analytically in various models, including the transmission line model and the cavity model, and by means of full-wave analysis. It has been found that this feeding technique exhibits behavior that follows the trigonometric function [62]:

$$R_{in}(y = y_0) = R_{in}(y = 0)\cos^2(\pi y_0 / L) \quad \textbf{3.24}$$

$$R_{in(y=0)} = \frac{1}{2(G_1 + G_{12})} \quad \textbf{3.25}$$

Where, L is the length of the patch and y_0 is the position of the feed from the edge along the direction of the patch length.

To find the input impedance, a simple approach has been developed using the transmission line model. This approach can be derived to find the inset length to achieve 50 Ω input impedance when using modern thin dielectric materials. Figure 3.13, is a graphical depiction of an inset fed microstrip patch antenna.

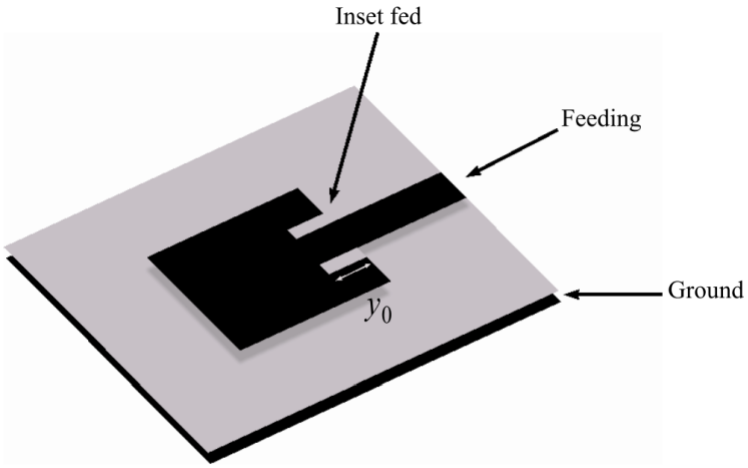

Figure 3.13. Inset fed patch antenna

The input impedance of an inset fed microstrip patch antenna depends mainly on the inset distance, y_0, and on the inset width which is the spacing between the feed line and the patch conductor. Variations in the inset length do not produce any change in

resonant frequency, but a variation in the inset width will result in a change in resonant frequency.

3.3.6 Polarization

The polarization of an antenna is the polarization of the radiated fields produced by an antenna, evaluated in the far field. It is defined as "the property of an electromagnetic wave describing the time varying direction and relative magnitude of the electric filed vector" [57]. In another word, polarization is the electric field vector of the radiated wave versus time of the orientation of the electric fields.

A linear polarized antenna radiates entirely in one plane containing the direction of propagation. In a circular polarized antenna, the plane of polarization rotates in a circle making one complete revolution during one period of the wave.

Figure 3.14 shows a linearly polarized wave. As illustrated, in a circularly polarized wave, the electric field vector remains constant in length but rotates around in a circular path.

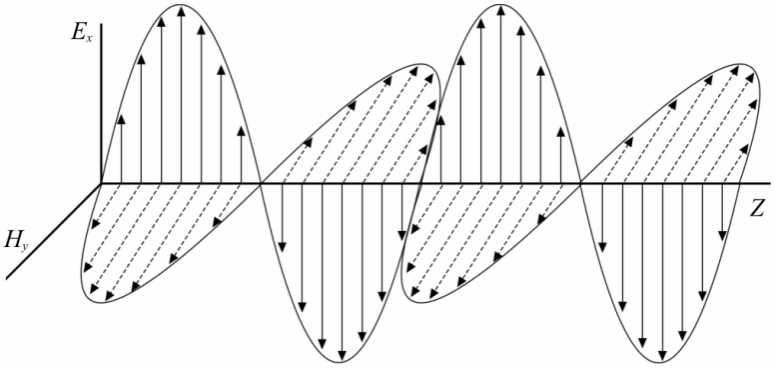

Figure 3.14. Linear polarized wave

In Figure 3.15, the vertical linear polarization is shown in (a) whereas in Figure 3.15(b) the horizontal linear polarization is presented. In 3.15 (c) a right hand circular

polarization and Figure 3.15(d) is the left hand circular polarization is illustrated. The left hand circular polarized wave is one in which the wave rotates counter clockwise whereas right hand circular polarized wave exhibits clockwise motion.

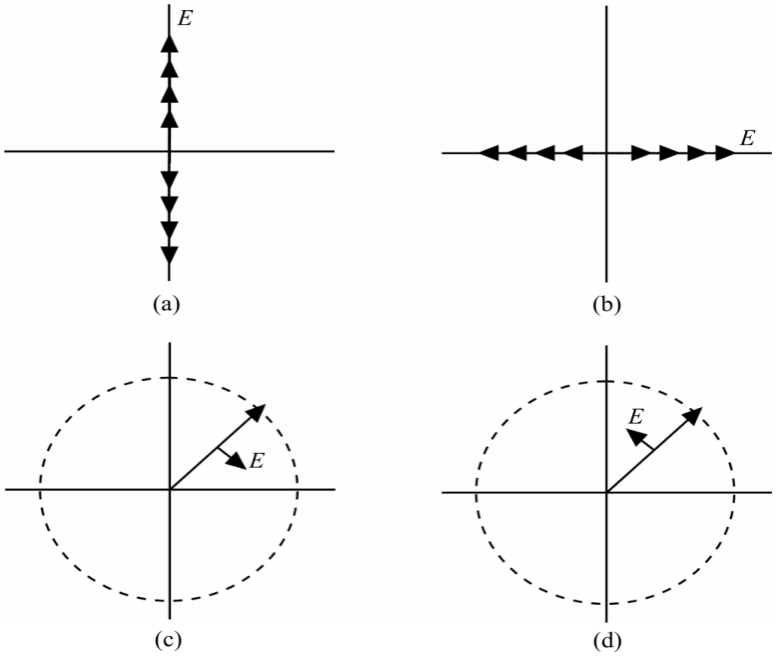

Figure 3.15. General polarization schemes

3.4 Antenna array

Antenna array or phased array is a set of antennas combined together to enhanced performance over that of a single antenna. Using a single patch antenna provide limited radiation pattern. However, if we joint multiple patch antennas "array", this will improve our radiation and will offer us flexibility to control the radiation. The main advantages of the antenna array are as follows:

- Increases the gain and performance of the whole antenna.
- Improves direction for the outgoing and incoming signals.
- Cancels undesired signals can be generated with different patch locations.

- Manoeuvres the antenna on a particular direction by reducing the beamwidth of the mainlobe.

3.4.1 Linear antenna array

Linear antenna array is geometrically structured in lines. The elements of the array are placed on the y- axis with a uniform spacing *d*. The actual radiation pattern of the linear antenna array is the magnitude of the product of the array factor and the element field [10].

$$AF = 1 + e^{j\psi} + e^{j2\psi} \_ e^{j3\psi} + ... + e^{j(N-1)\psi} \quad \textbf{3.26}$$

$$E_a(q) = \sum_{n=0}^{N-1} a_n e^{j(\psi_n + nkd\sin\theta)} \quad \textbf{3.27}$$

where;

$$\psi_n = -nkd\sin\theta_0 \quad \textbf{3.28}$$

Advantages:

- Linear array antenna is simple and easy to design.
- Improves antenna radiation pattern

Disadvantages:

- Linear antenna array can only scan the main beam in one polar plane (φ or θ)

The general form of an antenna array can be illustrated in below figure, Figure 3.16.

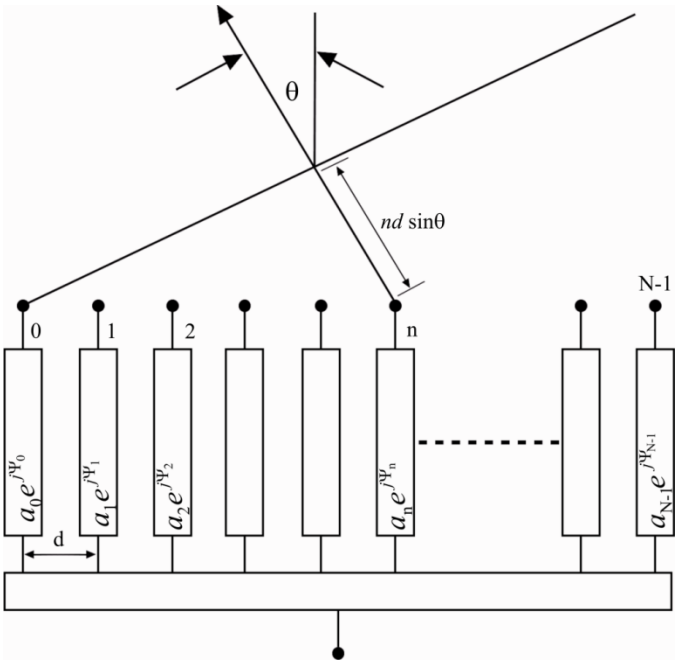

Figure 3.16. Linear antenna array

3.4.2 Planar antenna array

Planar array antenna is an antenna in which all of the elements, both active and parasitic, are in one plane. Since the elements are placed in two dimensions the array factor of a planar array can be expressed as the multiplication of the array factors of two linear arrays: one along the *x*-axis and one along the *y*-axis as [10]:

$$AF_{planar} = (AF_x).(AF_y) \tag{3.29}$$

$$AF_n(\theta,\phi) = \left\{\frac{1}{M}\frac{\sin(\frac{M}{2}\psi_x)}{\sin(\frac{\psi_x}{2})}\right\}\left\{\frac{1}{N}\frac{\sin(\frac{N}{2}\psi_y)}{\sin(\frac{\psi_y}{2})}\right\} \tag{3.30}$$

here;

$$\psi_x = kd_x \sin\theta\cos\phi + \beta_x \quad \textbf{3.31}$$

$$\psi_y = kd_y \sin\theta\sin\phi + \beta_y \quad \textbf{3.32}$$

where; k presents the wave vector and β is the phase difference.

Advantages:

- Planar arrays provide a large aperture and may be used for directional beam control by varying the relative phase of each element. In another word, arrays scan the main beam along both φ and θ.
- Planar arrays offer more gain and lower sidelobes than linear arrays, at the expense of using more elements.
- The design principles for planar arrays are similar to those for the linear arrays.
- A planar array may be used with a reflecting screen behind the active plane.

Disadvantages:

- Planar arrays design is complicated
- This type of antennas required more electronically controlled phase shifters.

Figure 3.17 shows the planar antenna array. The antenna array becomes a rectangular one and by changing the delay, the progressive phase shift is switched along the x direction.

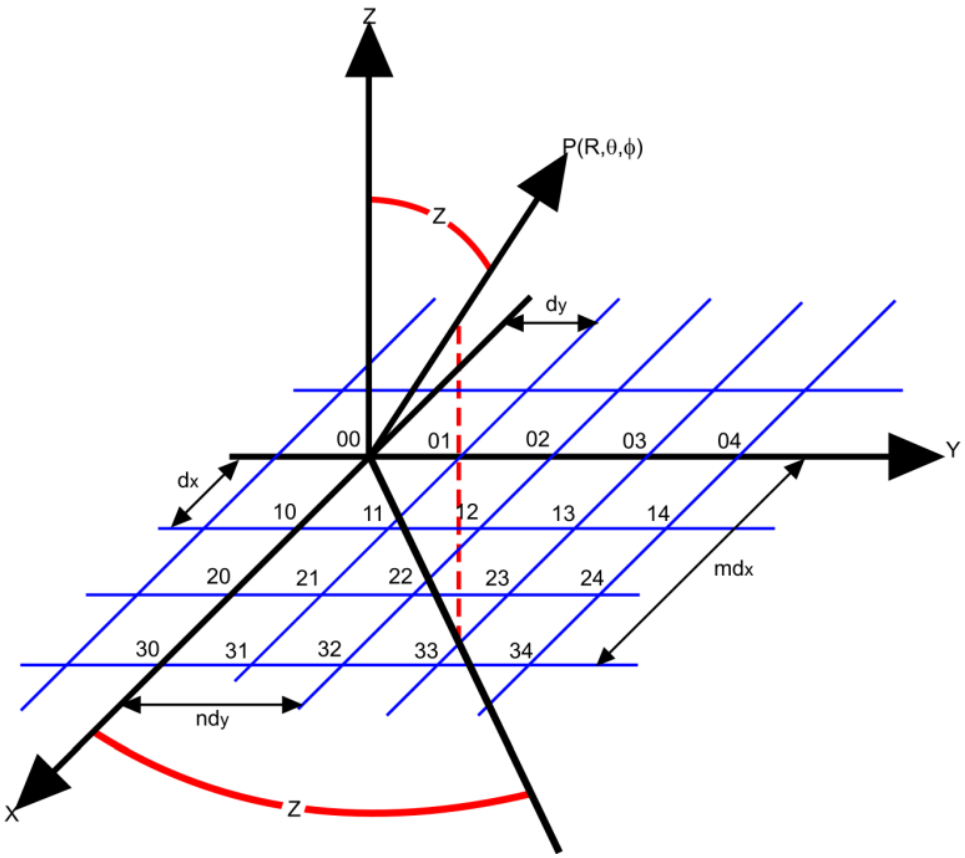

Figure 3.17. Planar antenna array

3.5 Microstrip antenna feed techniques

There are many techniques to feed the microstrip path. The four most popular feed techniques used are the microstrip line, coaxial probe (both contacting schemes), aperture coupling (non-contacting schemes).

In the contacting method, the RF power is fed directly to the radiating patch using a connecting element such as a microstrip line or a coaxial probe. In the non-contacting, electromagnetic field coupling is done to transfer power between the microstrip line and the radiating patch. The following figures, Figure 3.18, shows the most used types of microstrip antenna geometries.

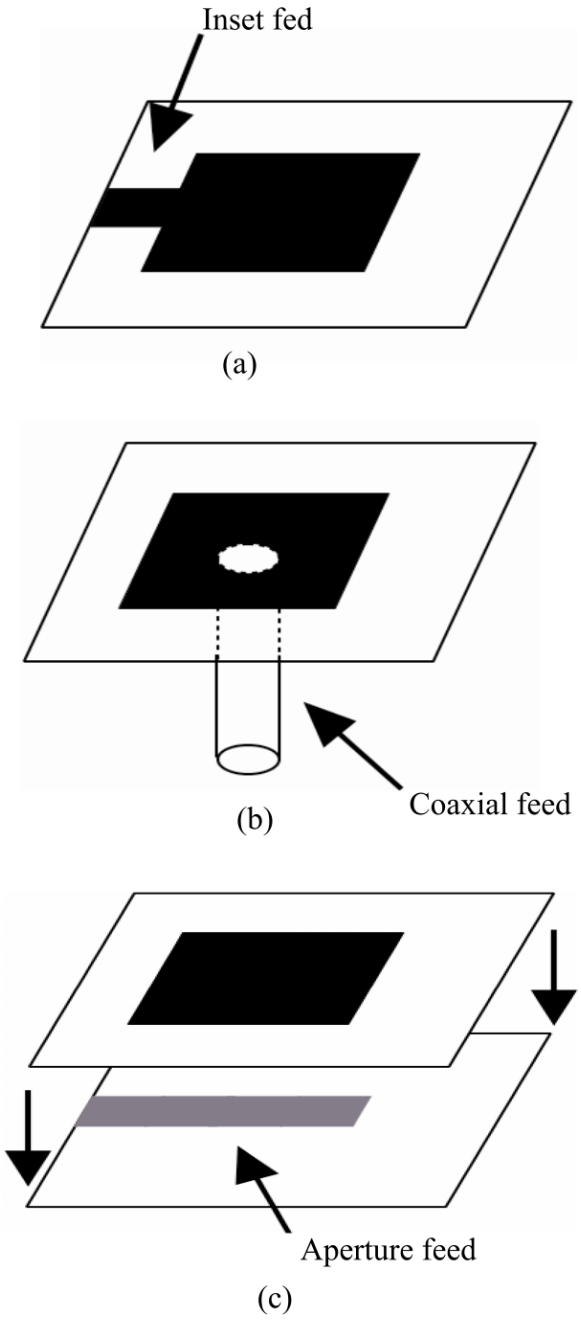

Figure 3.18. (a) Microstrip inset fed; (b) Coaxial probe; (c) Aperture feed line

The following table, Table 3.1, summarizes the characteristics of microstrip antenna feed techniques:

Table 3.1. Microstrip antenna feeding techniques comparison [9]

Characteristics	Microstrip Line feed	Coaxial Probe feed	Aperture Coupled feed
Spurious Feed Radiation	More	More	Less
Reliability	Better	Poor due to Soldering	Good
Ease of Fabrication	Easy	Soldering and Drilling is needed	Alignment Required
Impedance Matching	Easy	Easy	Easy
Bandwidth (Achieved with Impedance Matching)	2-5%	2-5%	2-5%

3.6 Summary

Microstrip patch antennas basically consist of a metallic patch on a grounded substrate. As explained in this chapter that the metallic patch geometry varies from one application to another. In Figure 3.2, a mixture of forms has been captured. However, the rectangular and circular patches are the most popular shapes because of ease of fabrication and analysis and their good radiation characteristics, especially low cross-polarization radiation.

CHAPTER IV

MICROMACHINED MICROSTRIP ANTENNA

Due to the fact that microstrip antennas can be planar or conformal, they are widely used in wireless communication applications. They can be fed in different techniques and also are compact and suitable for antenna array designs. One of the disadvantages of the microstrip antenna arrays is the excitation of surface waves in high dielectric constant substrates especially in cases where the bandwidth and the radiation efficiency demands large values of the substrate thickness. While high dielectric constant substrates provide the capability of small size circuits, micromachining techniques can locally synthesize a low dielectric antenna substrate [60] [63] [64] [65].

Micromachining of a high dielectric constant substrate, for example silicon, is a process where the semiconductor substrate is micromechanically altered, either by removing material from the substrate (bulk micromachining) or by adding layers and structures to the top of the wafer (surface micromachining) to modify the dielectric constant.

In this chapter, a detailed description of micromachined techniques to realize high performance antenna is provided.

4.1 Micromachining

As mentioned in chapter I, microstrip antennas on high dielectric substrates such as Silicon (Si) and Gallium arsenide (GaAs) experience degradation in performance. Silicon and Gallium based microstrip antennas suffer from low efficiency, narrow

bandwidth and poor radiation pattern due to surface waves. As a result, the antenna has undesired coupling between the various elements while used in array configuration.

From design prospective, microstrip antenna design requires the radiating patch to be printed on low-index material and the feeding network to be printed on the high-index material to ensure higher efficiency of the radiating patch and the feeding network. Consequently, the optimum antenna performance depends on the choice of the dielectric material as well as on the choice of the feeding network. This is achieved when radiated power occurs primarily as a space wave with little or no component of undesired surface waves. Table 4.1 compares performances of antennas built with a high index material (Silicon substrate, $\varepsilon_r = 11.8$) and a low index material (micromachined Silicon substrate, Synthesized Permittivity (ε_{synth}) = 1.85) :

Table 4.1. Comparison between high and low index materials

Parameter	Array on plain Silicon substrate	Array on micromachined Silicon substrate
Fabrication	batch fabricated	batch fabricated
Fabrication Cost	low cost	low cost
Efficiency	low	high
S11 Bandwidth	narrow	wide
Radiation pattern	degraded radiation patterns	elevated radiation patterns
Gain	Low	high
Directivity	Low	high

In order to get the best result and antenna performance, we have selected to work on high index material such as Silicon (ε_r= 11.8) and implement micromachining technique.

4.2 Bulk micromachining

There are various techniques to alter a substrate. Bulk micromachining refers to methods where parts of the wafer are selectively removed by etching processes. Two procedures are mainly used for bulk micromachining, chemical wet etching and dry etching. Usually silicon wafer is commonly used substrates for bulk micromachining because they can anisotropically wet etched, forming highly regular structures. Etching modes changes based on the specifications and requirements such as:

i. Isotropic etching

Isotropic etching, in semiconductor technology, removes material equally in all directions from a substrate via a chemical process using an etchant substance. The etchant substance could be a liquid that is corrosive or a chemically active ionized gas, known as plasma. The following figure, Figure 4.1, shows an example of wet chemically etched hole geometries which are commonly used in micromechanical devices.

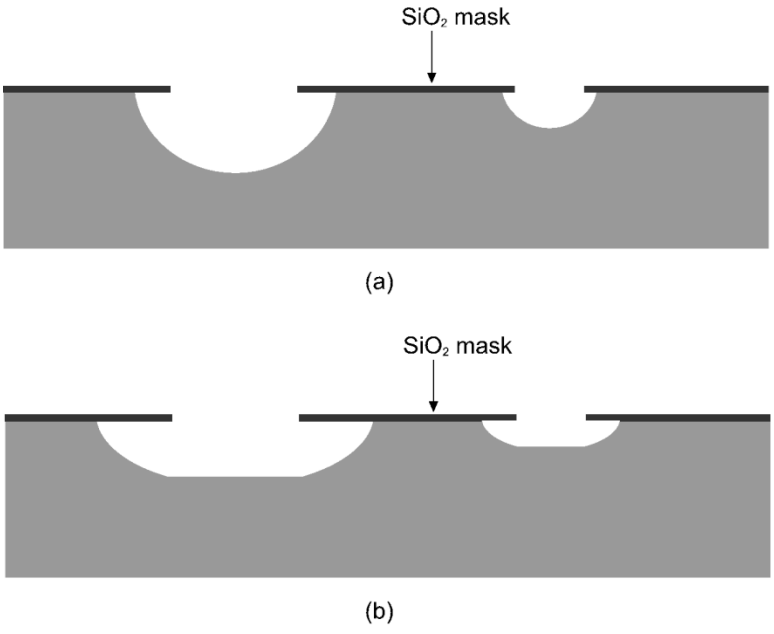

Figure 4.1. (a) Isotropic etching with agitation;

(b) Isotropic etching without agitation

ii. Anisotropic etching

Opposite to isotropic etching, anisotropic etches in certain directions faster than others and it is directionally dependent. Figure 4.2 presents two cases of different anisotropic etched geometries using wet chemicals.

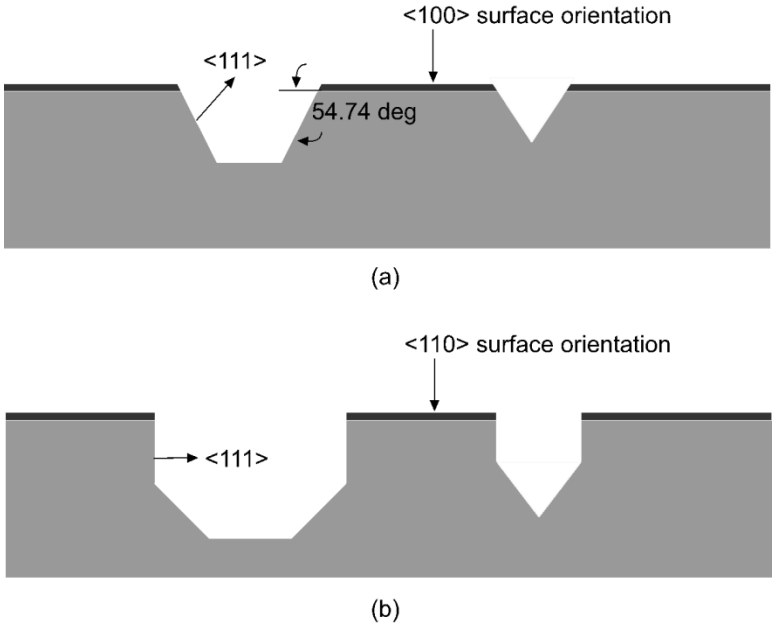

Figure 4.2. (a) Anisotropic etching on (100) surface;

(b) Anisotropic etching on (110) surface

4.3 Surface micromachining

Surface micromachining is another technology used for the fabrication of MEMS devices. Various ways of how surface micromachining is performed, depending on the materials and etchant combinations that are used. However, the common theme involves a sequence of steps starting with the deposition of thin film material as a temporary mechanical layer onto which the actual device layers are built; followed by the deposition and patterning of the thin film device layer of material which is referred to as the structural layer; then followed by the removal of the temporary layer to release the

mechanical structure layer from the constraint of the underlying layer, thereby allowing the structural layer to move. An illustration of a surface micromachining process is shown in Figure 4.3, wherein an oxide layer is deposited and patterned. This oxide layer is temporary and is commonly referred to as the sacrificial layer. Subsequently, a thin film layer of Polysilicon is deposited and patterned and this layer is the structural mechanical layer. Lastly, the temporary sacrificial layer is removed and the Polysilicon layer is now free to move as a cantilever.

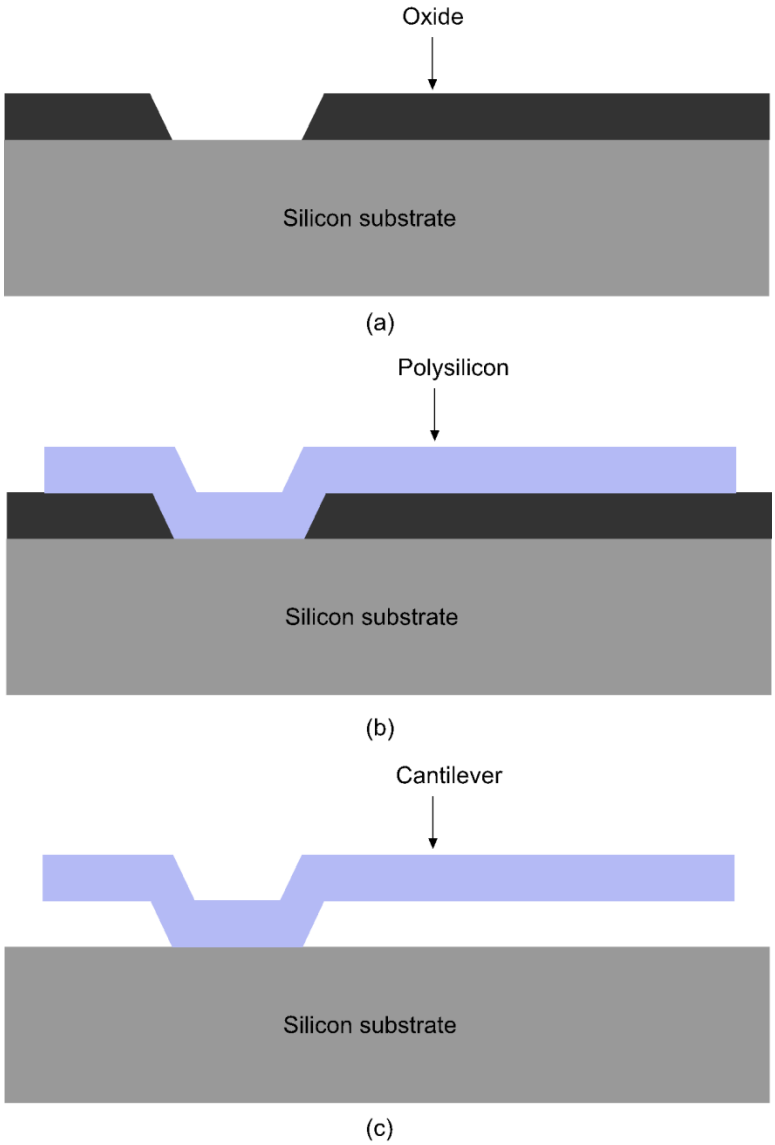

Figure 4.3. Illustration of a surface micromachining process

In this chapter, we will introduce a new approach that combines bulk and surface micromachining techniques to fabricate a microstrip antenna array. The approach is to etch away a series of rectangular air cavities under each of the antenna patches. The synthesized dialectic constant can be control with choice of the substrate and the air cavity thickness. This technique has a winning feature of compactness, which is an important feature in communication antenna applications. Using this technique, the suppression of surface wave propagation and the in-phase refection coefficients help to improve antenna's performance such as increasing the antenna gain, efficiency and reducing back radiation [66] [67].

4.3 Synthesized permittivity

Extensive research on MEMS over the past decade has contributed to new fabrication technologies for high performance millimeter-wave systems, including surface and the bulk micromachining. This design shows an improvement over conventional designs where the bandwidth and the efficiency increase by 50% and 25%. Table 4.2 presents a comparison between a high index antenna and a micromachined antenna fabricated on a GaAs substrate. The improvement of the antenna is clear and it provides better results:

Table 4.2. Micromachined solution on a GaAs (ε_r =12.9) with air cavity [10]

Important antenna parameters	Array on plain GaAs substrate	Array on micromachined GaAs substrate	Improvement
S_{11} bandwidth	887 MHz	1426 MHz	539 MHz
Directivity	9.2 d	12.6 d	3.4
Efficiency	63%	80%	17%
Gain	7.2 dB	11.6 dB	4.4
S21	-26.5 dB	-25.7 dB	-0.8

4.3.1 How micromachined substrates work

- The high-index material is removed laterally underneath the patch antenna to produce a cavity.
- This cavity consists of a combination of air and substrate with equal and unequal thicknesses and provides the low effective dielectric constant for the patch region.
- The below expression represent the synthesized dielectric constant of mixed regions [60]:

$$\varepsilon_{synthesized} = \left(\frac{h_{material}}{\varepsilon_{material}} \right) + \left(\frac{h_{air}}{\varepsilon_{air}} \right)^{-1} \times (h_{eq}) \qquad \textbf{4.1}$$

where;

$$h_{eq} = h_{material} + h_{air} \qquad \textbf{4.33}$$

The following figure, Figure 4.4, explain the geometry of the micromachined substrate that includes multiple layers:

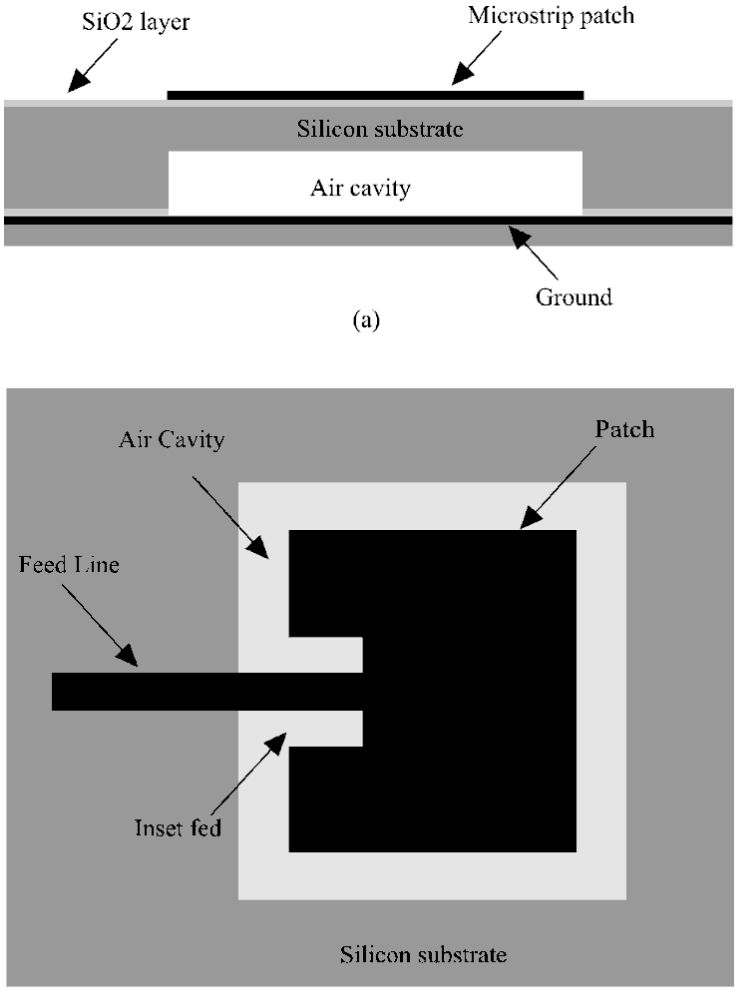

Figure 4.4. Micromachined patch antenna; (a) side view; (b) top view

4.4 Summary

Micromachining technique allows etching a cavity directly under the area of microstrip antenna, and then fills the cavity with lower permittivity materials, such as air or silicon dioxide. A metal layer is deposited between the low permittivity material and the silicon underneath. The thin layer of low permittivity substrate can reduce the loss and the excitation of surface waves. The tradeoff is that the very small thickness of this

layer makes the realization of practical bandwidths for this type of microstrip antennas very difficult. Finding the most efficient thickness, in term of fabrication feasibility and bandwidth of the antenna, is the most critical problem of these designs.

In order to achieve a compact microstrip patch antenna array, we incorporated micromachining techniques to design a 77 GHz microstrip antenna array. The advantages of implementing such technology result in high efficiency, wide bandwidth and good radiation pattern. Whereas the choosing of rectangular shape patch offers good directivity and simplicity in constructing. The gain of the selected patch antennas can be easily increased by adding higher number of elements. This structure made our work flexible and easy to manipulate.

CHAPTER V

ANTENNA ARRAY DESIGN, SIMULATION AND FABRICATION

In this chapter, detailed design of a 77 GHz reconfigurable micromachined microstrip antenna array for use in the target tri-mode automotive radar is presented. Design concepts and mathematical models as described in the previous chapters were used to determine the initial specifications. A full wave analysis using XFDTD™ has been carried out to optimize the geometry that resulted in further improvement of the performance parameters. A fabrication process table has been developed to fabricate the antenna array.

5.1 Microstrip antenna design specifications

The designed microstrip antenna array is basically a planar array of rectangular microstrip radiating patches. The antenna array is fed by the Rotman lens as shown in figure 2.5 in a corporate feed arrangement along one axis while along the other axis, the successive patches are series fed using microstrip feed lines. The phase alteration among the Rotman lens array ports of a signal input at a specific beam port will feed the antenna array with different time delays to steer the antenna beam in any of the specified directions. Control of the number of patches in each of series fed columns using switches will change the radar from short range to mid-range to long range by dynamically changing the array factor following (3.30). The antenna array is designed to operate at 77 GHz center frequency with sufficient bandwidth to support FMCW operation. To increase the efficiency and bandwidth, high resistivity float zone micromachined silicon substrate with dielectric constant 11.8 and a loss tangent (tan δ) of 0.0005 has been

selected to fabricate the antenna array. The height of substrate (h) has been chosen to be 500 μm. Part of the Silicon substrate beneath the patches was removed using Bosch™ Deep Reactive Ion Etching (DRIE) technique to create a rectangular cavity that reduces the effective dielectric constant of the substrate.

[60] has presented this approach to integrate patch antennas into circuit designs on high dielectric constant substrates without losing the advantages of low dielectric constant materials, the regions in the substrate, which will house the radiating elements must have low dielectric constant of refraction. This is achieved by using micromachining to eliminate a portion of the substrate material [25].

The Deep Reactive Ion Etching (DRIE) of Silicon has opened new fields of application in MEMS and device integration. Opposite to the wet anisotropic etching, the DRIE process, well-known as Bosch process, prevents lateral etching of the Si resulting in highly anisotropic etch profiles at high etch rates and with high aspect ratio compare to wet chemical etching. Figure 5.1 is an example of an etched silicon substrate using the DRIE process to create air cavity under the selected patch. By combining Silicon micromachining substrate and microstrip line feeding techniques, a highly efficient patch antenna can be made. A thick wafer is selected for the upper wafer to obtain good radiation characteristics where a cavity is opened underneath the patch. A thinner wafer is selected to hold the ground plane lines.

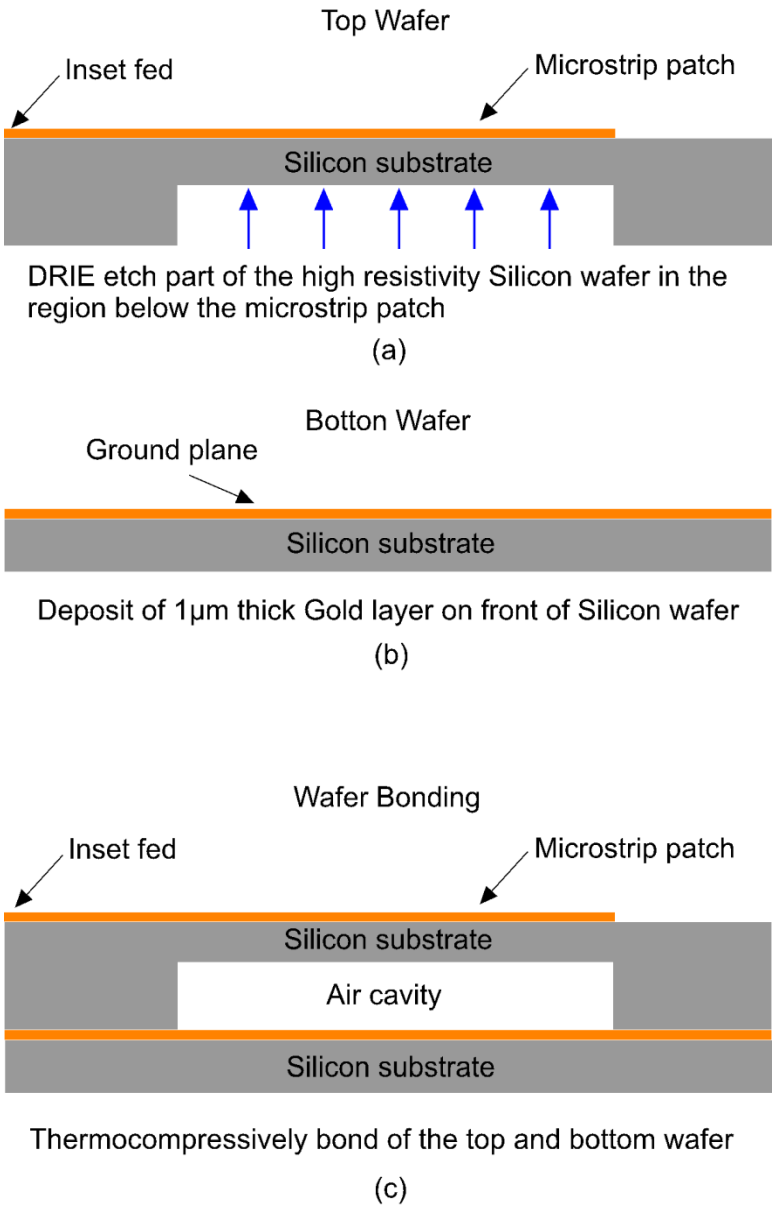

Figure 5.1. DRIE process or Bosch process, (a) top wafer DRIE etch part of the Silicon substrate, (b) bottom wafer topped with a ground plane, (c) Thermocompressively bond of the two wafers

An essential designing point that must be addressed is that for designing a high frequency patch antennas the requirements on the substrate are vastly different for the

radiating patch element and the feed-line. By using microstrip line between the patch and the feed-line, a high permittivity substrate could be chosen for the microstrip feed, while a substrate with a lower dielectric constant could be selected for the patch-antenna element.

5.2 Design procedure

In designing a micromachined rectangular patch microstrip antenna, the following formulas were implemented as an outline in designing procedures.

i. Synthesized dielectric constant

As mentioned in the previous chapter, the following expression represents the synthesized dielectric constant of mixed regions of air and silicon below the patch. To produce the mixed substrate region, silicon micromachining is used to laterally remove the material from underneath the specified cavity region resulting in two separate dielectric regions of air and silicon [60]:

$$\varepsilon_{synthesized} = \left(\frac{h_{material}}{\varepsilon_{material}} \right) + \left(\frac{h_{air}}{\varepsilon_{air}} \right)^{-1} \times (h_{eq}) \qquad \textbf{5.1}$$

Add a diagram that shows h_{material} and h_{air}.

where,

$$h_{eq} = h_{material} + h_{air} \qquad \textbf{5.2}$$

ii. Effective permittivity

An equivalent dielectric constant ε_{reff} needs to be calculated just like the microstrip line. This equivalent constant is used to replace the substrate and the surrounding air. It can be calculated as shown in following equation:

$$\varepsilon_{reff} = \frac{\varepsilon_r + 1}{2} + \frac{\varepsilon_r - 1}{2}\left[1 + 12\frac{h}{W}\right]^{-1/2} \qquad W/h > 1 \qquad \textbf{5.3}$$

where;

ε_r is the dielectric constant of the substrate, in our case the synthesized dielectric constant.

h is the height of the substrate.

W is the width of the patch.

iii. Patch width

For efficient radiation, the width of the patch W is given by [10] as:

$$W = \frac{c}{2f\sqrt{\frac{(\varepsilon_r + 1)}{2}}} \qquad \textbf{5.4}$$

where;

f is the operated frequency.

ε_r is the dielectric constant of the substrate, in our case the synthesized dielectric constant.

c is the free space velocity of light, which is $3\text{x}10^8$ m/s.

iv. Patch effective length

For a given resonance frequency f_0, the effective length is given by [10]:

$$L_{eff} = \frac{c}{\sqrt{\varepsilon_{reff}}}(1/2f) \quad \textbf{5.5}$$

where;

f is the operating frequency.

ε_{reff} is the effective dielectric constant.

c is the free space velocity of light, which is $3x10^8$ m/s.

v. Patch electrical length extension

Considering the fringing fields at the ends of the patch the electrical length of the element is longer than the physical length. Calculating the patch length extension (ΔL) can be determined using the following Hammerstad equation [10]:

$$\Delta L = 0.412h\frac{\left(\varepsilon_{reff}+0.3\right)\left(\frac{W}{h}+0.264\right)}{\left(\varepsilon_{reff}-0.258\right)\left(\frac{W}{h}+0.8\right)} \quad \textbf{5.6}$$

vi. Patch electrical length

As shown in Figure 3.4, the effective length L_{eff} of the patch [10]:

$$L_{eff} = L + 2\Delta L \quad \textbf{5.7}$$

5.3 Single patch design calculation

The essential parameters used for designing the rectangular microstrip patch antenna are listed in the following table, Table 5.1:

Table 5.1. Single patch calculation

Parameter Description	Value
Dielectric constant of Silicon (ε_r)	11.8
Silicon substrate loss tangent (tan δ)	0.0005
Height of Silicon substrate	500 μm
Air cavity length (L)	1.504 mm
Air cavity width (W)	1.90 mm
Air cavity thickness	250 μm

To integrate the microstrip patch antennas into circuit designs on high dielectric substrates (Silicon) without losing the advantages of low dielectric constant materials (air), the regions in the substrate, which will house the radiating elements, must have low refraction. This is achieved by using micromachining technique to eliminate a portion of the substrate material. The micromachined antenna configuration consists of a rectangular patch centered over the cavity, sized according to the effective cavity region, and fed by a microstrip line. To produce the mixed substrate region, silicon micromachining is used to laterally remove the material from underneath the specified cavity region resulting in two separate dielectric regions of air and silicon. In this work, the amount of silicon removed 50% of the original Silicon substrate thickness underneath the patch and a micromachined model was described in the previous chapter that provides the calculation of the synthesized permittivity for low dielectric constant environment for the patch.

XFDTD™ 3-D and MATLAB are used for simulation and design calculations of the microstrip antenna. The initial calculation of the microstrip antenna parameters was completed using MATLAB and with XFDTD™ 3-D full wave simulation software from Remcom™ the antenna is designed, simulated and optimized. Utilizing XFDTD™'s

parameter sweep feature, an increment within the antenna parameters was applied and simulated at every parameter change. The effectiveness of the design is confirmed through proper simulation results and the return loss, VSWR, Directivity, gain, radiation patter were evaluated at each parameter adjustment. Based on the best result, the antenna design parameters were selected. Table 5.2 presents the mathematical calculations of a single patch along with the optimized parameters.

Table 5.2. Single patch mathematical and optimized parameters

Parameter Description	Calculation	Optimization
Patch length (L)	1.24 mm	1.50 mm
Patch width (W)	1.63 mm	1.90 mm
Inset fed (Y_0)	0.41 mm	0.35 mm
Lambda (λ)	3.8961	Same
Half lambda ($\lambda/2$)	1.95	Same
Synthesized Permittivity (ε_{synth})	1.85	Same
Effective Permittivity (ε_{reff})	1.62	Same

5.4 Antenna array

As mentioned in the previous chapters, our designed is prepared for automotive radar application according to the coverage. Short range radar (SRR), medium range radar (MRR) and long range radar (LRR) are used in cruise control and collision avoidance. This section presents the simulation results of the three antenna arrays of our tri-mode radar.

Radars and antenna arrays come in various shapes and forms. The types of radars and antenna geometries are typically structured based on the purpose of the application. For short range radars, the main aspect is the range accuracy, while for mid-range and long-range radar systems the key performance parameter is the detection range. Short

range radar (range to tens meters) and mid-range radar systems (range from tens to forty meters) enable several applications such as blind-spot detection and pre-crash alerts [42]. It can also be used for implementation of "stop–and-go" applications in city traffic. Whereas, the long-range radar (hundreds of meters) is utilized in adaptive cruise-control systems. These systems can provide enough accuracy and resolution for even relatively high speeds (~120 mph).

The following table, Table 5.3, provides some of the radars along with the antenna arrays in use that are close to our design requirement. Based on these requirements, the SRR, MRR, and LRR antenna arrays were designed and fabricated.

Table 5.3. Different radars and antenna arrays

Year	Frequency	Radar	Antenna	Azimuth	Gain	BW
2005 [45]	76.5 GHz	SRR	Rectangular Microstrip (4x12)	±25.5°	17.8 dBi	1.0 GHz
2005 [45]	76.5 GHz	SRR	Rectangular Microstrip (2x12)	±39.3°	15.5 dBi	1.0 GHz
2010 [46]	34.5 GHz	SRR	Rectangular Microstrip (1x1)	60°	9.0 dBi	1.2 GHz
2005 [47]	122 GHz	SRR	Rectangular Microstrip (1x1)	90°	3.2 dBi	2.0 GHz
2004 [48]	24 GHz	MRR	Rectangular Microstrip (4x6)	±12°	N/P	500 MHz
2008 [49]	140 GHz	LRR	Rectangular Microstrip (2x4)	20°	12 dBi	2.0 GHz
2010 [50]	77 GHz	LRR	Rectangular Microstrip (8x8)	±9°	20 dBi	1.0 GHz

Derived from those requirements, the design of our reconfigurable antenna array was developed based on range capability. As for the number of array ports assigned to each of the antenna is founded on the number of output ports provided by the Rotman lens that radiates the signal in a specific direction.

For the target automotive radar, the lens center frequency has been selected as 77 GHz. As the lens would be used in tri-mode FMCW radar, the lens bandwidth has been selected to be 8 GHz to match with the maximum chirp bandwidth of the FMCW signal. Number of beam ports has been chosen as 3 at three perfect focal points and the number of array ports has been chosen to be 5 to minimize the lens width.

In this project, we have designed and fabricated a micromachined microstrip antenna array on 77 GHz frequency. The antenna consists of five arrays since our design is intended to work with Rotman lens of five array ports that realizes the directional beams without any microelectronic signal processing. Figure 5.2 explains the general system concept of the design that includes the major components Rotman lens, MEMS SPST RF switches, and the micromachined microstrip antenna array.

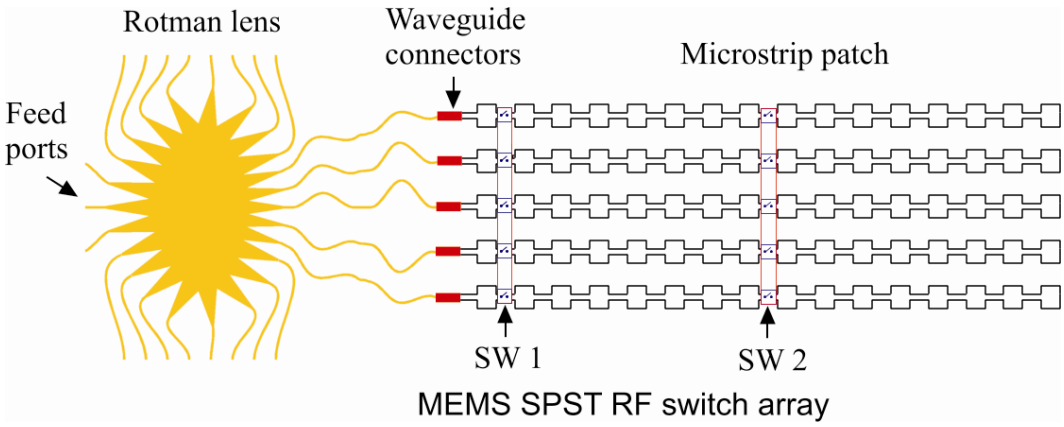

Figure 5.2. System concept of Rotman Lens, antenna array and switches

The above figure, illustrates the antenna arrays designed to work with Rotman lens. The MEMS based Rotman lens and RF switches combination central to this thesis can be used in conjunction with a reconfigurable patch antenna array in order to

accomplish SRR, MRR and LRR beamforming using the same hardware. The control of such a system would be easily realizable digitally by means of the FPGA control algorithm.

5.4.1 Short range antenna array

After finding the actual dimensions of the patch, the desired short range antenna array is designed. After calculation and optimization using XFDTD™ 3-D for the desired output the parameters is given in following table, Table 5.4:

Table 5.4. Short range antenna array parameters

SRR Parameter	Value
SRR array antenna	5 x 1
SRR length (L)	3.35 mm
SRR width (W)	11.49 mm
Frequency (f)	77 GHz
Silicon Substrate thickness	500 μm
SiO_2 layer thickness (top)	1.5 μm
SiO_2 layer thickness (bottom)	1.5 μm
Copper patches layer (Cu)	0.5 μm
Gold ground layer (Au)	0.5 μm
Array Element Spacing	2.4 mm

Short range antenna was designed based on the above parameters and the spacing between the elements from the centre of the feed point to the other center of the feed point is based on the Rotman lens array ports spacing (2.4mm) as shown the following figure:

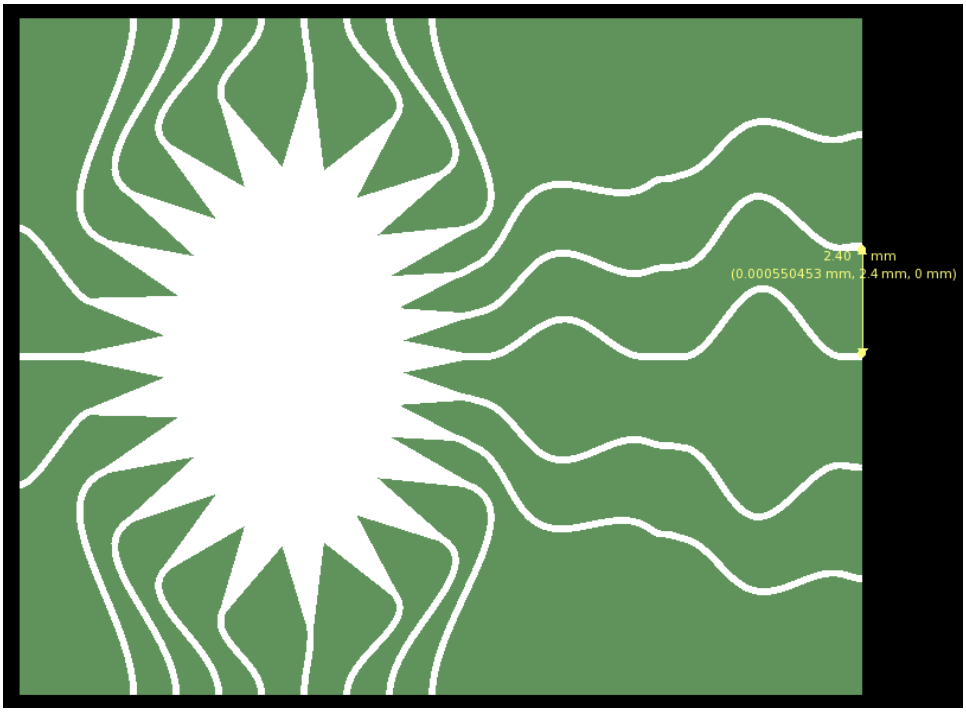

Figure 5.3. (3 beam ports, 5 array ports, and 16 dummy ports) Rotman Lens

The size of the short range antenna array was determined to be 5 x 1 following the short range radar specifications. The analysis and the optimization were carried using XFDTD™ 3-D full wave simulation software from Remcom™. In another word, a sweep parameter was applied on the SRR to generate a good radiation pattern that falls in the short range automotive requirements. Figure 5.4 shows a top and a 3D view of the design from XFDTD™.

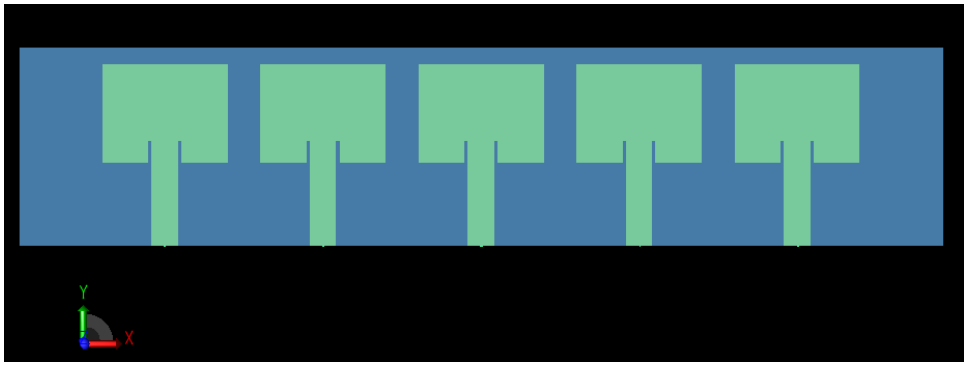

(a)

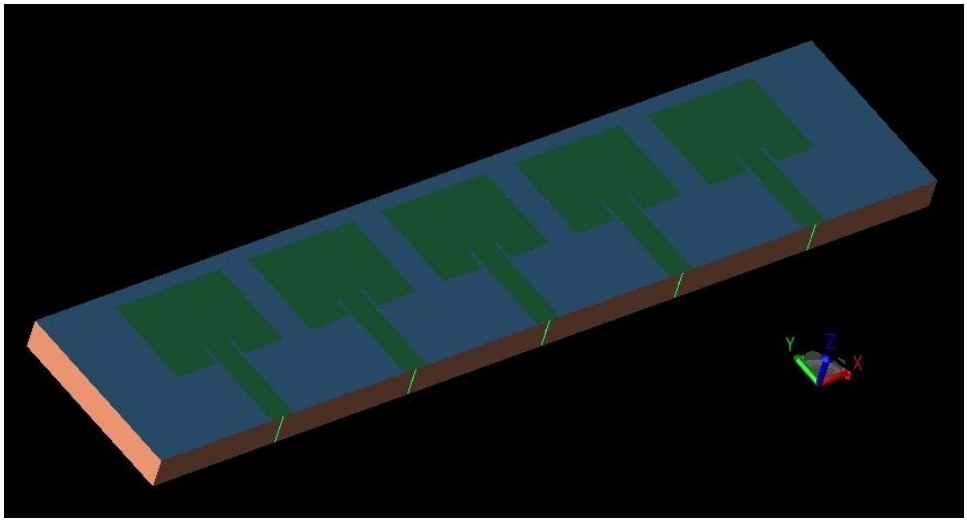

(b)

Figure 5.4. 3D view of the SRR design from XFDTD™(a) top view (b) 3D view

The Half Power Beamwidth (HPBW) is the angular separation in which the magnitude of the radiation pattern decreased by -3 dB from the peak of the main beam. Figure 5.5 illustrates the Azimuth and Elevation angular coverage, at -3 dB, the value shown is 5.8 dBi for the short range antenna. Thus, the half-power beamwidth for the SRR is 40 degrees.

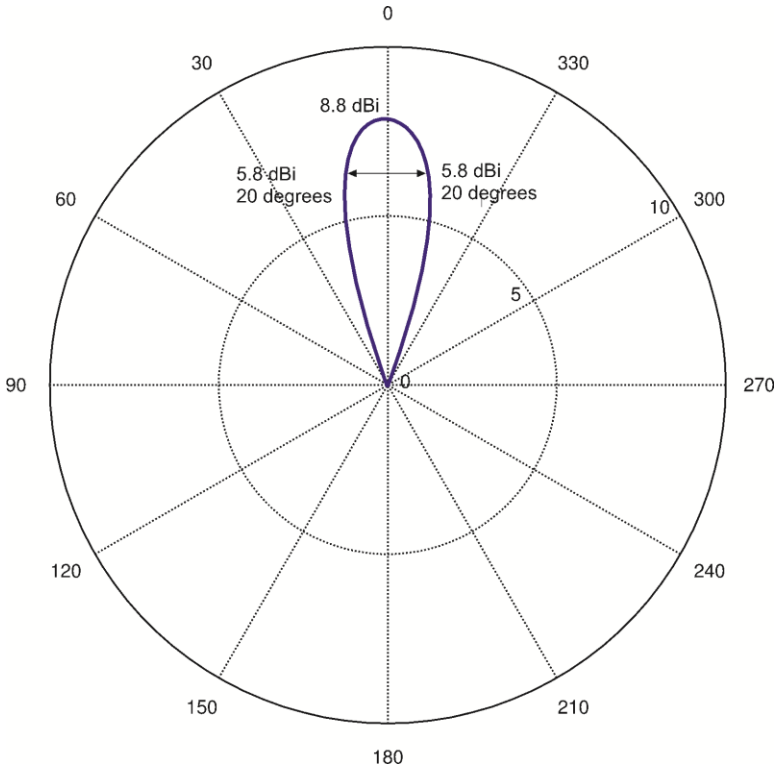

(a)

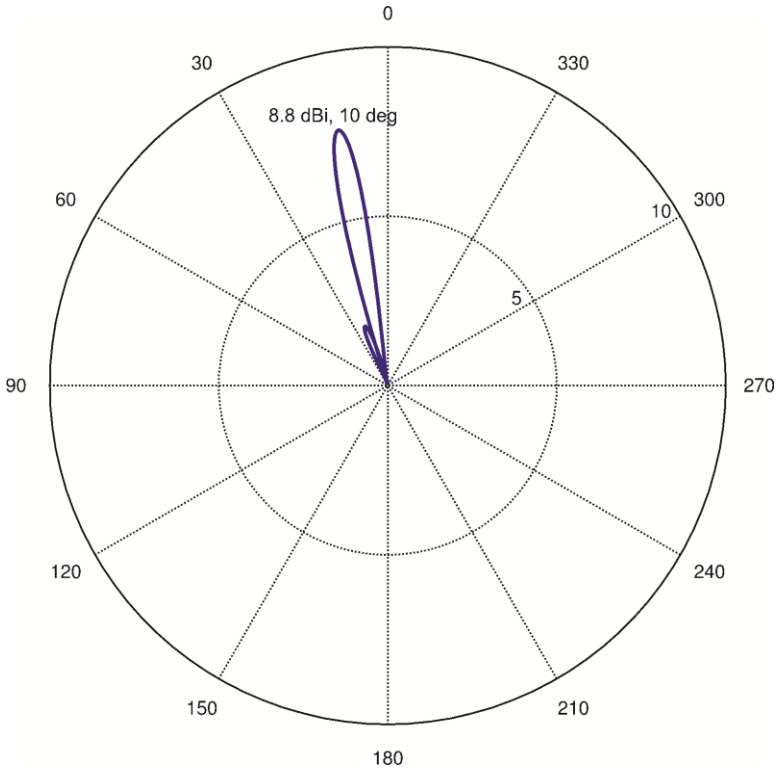

(b)

Figure 5.5. SRR maximum radiation occurs at gain of 8.8 dBi, (a) Azimuth angle, (b) Elevation angle

whereas the term elevation is referred to the vertical plane pattern. When used to describe antenna patterns, these terms assume that the antenna is mounted in the orientation in which it will be used.

The bandwidth was taken S11 parameter at –10dB. The bandwidth of simulated results is 1.2 GHz for the SRR as shown in Figure 5.6.

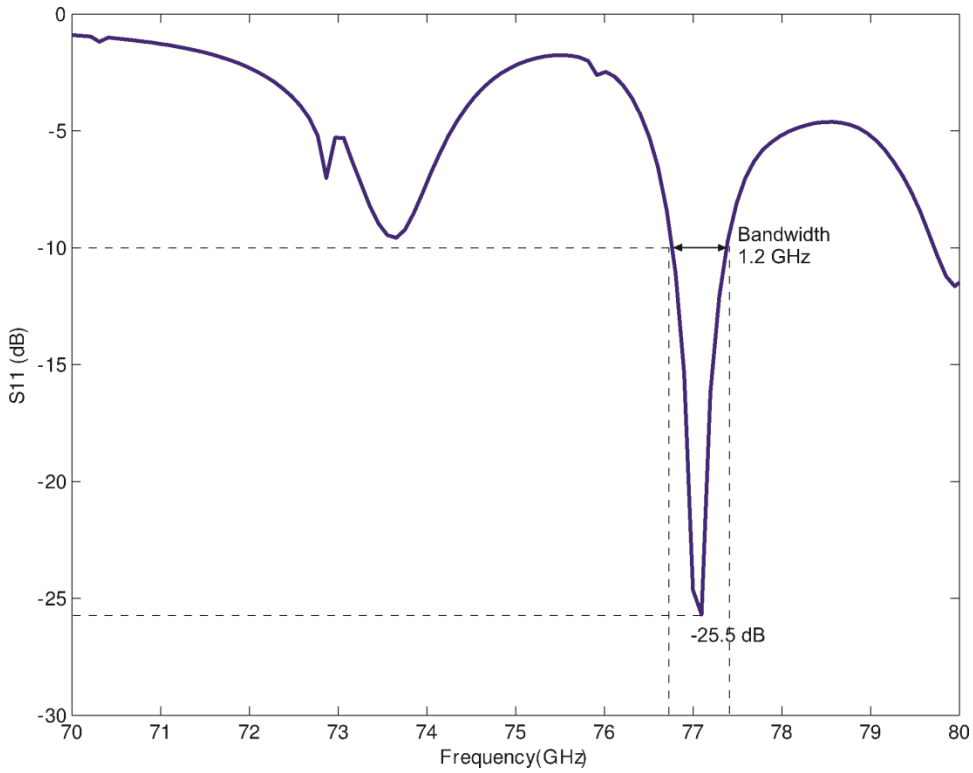

Figure 5.6. SRR S11 parameter is -25.5 dB

VSWR stands for voltage standing wave radio. It is the ratio of power that is reflected back down the antenna lead from the antenna. The follwoing figure, Figure 5.7, shows the VSWR of the SRR antenna array is 1.2. The value of VSWR for SRR is less than 2 at the operating frequency. This is considered a good value, as the level of mismatch is not very high.

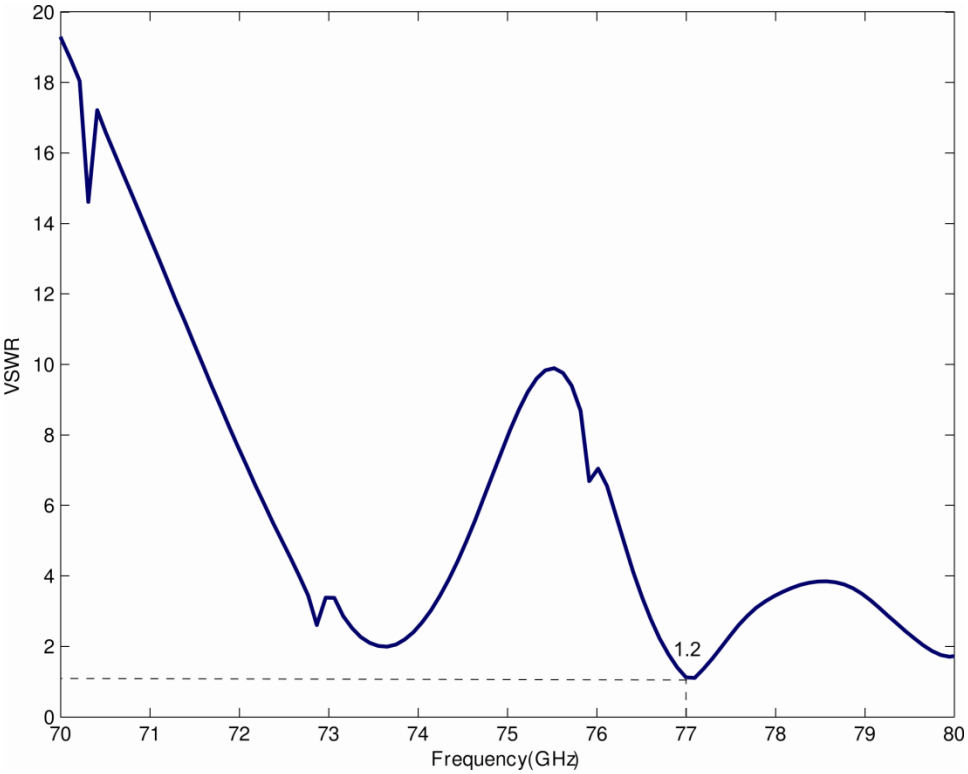

Figure 5.7. SRR VSWR is 1.2

XFDTD™ 3-D full wave simulation software from Remcom™ is the market's most modern 3D electromagnetic simulation software for modeling and EM simulation. It simplifies the workflow with an overall focus on the iterative nature of the design process. This software provides us with time and frequency domain simulation that is close to the real world application. The following figure, Figure 5.8, is a SRR radiation 3D model generated by XFDTD™ simulation software:

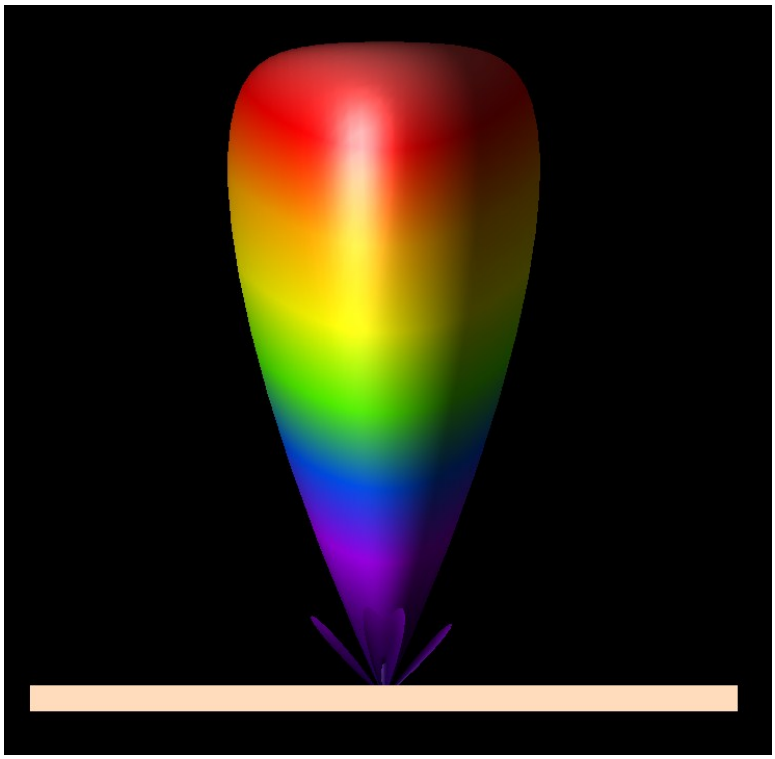

Figure 5.8. XFDTD™ SRR radiation pattern

The above antenna array elements are separated almost by one-half of the wavelength and are radiating in-phase, that is, when one patch is at the positive peak, the other is also at a positive peak. This type of array is called a "broadside array" because most of the radiation is in the direction that is broadside to the line of the antenna array.

Table 5.5 summarizes the fundamental results of the short range array antenna (1x2) designed for this project. As mentioned earlier, based on the short range requirements it is necessary to have wide angular beamwidth coverage (40 degrees) along with a good antenna gain (8.8 dBi).

Table 5.5. SRR summary table

Parameters	Value
Gain	8.8 dBi
Azimuth angle	0°
Elevation angle	10°
-3dB Beamwidth (HPBW)	40°
S11 Parameter (return loss)	-25.5 dB
Bandwidth	1.2 GHz
Radiation Efficiency	97 %
VSWR	1.2

5.4.2 Mid-range antenna array

Following the SRR procedure, to develop the MRR, a number of patches were added to meet the mid-range radar specifications. Using XFDTD™ 3-D software, the mid range antenna array is designed, optimized and analyzed. The following table, Table 5.6, shows the detailed dimensions of the MRR developed for this project:

Table 5.6. Mid-range antenna array parameters

MRR Parameter	Value
MRR array antenna	5 x 8
MRR length (L)	18.65 mm
MRR width (W)	11.49 mm
Frequency (f)	77 GHz
Silicon Substrate thickness	500 μm
SiO_2 layer thickness (top)	1.5 μm
SiO_2 layer thickness (bottom)	1.5 μm
Copper patches layer (Cu)	0.5 μm
Gold ground layer (Au)	0.5 μm
Array Element Spacing	2.4 mm

The mid-range antenna array was designed based on the above parameters listed. Following the short range, the spacing between the elements is 2.4mm based on the Rotman lens array ports spacing (2.4mm). The size of the antenna array is 5 x 8 and the

spacing between them was optimized and analyzed using XFDTD™ 3-D full wave simulation software from Remcom™. Figure 5.9 shows a top and a 3D view of the mid-range antenna radar design.

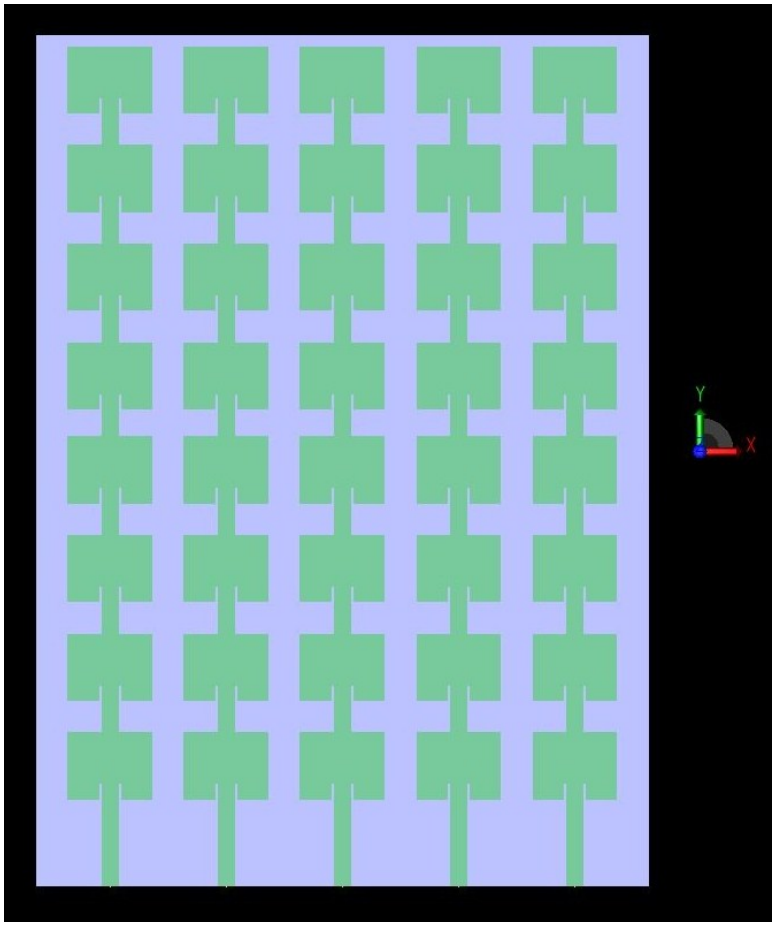

(a)

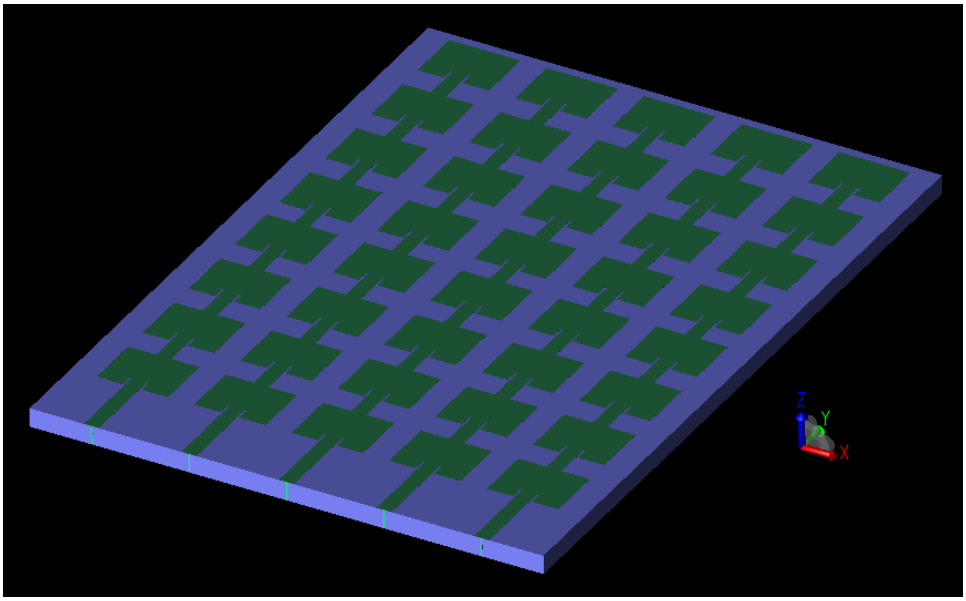

(b)

Figure 5.9. 3D view of the MRR design from XFDTD™(a) top view (b) 3D view

The figure below, Figure 5.10, at – 3 dB, the value shown is 12 dBi. Thus, the half-power beamwidth (HPBW) for the MRR is 26 degrees. As for the azimuth and elevation orientation, it was carried in coincide with the short range antenna.

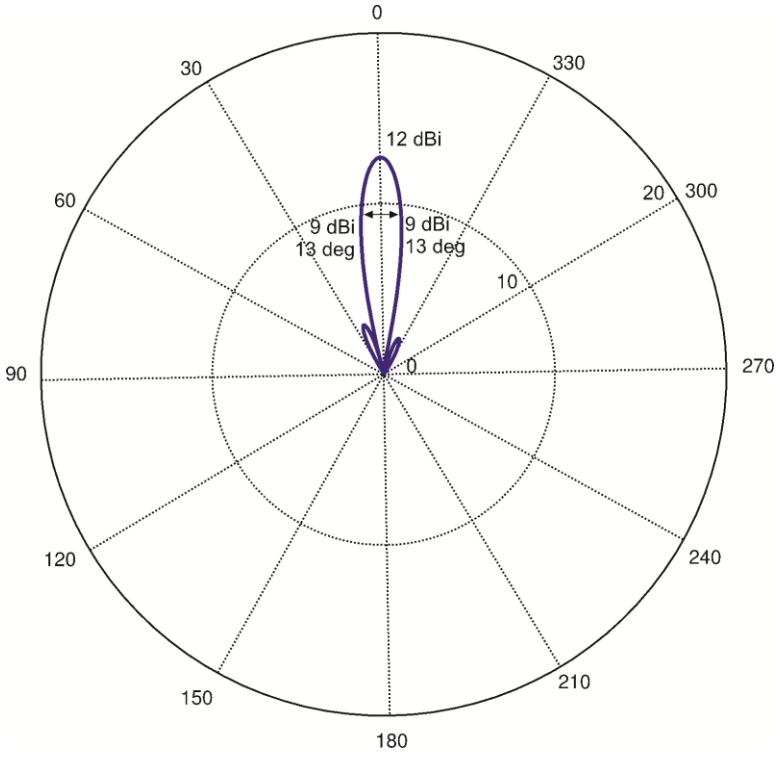

(a)

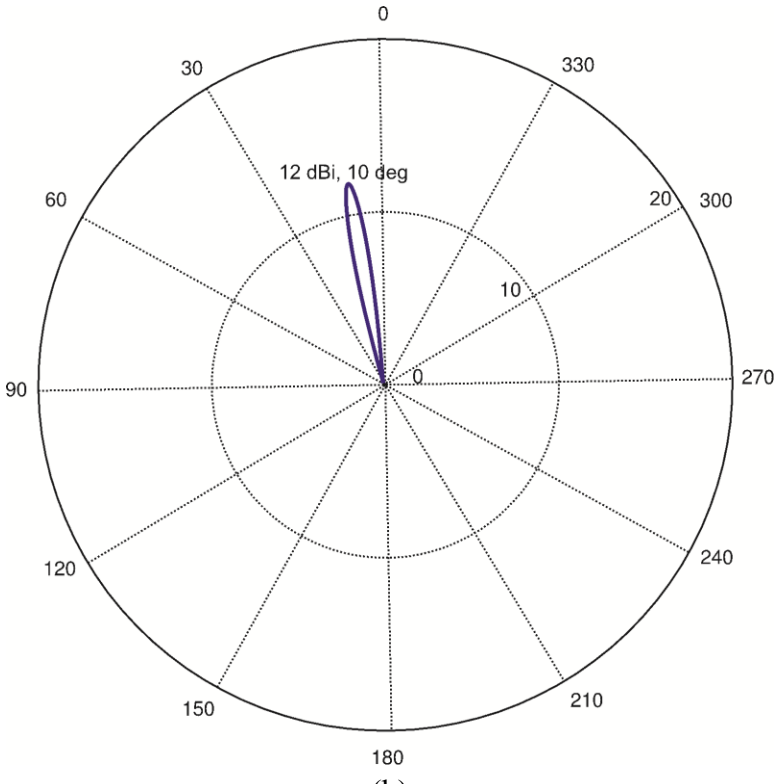

(b)

Figure 5.10. MRR maximum radiation occurs at gain of 12 dBi, (a) Azimuth angle, (b) Elevation angle

The bandwidth was taken at –10dB. The bandwidth of the simulated results is 1.2 GHz for the MRR as shown in Figure 5.11.

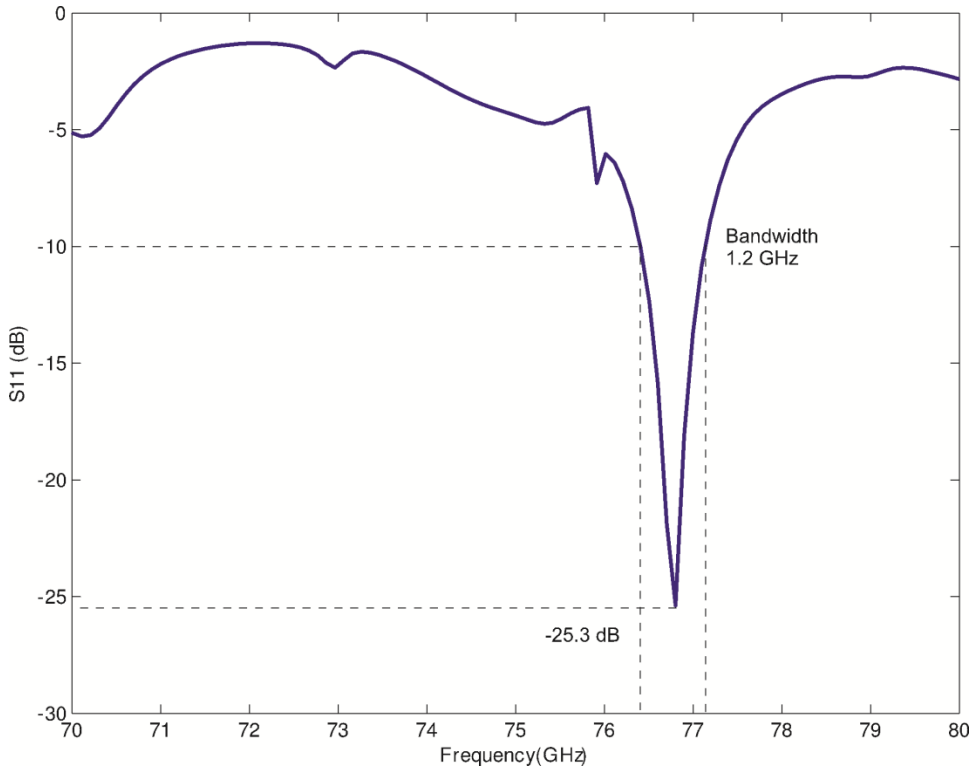

Figure 5.11. MRR S11 parameter is -25.3 dB

The follwoing figure, Figure 5.12, shows the VSWR of the MRR antenna array is 1.2. The value of VSWR for MRR is less than 2 at the operating frequency. This is considered a good value, as the level of mismatch is not very high.

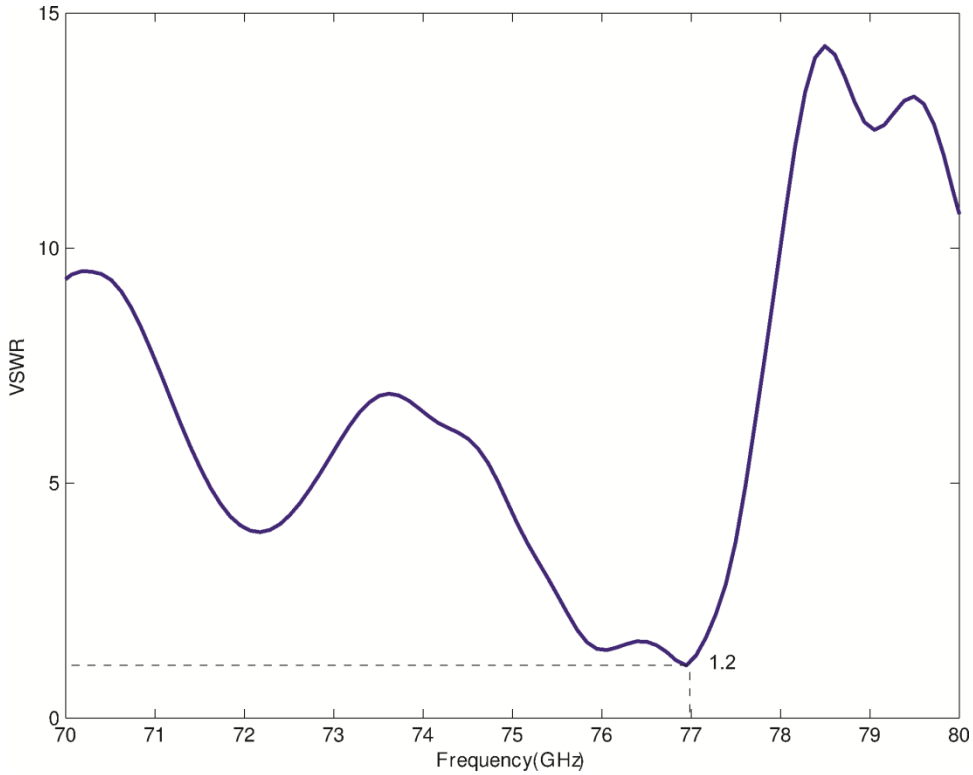

Figure 5.12. MRR VSWR is 1.2

Similar to SRR, the radiation of the MRR antenna is a broadside radiation which is perpendicular to the surface of the array. The following figure, Figure 5.13, illustrtes the simulation done by XFDTD™ 3-D software.

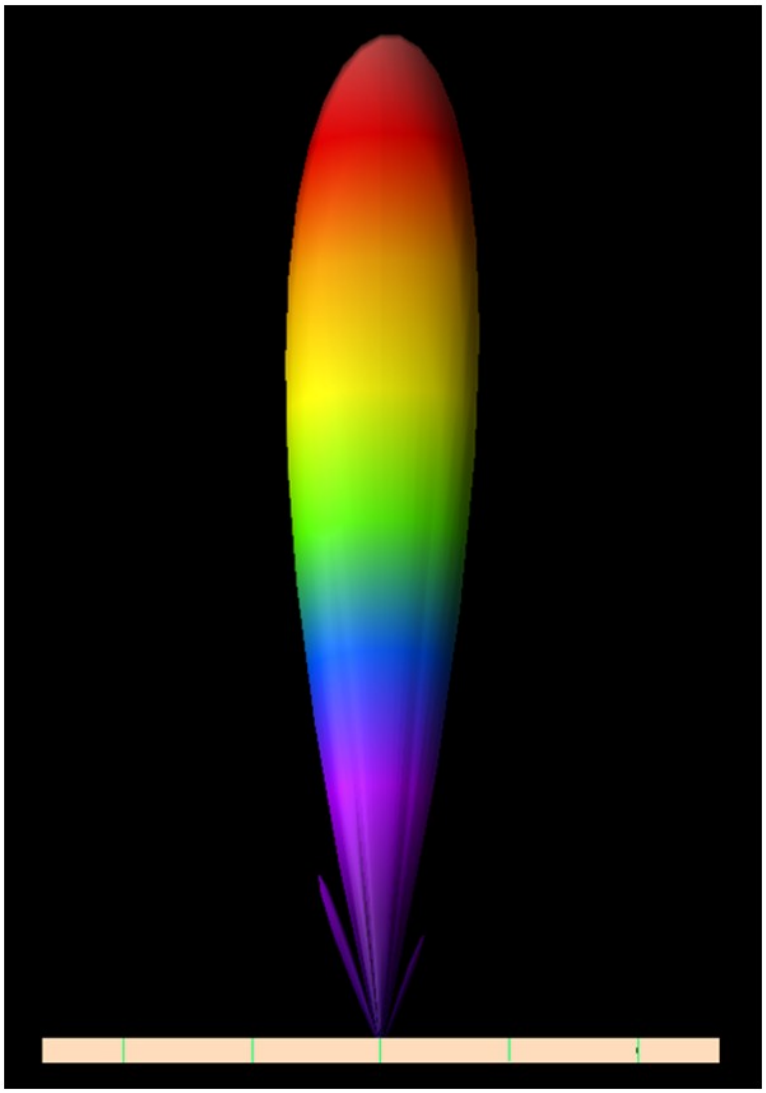

Figure 5.13. XFDTD™ MRR radiation pattern

The summarized results of MRR in Table 5.7, presents a close value to the available automotive mid-range radar specifications specified in the previous sections. The following table lists all the necessary parameter values of the MRR:

Table 5.7. MRR summary

MRR Parameter	Value
Gain	12 dBi
Azimuth angle	0°
Elevation angle	10°
-3dB Beamwidth (HPBW)	26°
S11 Parameter (return loss)	-25.3 dB
Bandwidth	1.2 GHz
Radiation Efficiency	94 %
VSWR	1.2

5.4.3 Long range antenna array

Following the SRR and MRR course of action, a number of patches were added to meet the long range radar specifications. Using XFDTD™ 3-D software, the long range antenna array is designed, optimized and analyzed. The following table, Table 5.8, shows the detailed dimensions of the long range radar (LRR):

Table 5.8. Long range antenna array parameters

LRR Parameter	Value
LRR array antenna	5 x 14
LRR length (L)	31.75 mm
LRR width (W)	11.49 mm
Frequency (f)	77 GHz
Silicon Substrate thickness	500 μm
SiO_2 layer thickness (top)	1.5 μm
SiO_2 layer thickness (bottom)	1.5 μm
Copper patches layer (Cu)	0.5 μm
Gold ground layer (Au)	0.5 μm
Array Element Spacing	2.4 mm

Figure 5.14, illustrate the LRR design from top and 3D view respectively in XFDTD™ 3-D software.5

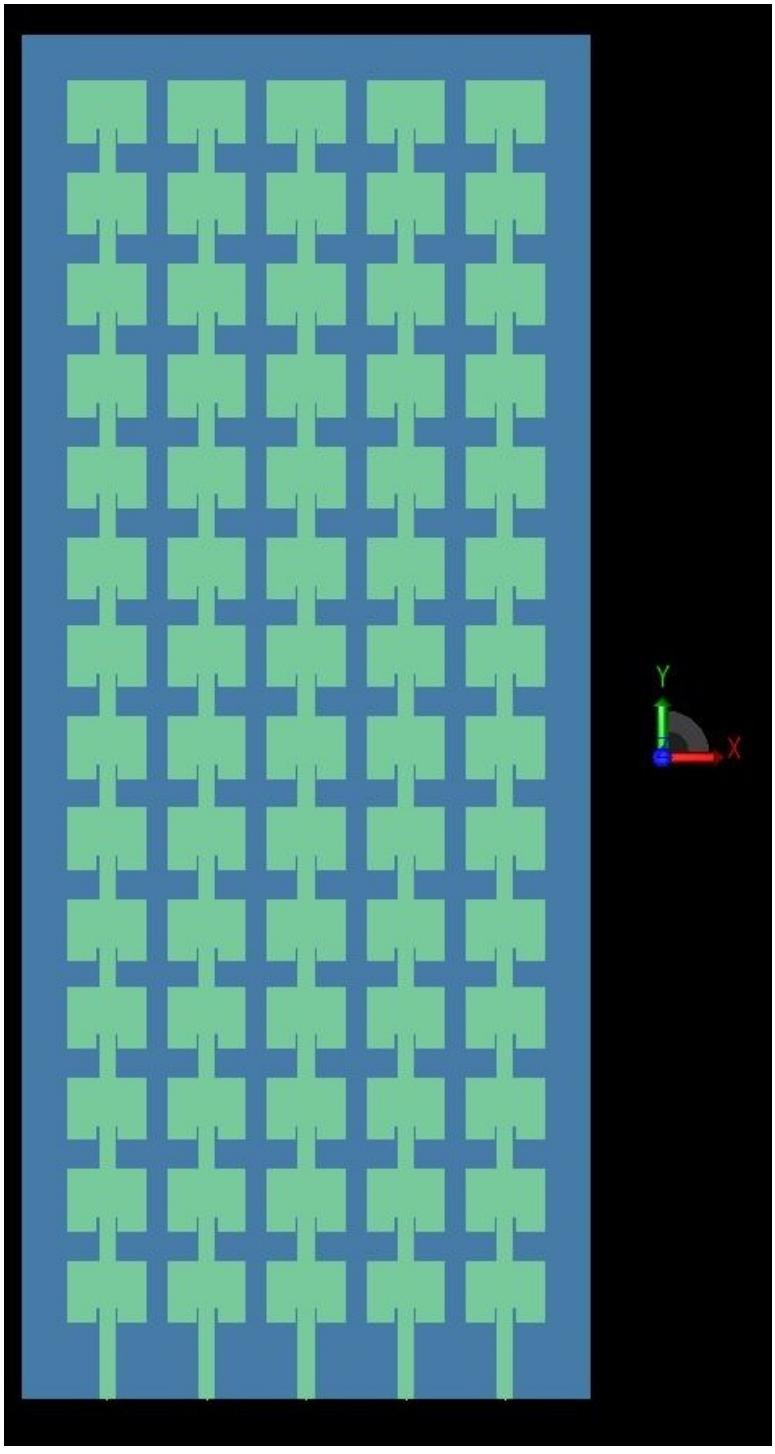

(a)

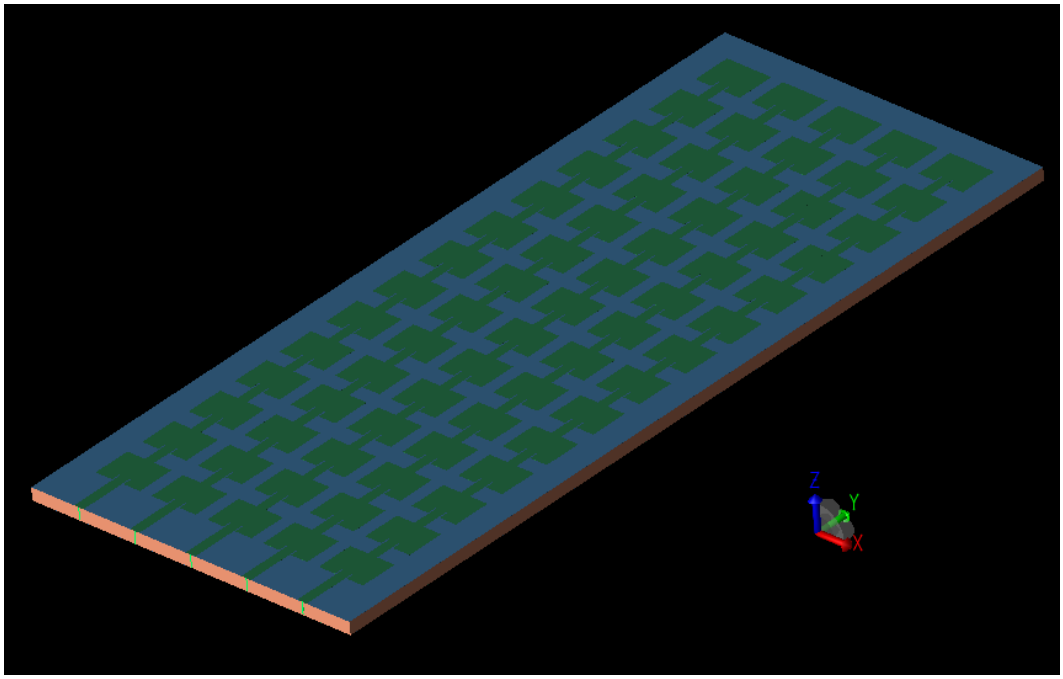

(b)

Figure 5.14. 3D view of the LRR design from XFDTD™(a) top view (b) 3D view

The normalized value of the radiation pattern gives the half-power beamwidth (HPBW) value. From Figure 5.15 below, at - 3dB, the values shown are 17.5 dB. Thus, the half-power beamwidth for the SRR is 11 degrees.

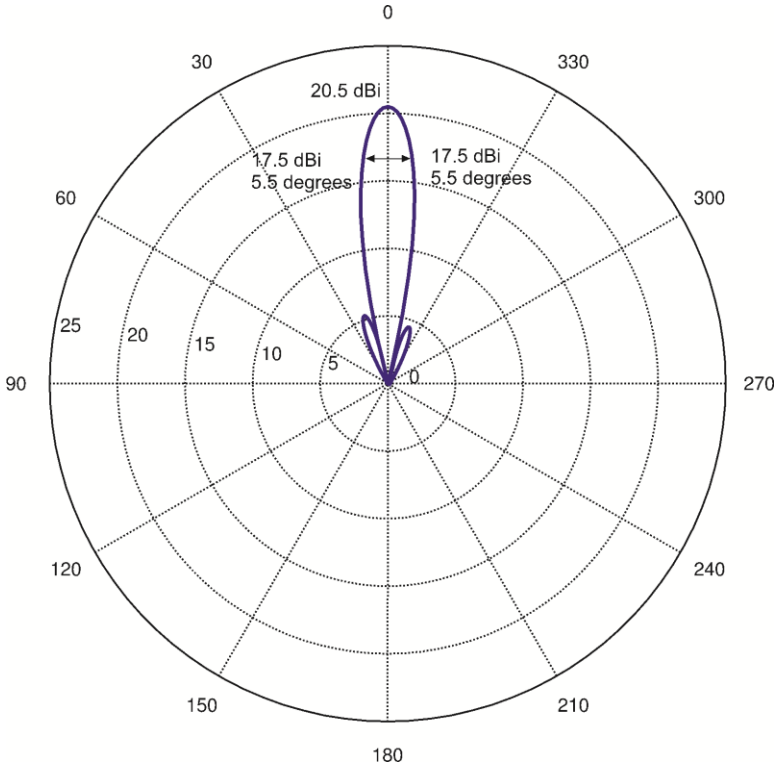

(a)

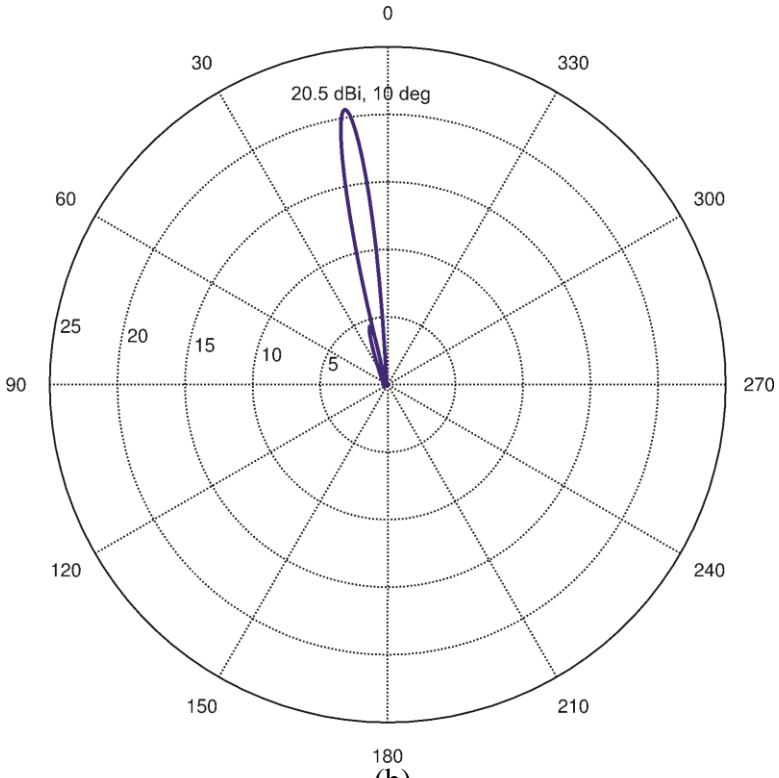

(b)

Figure 5.15. LRR maximum radiation occurs at gain of 20.5 dBi, (a) Azimuth angle, (b) Elevation angle

The bandwidth was taken at –10dB. The bandwidth of simulated results is 1.8 GHz for the LRR as shown in Figure 5.16.

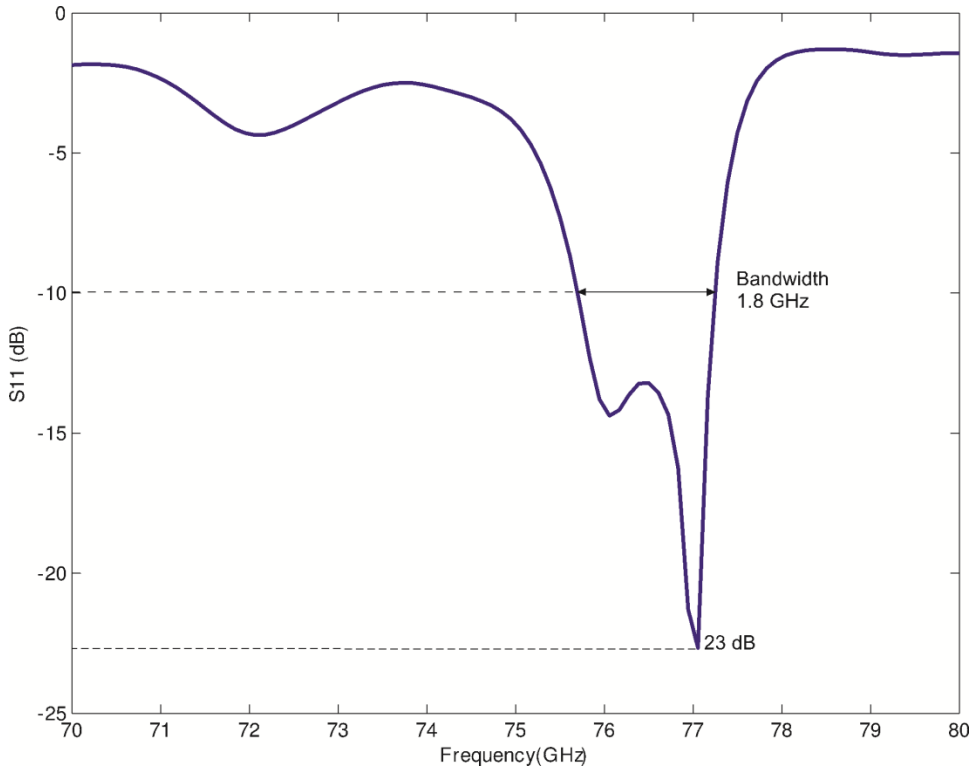

Figure 5.16. LRR S11 parameter is -23 dB

The follwoing figure, Figure 5.17, shows the VSWR of the LRR antenna array is 1.1. The value of VSWR for LRR is less than 2 at the operating frequency. This is considered a good value, as the level of mismatch is not very high.

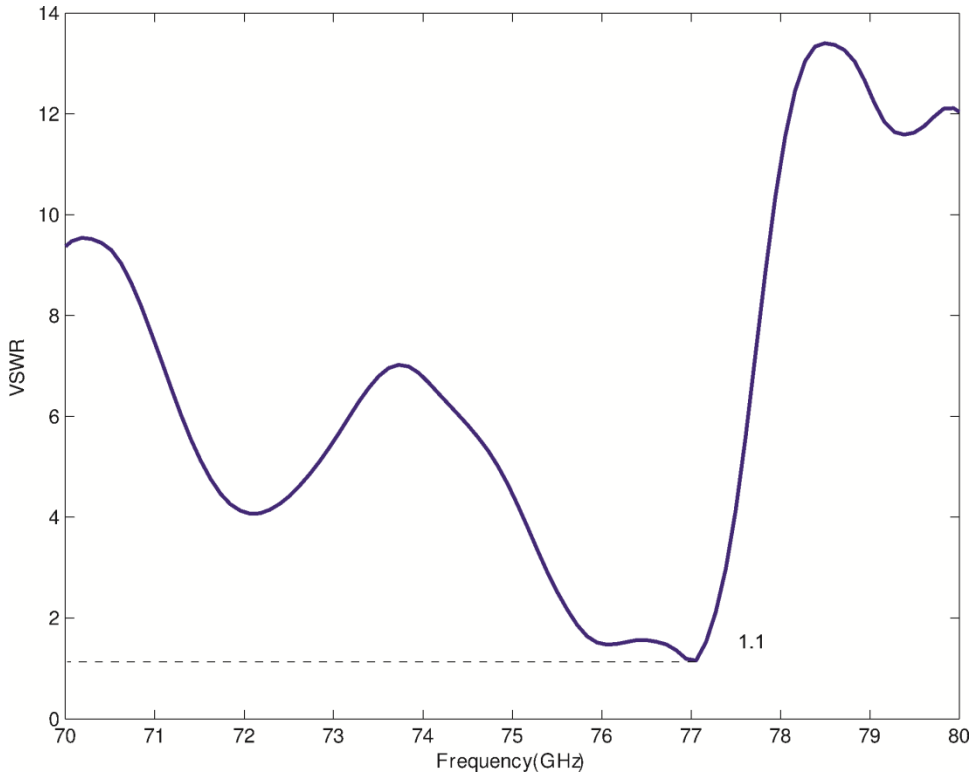

Figure 5.17. LRR VSWR is 1.1

The LRR radiation is shown the following figure, Figure 5.18. The maximum gain of this radiation is 20.5 dBi which is very good comparing available long range antennas in the market.

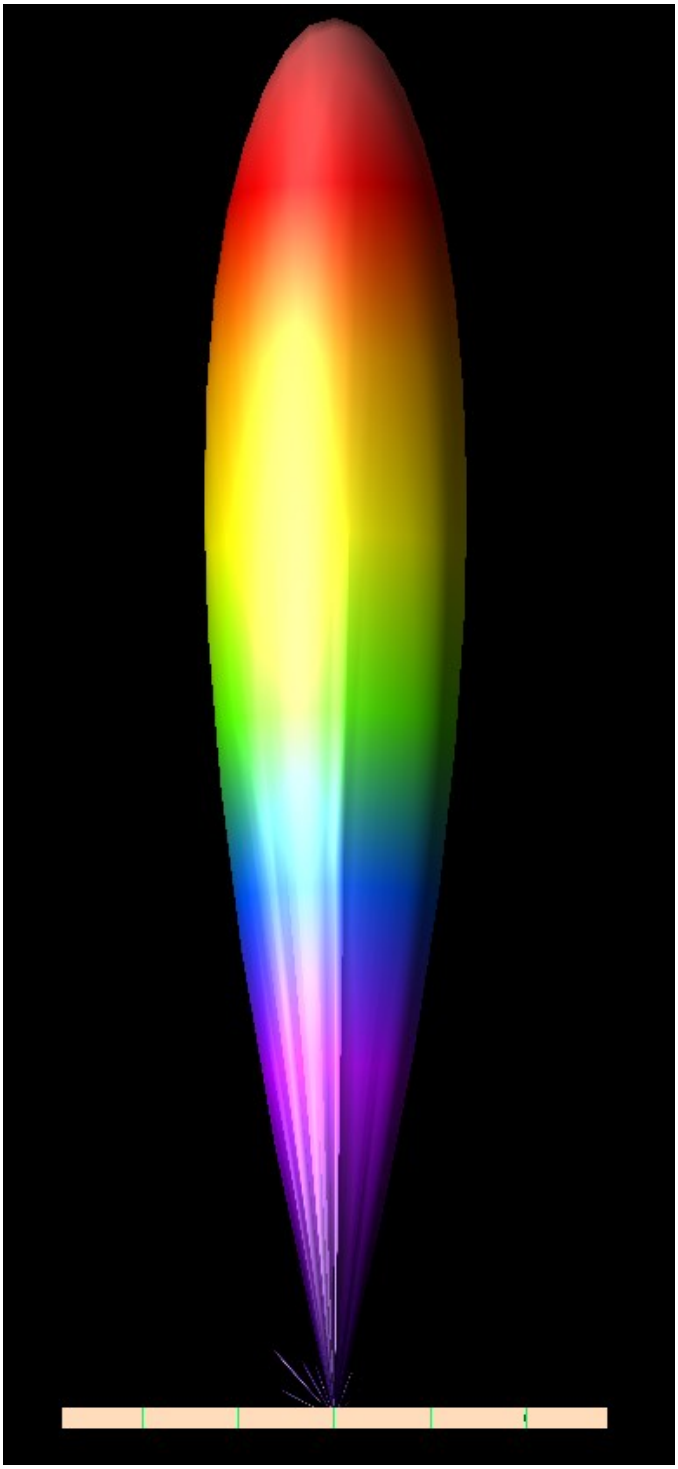

Figure 5.18. XFDTD™ LRR radiation pattern

To summarize the results of the LRR antenna that was designed, the following table, Table 5.9, is presented:

Table 5.9. LRR summary

Parameters	Value
Gain	20.5 dBi
Azimuth angle	0°
Elevation angle	10°
-3dB Beamwidth (HPBW)	11°
S11 Parameter (return loss)	-23 dB
Bandwidth	1.8 GHz
Radiation Efficiency	90 %
VSWR	1.1

5.5 Fabrication

Micromachined microstrip antenna array provides several advantages compared to conventional microstrip antenna array. Advantages of micromachining in microstrip patch antennas are comprehensive. In a single patch scenario, this approach can reduce the effective dielectric constant of the substrate by selectively removing material underneath the patch. This alteration improves the radiation efficiency and bandwidth of the selected antenna. As for antenna arrays scenario, in addition to radiation efficiency and bandwidth improvement, micromachined reduces the mutual coupling of the microstrip due to surface waves which are exist on high dielectric constant substrates.

In our fabrication, we have separated our process in three different structures. Top wafer take in account deposition of the gold patch on top of the silicon wafer and alteration of the substrate beneath selected patches. Bottom wafer includes depositions of the ground plane on top of a silicon bottom wafer. The last process is to bonding between

the top and bottom wafers to form our antenna array. A detailed explanation of the fabrication process is followed.

i. Top wafer

Step 1. Preparation of 500 µm silicon wafer followed by a cleanup (4" diameter, double-side polished, float zone <111>, boron doped to 1000 - 1750 ohm-cm) with 3:1 H_2SO_4:H_2O_2 solution.

Figure 5.19. Preparation of silicon wafer

Step 2. Thermally grow wet Silicon dioxide "SiO_2". Then, sputter Chromium "Cr" & Copper "Cu" on front of the wafer. A lithographically pattern front patches with mask #1. After that a wet-etch process through Cu. Strip photoresist and Ion-mill through Cr.

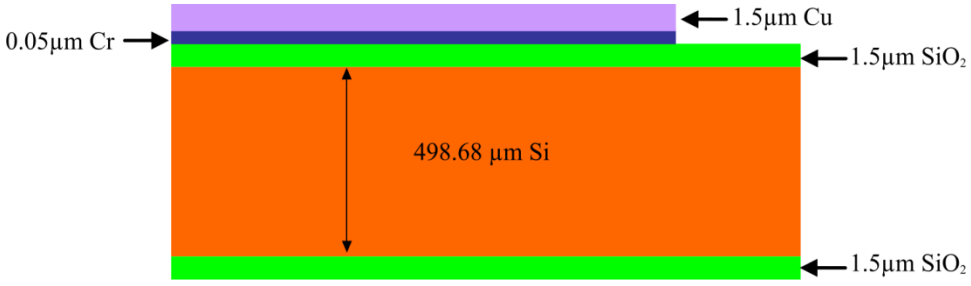

Figure 5.20. Alteration and lithography

Step 3. Lithographically pattern back holes with mask #2. Deposit Chromium "Cr" and Gold "Au" on back.

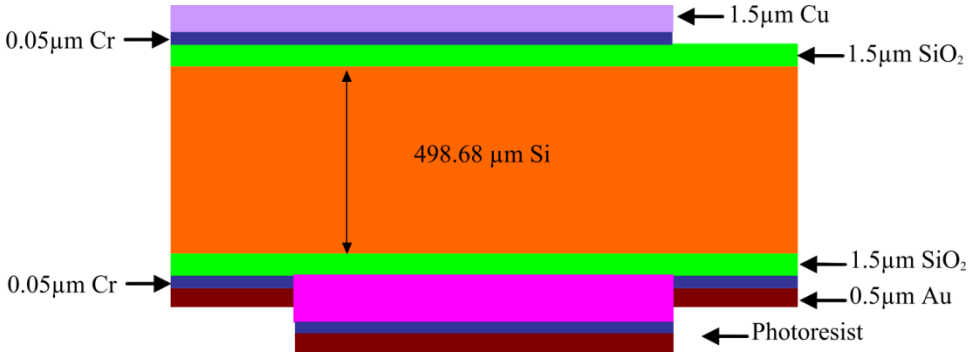

Figure 5.21. Alteration and lithography

Step 4. Strip photoresist. Cover front with photoresist, & wet-etch SiO_2. Strip photoresist. Re-pattern back holes with mask #3 using Bosch DRIE process into back.

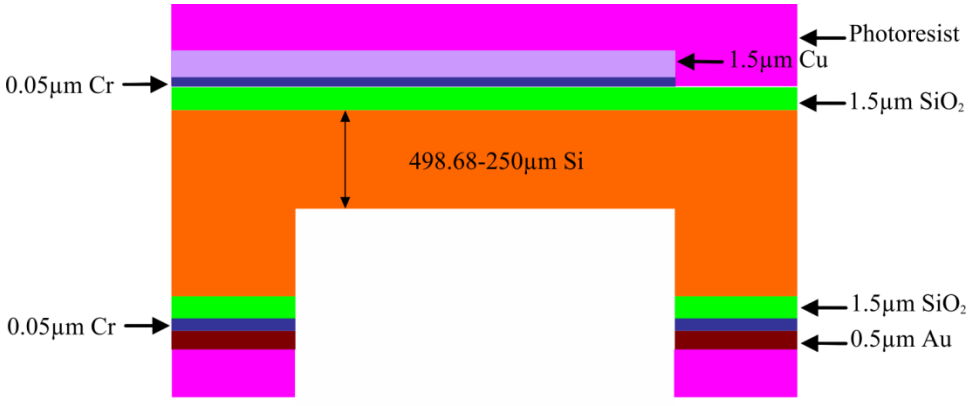

Figure 5.22. Strip photoresist

Step 5. Strip photoresist.

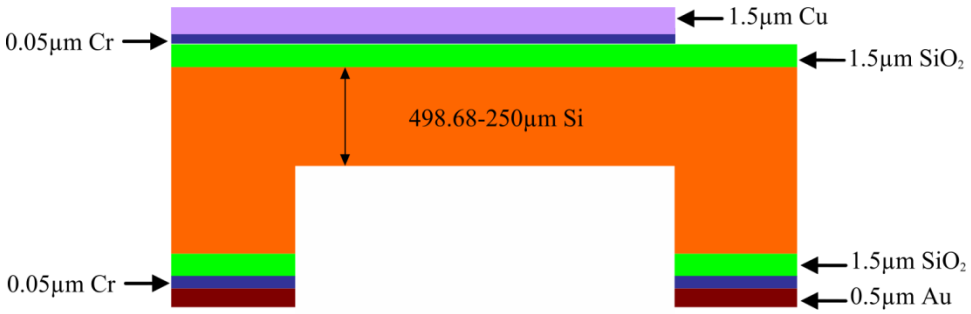

Figure 5.23. Strip photoresist

ii. Bottom wafer

Step 6. Clean 500 µm of silicon wafer (4" diameter) with 3:1 H_2SO_4:H_2O_2 solution.

Figure 5.24. Preparation of bottom wafer

Step 7. Deposit of Cr and Au layers on front of the wafer.

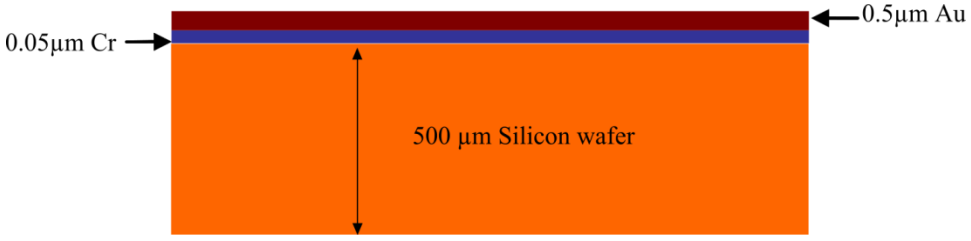

Figure 5.25. Depositions of Cr and Au

iii. Wafer bonding

Step 8. This is the last process of our fabrication and it incorporates thermo compressively gold to gold bonding between our two wafers. Thermocompressively bond of the two wafers and dice them.

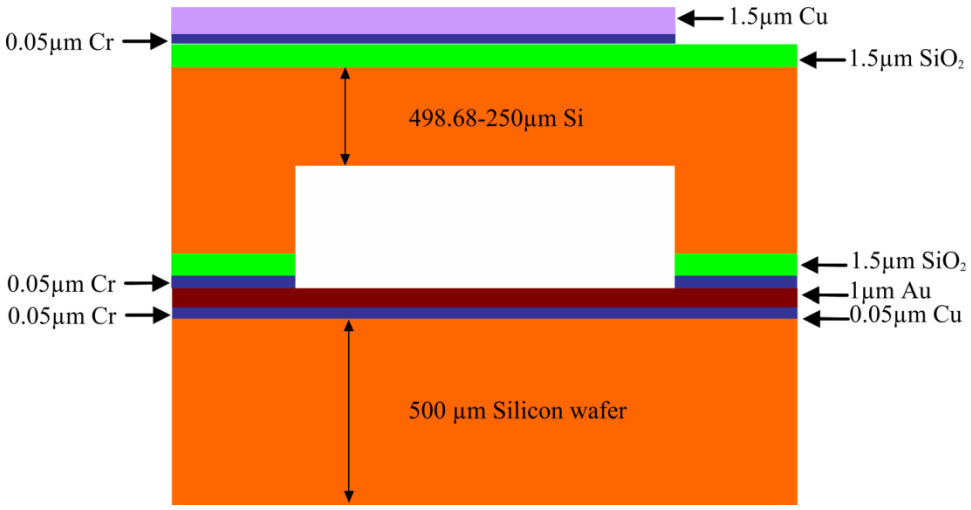

Figure 5.26. Wafer bonding

5.6 Summary

The antenna array structure is designed and optimized using XFDTD™ 3-D full wave simulation software from Remcom™. Using MATLAB, we have calculated the initial patch and microstrip line dimensions and then optimized it for better simulation results. Using the transmission line model, it was possible to model and analyze inset fed patch antenna designs. It was also possible to locate the accurate inset length needed for given 50 Ω input impedance. Further modification and the implementation of micromachined technology of the initial design provided an improvement in the bandwidth and efficiency as shown in this chapter. To that end, parametric analysis of the

substrate thickness, inset feed location and patch thickness also studied to optimize the initial geometry to obtain better overall results.

The following figures are captured pictures of the fabricated microstrip micromachined antenna array on a silicon based micromachined substrate with copper patches and gold ground layer. Figure 5.27 shows the micromachined air cavities of the antenna array that was etched away using Bosch DRIE process.

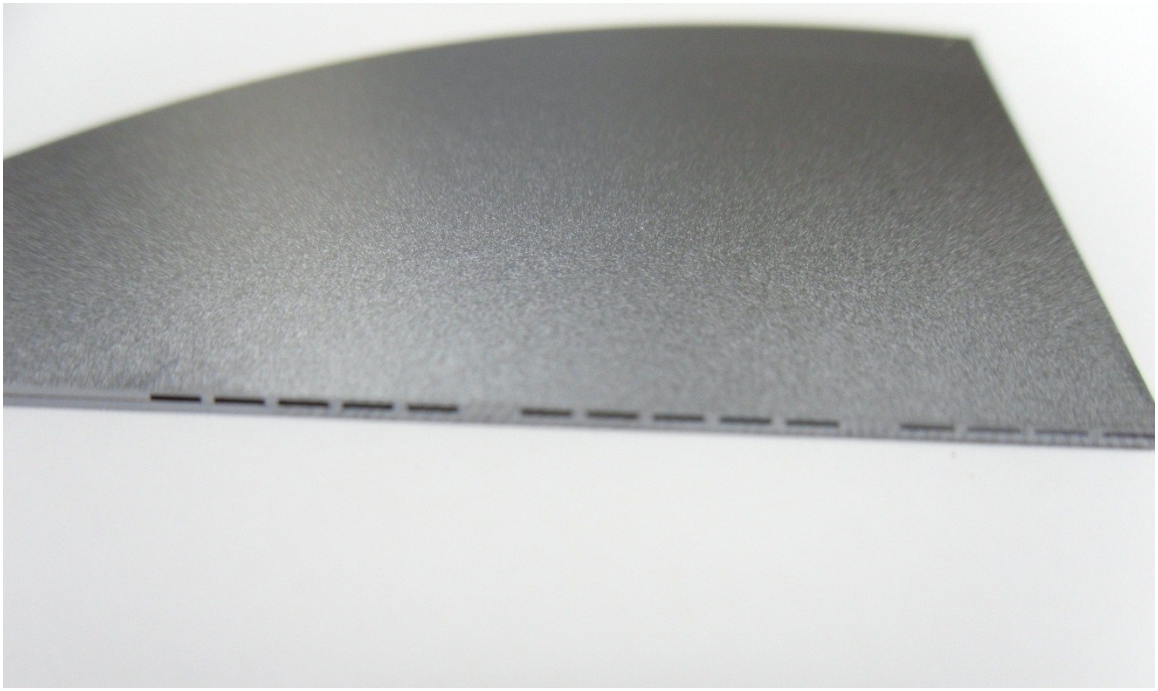

Figure 5.27. This photograph is a cross-section of the antenna array that shows the top layer with the micromachined air cavities

Figure 5.28 demonstrations the top view of the fabricated antenna on a silicon wafer. A lithographically pattern was done on the front patches using mask #1. After that a wet-etch process through Cu was applies.

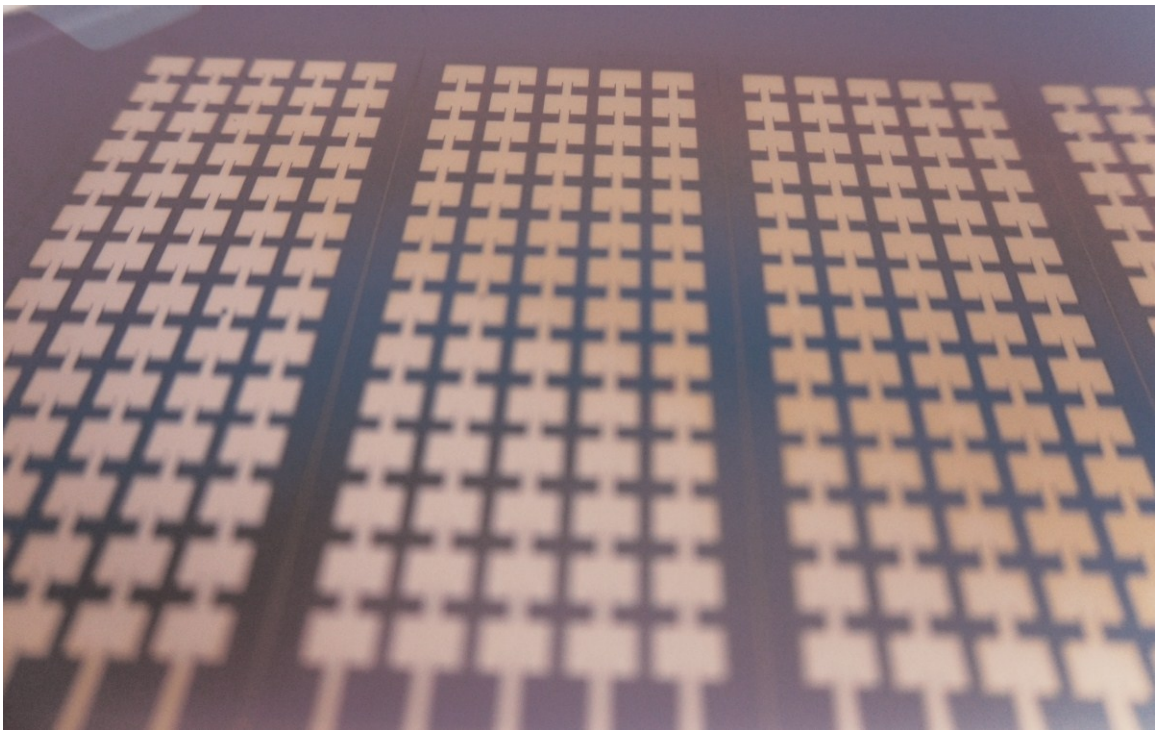

Figure 5.28. This photograph shows the top layer of the antenna array

CHAPTER VI

CONCLUSION AND FUTURE WORK

This chapter concludes with a summary for the work done for this thesis and the future prospects of the 77 GHz reconfigurable micromachined microstrip antenna array. A rundown on the topics covered during this thesis is presented, including design and simulation analysis. Subsequently, the future work that is essential for this project to succeed, especially measurement and performance testing to validate the range met all the required automotive specifications and exhibit excellent accuracy.

6.1 Conclusion

A 77 GHz reconfigurable micromachined microstrip antenna array has been developed to work with the Rotman lens beamformer designed at the University of Windsor for automotive collision avoidance system.

This thesis explained the theory behind microstrip antennas and a deep explanation of the antenna arrays. Background information with regard to microstrip planar antenna arrays is demonstrated, followed by a literature review on micromachined technology and how it can be implemented to benefits our application. In this section, we will highlight some of the unique properties of our design.

A clear improvement of the radiation efficiency and patterns of microstrip antennas on high dielectric-constant substrates (Silicon) has been demonstrated, resulting from a local reduction of the substrate dielectric constant underneath the antenna patches using micromachining techniques. As expected, the synthesized microstrip antenna array resulted in high efficiency, wide bandwidth and good radiation pattern. Whereas the use

of rectangular patch geometry provided good directivity and simplicity in design and fabrication process.

Based on the simulations obtained in chapter 5, the microstrip antenna arrays have been successfully designed and centered at 77 GHz frequency using XFDTD™ 3-D full wave analysis software, carrying an optimization to the geometry, resulted in further improvement of the simulation parameters.

The antenna array for LRR has showed a pretty high gain with up to 20.5 dBi and a narrow beamwidth of 11 degrees. The attractive part of this design that it is compact in size and provide high radiation efficiency of 90%. As for the mid-range antenna array, a gain of 12 dBi and a beamwidth of 26 degrees are been generated. The radiation efficiency of this antenna array is 94%. Whereas the short range antenna array, came with a good gain of 8.8 dBi and a wide beamwidth of 40 degrees. The radiation efficiency is very high and it is 97%. The mid and short range antenna arrays provided a wider angular coverage as proposed for short range radar specifications.

The S11 parameter for all the antenna arrays have a magnitude of much less than -10dB at the operating frequency 77 GHz, which means that those antennas doesn't have many losses while transmitting the signals. As for the voltage standing wave ratio (VSWR), it is not ideal; however, we obtained a value of under 2 which is consider acceptable and the level of mismatch is not high.

The antenna arrays bandwidth was determined from S11 parameter at -10dB for SRR (1.2 GHz), MRR (1.2 GHz) and LRR (1.8 GHz). Clearly, the antenna bandwidth of the compact design with less number of elements is reduced. This is to be expected owing to the antenna size reduction.

6.2 Future work

Although we have presented a thorough analysis of the work of the reconfigurable antenna array and the feed structure, there are still tasks remaining in several areas.

- Performance analysis and measurement results for the fabricated antenna array
- Study of the radiation pattern and guarantee acceptable frequency bandwidth for each of the antenna arrays LRR, MRR, and SRR
- Integrate MEMS RF switches between the arrays
- Combine the designed and fabricated Rotman lens, developed at University of Windsor MEMS lab, to work with the designed antenna array
- Implement the FPGA / ASIC algorithm to control the operation of the MEMS SPST switches to dynamically alter the beamwidth of the antenna array to cycle the radar constantly from short-range (SRR) to mid-range (MRR) to long range (LRR) mode.

After dicing the fabricated antenna and incorporating the SPST RF MEMS switches, the final shape of the antenna will look as presented in the following figure, Figure 6.1:

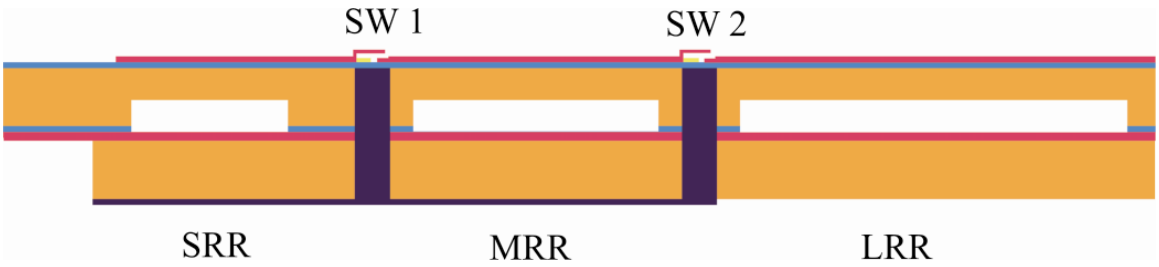

Figure 6.1. Reconfigurable Antenna Array

APPENDIX A

MATLAB CODE

```
clc
% function [length, delta_length, Leff]=cal_len_patch(Er, w, d, fr)
% fr= Resonant Frequency in GHz.
% w= Width of the microstrip
% h= Thickness of the microstrip
% Er = Di electric Constant
% Antenna THeory: Analysis and Design -Balanis

fr= 77e9; %77GHz frequesncy
Er= 1.85;   % Synthesized Dielectric Constant
h= 0.25  ; %mm
c=((3e8)*1000); %speed of light(mm/sec) if in m/sec then 3e8 only!

Zc=50; % Charactar
%width calculation
A_width= c/(2*fr);
B_width= 1/(sqrt((Er+1)/2));
width =(A_width)*(B_width);

% width feed line calculation
% function [ratio, width]=width_feedline(Zc, Er, h);
% Equation by Wheeler and Hammerstad
% w=width
% h=thickness
% Er= Relative permittivity
% the formula I have used here have been taken from the book called:
% Microstrip filters for RF/microwave applications, Jia-Sheng G. Hong,
M.J. Lancaster
% http://www.rfdh.com/rfdb/msline.htm
% Microwave Engineering - Third edition- David Pozar
% Microwave filters, Impedence-matching, Networks, and Coupling
structures - Mathaei Young Jones
% Passive and Active filters- Theory and implementations - Wai-kai-
Chen.
% Digital Signal Processing using MATLAB- Vinay K Ingle.
% Stripline Circuit design- Harlan Howe
% Approximate expressions for W/h in terms of Zc and Er derived by
Wheeler and Hammerstad


Er1_wf=(Er+1);
Er2_wf=(Er-1);
Er12=(Er2_wf/Er1_wf);
A_wf=(Zc/60);
B_wf=(A_wf*((Er1_wf/2)^0.5));
C_wf=(B_wf + (Er12*(0.23 + (0.11/Er))));
K_wf= (8 * (exp(C_wf)));
M_wf= ((exp(2*C_wf)) - 2);
ratio = (K_wf/M_wf);
 if ratio >= 2
```

```
    T=(60*(pi^2))/(Zc*sqrt(Er));
    F=(Er2_wf/(2*Er))*(log(T-1) + 0.39 - (0.61/Er));
    ratio = ((2/pi)*((T-1) - (log((2*T)-1)) + F));
 end
width_feedline=ratio*h;

%[Eeff, w_over_h]=calc_Eeff_patch(Er, w, h);

w_over_h= width / h;
Er1     = ((Er+1)/2);
Er2     = ((Er-1)/2);
h_over_w= (1/w_over_h);
A_eff   = sqrt(1+(12*h_over_w));
if w_over_h >= 1
    Eeff= (Er1 + (Er2*(1/A_eff)));
end
if w_over_h < 1
    B_eff= 0.04*((1-w_over_h)^2);
    Eeff =(Er1 + (Er2*((1/A_eff) + B_eff)));
end
numerator= ((Eeff +0.3)*(w_over_h+0.264));
denom=((Eeff - 0.258)*(w_over_h + 0.8));
deltaL_over_h = 0.412*(numerator/denom);
delta_length = deltaL_over_h * h;

%Lenght and effective lenght of the path antenna calculation
%length =(A_eff*((Eeff)^(-0.5)))-(2*(delta_length));
length =(c/(2*fr)*((Eeff)^(-0.5)))-(2*(delta_length));
Leff = length+(2*delta_length);

% Calculations of the yo (inset_feed in inch)
% function yo= inset_feed(length, width, fr, Zc, h)
% This function calculates the input impedance for the antenna and
calculates the position of inset feed point where the
% input impedance in 50 ohm.
lamda_o=c/fr; %mm
lamdaby2=lamda_o/2;
ko=(2*pi)/lamda_o;
A_yo=(1/(120*(pi^2)));
% Reference: Page : 732 (Antenna Theory: Analysis and design)
F1=0;
for theta=[0:1:180]*pi/180
    z=ko*length*sin(theta);
    J = besselj(0,z);
    I =
(((sin((ko*width/2)*cos(theta)))/cos(theta))*((sin((ko*width/2)*cos(the
ta)))/cos(theta)))*J*((sin(theta))^3)*(pi/180);
    F1=I+F1; %current (I1=F1)
end
g12=F1*A_yo;
F3=0;
% cacluation of G1 (conductance):
for phi=[0:1:180]*pi/180
```

```
    F2 =
(((sin((ko*width/2)*cos(phi)))/cos(phi))*((sin((ko*width/2)*cos(phi)))/
cos(phi)))*(sin(phi).^3)*(pi/180);
    F3=F2+F3;
 end
 g1=F3*A_yo;
 g12=6.1683e-004;
if (width > lamda_o)
    g1=(1/120)*(width/lamda_o);
end
if (width < lamda_o)
    g1=(1/90)*((width/lamda_o)^2);
end
Rin=(1/(2*(g1+g12))); %input impedance of the antenna from Microstrip
Antennas chanpter 14 page 825
yo= (acos(sqrt(Zc/Rin))*length)/pi;% inset feed point from Microstrip
Antennas chanpter 14 page 825

W_waveport = 3* width_feedline;
H_waveport = 4* h;

%A Dual frequency Series Fed Patch Array Antenna
%For a standard array antenna each lamda/2 - patch must be seperated by
%lamda/2 transmission line.
Lg = 6*h + length;
Wg = 6*h + width;


lamda_o
lamdaby2
length
width
% Eeff
% Leff
% width_feedline
yo
% W_waveport
% H_waveport
%
% Lg
% Wg

% [direct, directdB, Prad]=directivity(-90, 90, 0.1, 180, fr, width,
Leff, h)
% figure (1);
% [E_plane, phi]= e_plane1(fr, width, Leff, h, directdB);
% figure (2);
% [h_plane, theta]= h_plane1(fr, width, Leff, h, directdB);
% [radiation]= radiation_intensity(fr ,theta, phi, width, Leff, h);

function [direct, directdB, Prad]=directivity(phiMin, phiMax, thetaMin,
thetaMax, fr, width, Leff, h)
Umax=0;
Umax=0;
d_theta=pi/180;
```

```
d_phi=pi/180;
Prad=0;
phiMin1=phiMin+1;
%double integration
for phi = phiMin1:phiMax
    phi_rad=phi*pi/180;
    thetaMin1=thetaMin +1;
    for theta=thetaMin1:thetaMax
        theta_rad=theta*pi/180;
        radiation = radiation_intensity(fr ,theta_rad, phi_rad, width,
Leff, h);
        if radiation > Umax
            Umax=radiation;
        end
        UA= d_theta* d_phi * radiation*sin(theta_rad);
        Prad=Prad+UA;
    end
end
    direct= 4*pi* Umax/Prad;
    directdB=10*log10(direct);

function [E_plane, phi]= e_plane1(fr, width, Leff, h, directdB);
r=1;
phi = (-pi/2):(pi/1000):(pi/2);
%fr=fr*(1e+9);
fr= 7.7000e+010; %77GHz frequesncy
c=((2.9986e8)*1000);
lamda_o=c/fr; %mm
ko=(2*pi)/lamda_o;
const=((j)*width*ko*(exp((-j)*ko*r)))/(pi*r);
B=sin(((ko*h)/2)*cos(phi));
C= (((ko*h)/2)*cos(phi));
%B= (sin(((ko*h)/2)*cos(phi)))/(((ko*h)/2)*cos(phi));
D=B/C;
%E=cos(((ko*Leff)/2)*cos(phi));
E= cos(((ko*Leff)/2)*sin(phi));
%E_plane= 20*log10(abs(const*D*E));
plane1=abs(const*D*E);
plane_max=max(plane1);
E_plane = (20*log10(plane1/plane_max)) + directdB; %normalizing
polarhg(phi',E_plane','rlim',[-30 10],'rtick',[-30 -20 -10 0 10],
'tstep',60,'color','b'), title ('E-Plane E(\phi) (normalized)' );
plotedit on;

function [h_plane, theta]= h_plane1(fr, width, Leff, h, directdB);
fr= 7.7000e+010; %77GHz frequesncy
c=(2.9986e+8)*1000; %mm/sec
%c=((2.9986e8)*100)/2.54; %speed of light(inch/sec)
lamda_o=c/fr; %in
ko=(2*pi)/lamda_o;
theta = (0.01):(pi/1000):pi;
%phi=-90:5:90;
r=1;
%const=((-j)*2*width*ko*(exp(-j*ko*r)))/(4*pi*r);
const=((j)*width*ko*(exp((-j)*ko*r)))/(pi*r);
%B=   sin(((ko*width)/2)*cos(theta));
```

```
%C=(((ko*h)/2)*cos(theta));
B= ((sin(((ko*width)/2)*cos(theta)))/(((ko*width)/2)*cos(theta)));
C= (sin(((ko*h)/2)*sin(theta)))/(((ko*h)/2)*sin(theta));
%B=(sin((ko*width*cos(theta))/2))/((ko*width*cos(theta)/2));
D= sin(theta);
% used the equation from the book : " Microstrip Antenna by I.J. Bahl
%plane= ((20*log10(abs(const*(B*C*D)))));
plane1 = (abs(const*(B*C*D)));
plane_max=max(plane1);
h_plane = (20*log10(plane1/plane_max)) + directdB;
%offset = 40;
%plane = plane - max(plane);
%checking the negative values of plane
%for n=1:1:(i-1)
%    if ((plane(n)+offset) < 0)
 %       plane(n)=0;
 %   end
 %end
%plane(1000)
%plane1=max(abs(plane))
%plane1=max(abs(plane))
%plane2=min(abs(plane))
%[E_plane, phi]= e_plane(fr, width, Leff, h);
%[phi,RHO] = cart2pol(theta,h_plane);
%hplane=abs(h_plane);
%a=plane + plane1;
%min(a)
%max(a)
%polarhg(theta, plane +offset ,'g'), title ('H-Plane E(\theta)' );
polarhg(theta',h_plane','rlim',[min(h_plane) 10],'rtick',[-30 -20 -10 0
10],'tstep',30,'color','r'),...
title ('H-Plane E(\phi) (normlized)' );
plotedit on;
max(theta)*180/pi
min(theta)*180/pi
%'rtick',[-30 -20 -10 0 10],

function radiation = radiation_intensity(fr ,theta, phi, width, Leff,
h)
phi = (-pi/2):(pi/1000):(pi/2);
theta = (0.01):(pi/1000):pi;
r=1;
%fr=77*(1e+9);
c=(2.9986e+8)*1000; %mm/sec
fr= 7.7000e+010; %77GHz frequesncy
%c=((2.9986e8)*100)/2.54; %speed of light(inch/sec)
lamda_o=c/fr; %in
ko=(2*pi)/lamda_o;
const=((j)*ko*h*width*(exp((-j)*ko*r)))/(2*pi*r);
X=(ko*h/2).*(cos(phi(1:997)).*(sin(theta(1:997))));
Y=(ko*width/2)*cos(theta);
%radiation=
((abs(const*(sin(X)/X)*(sin(Y)/Y)*sin(theta)))^2)/(2*120*(pi^2));
radiation=
((abs(const.*(sin(X)./X).*(sin(Y)./Y).*sin(theta))).^2)./(2.*120.*(pi.^
2));
```

FABRICATED MICROSTRIP ANTENNA ARRAY

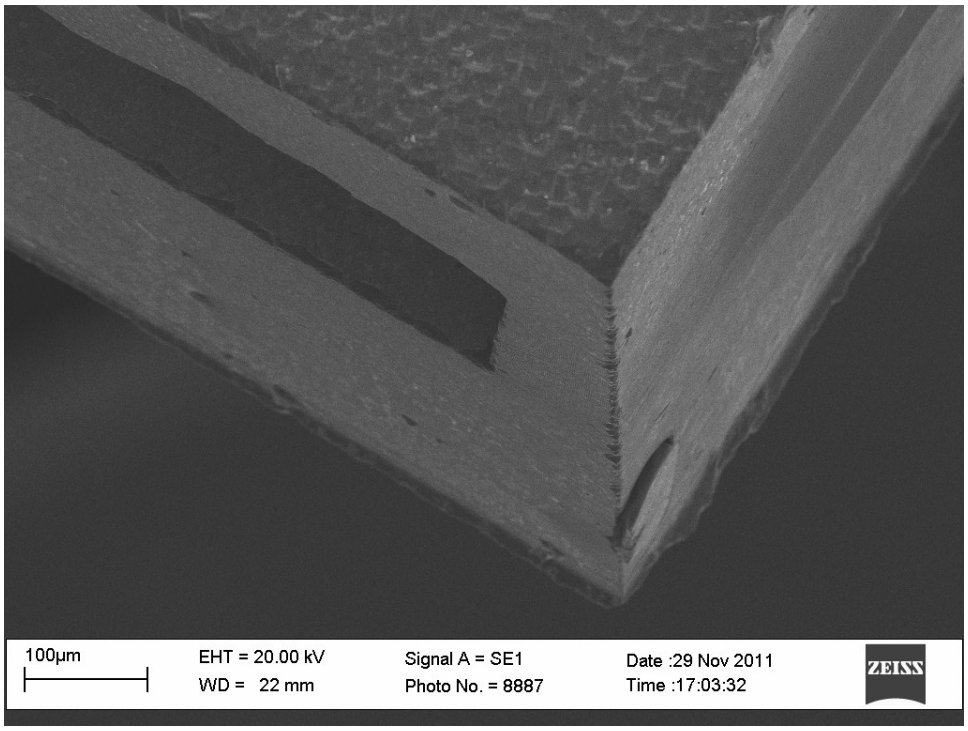

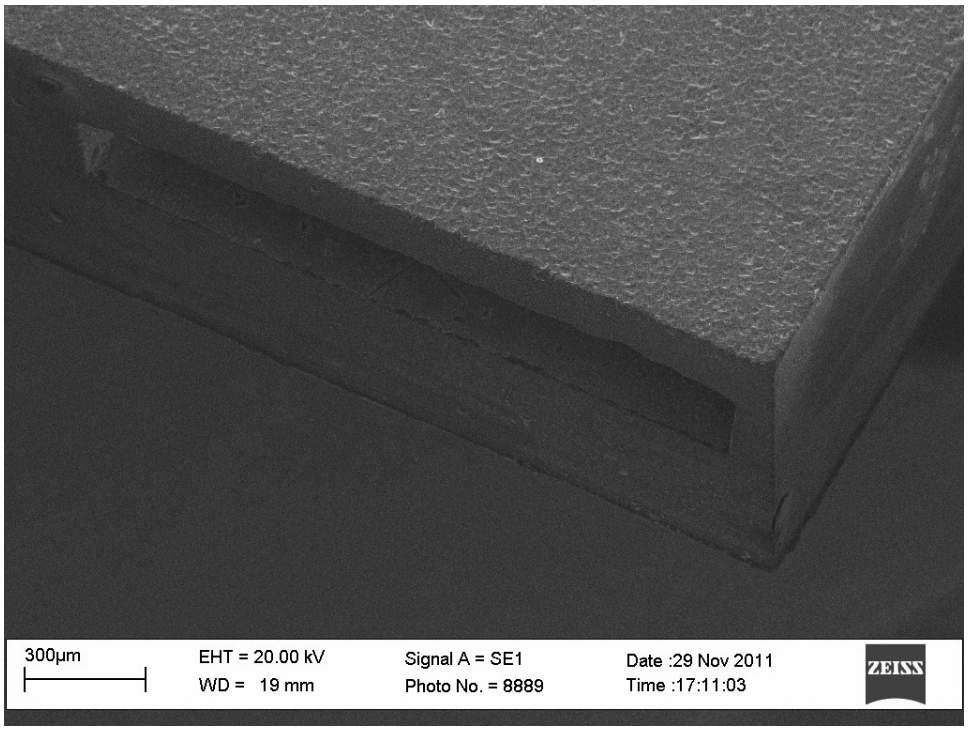

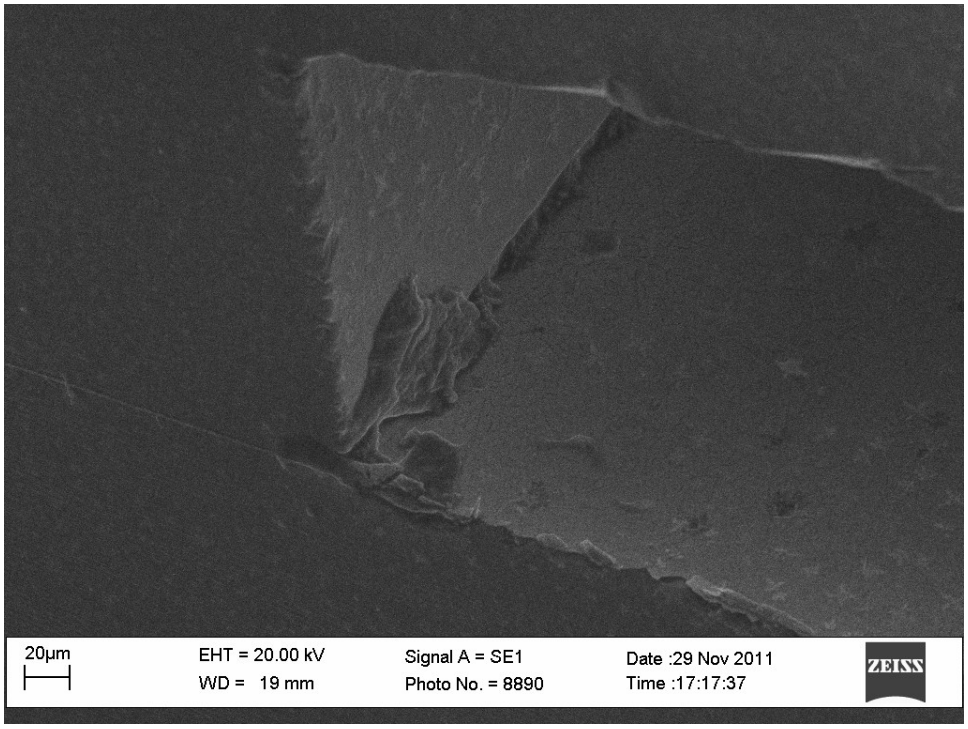
20µm
EHT = 20.00 kV
WD = 19 mm
Signal A = SE1
Photo No. = 8890
Date :29 Nov 2011
Time :17:17:37
ZEISS

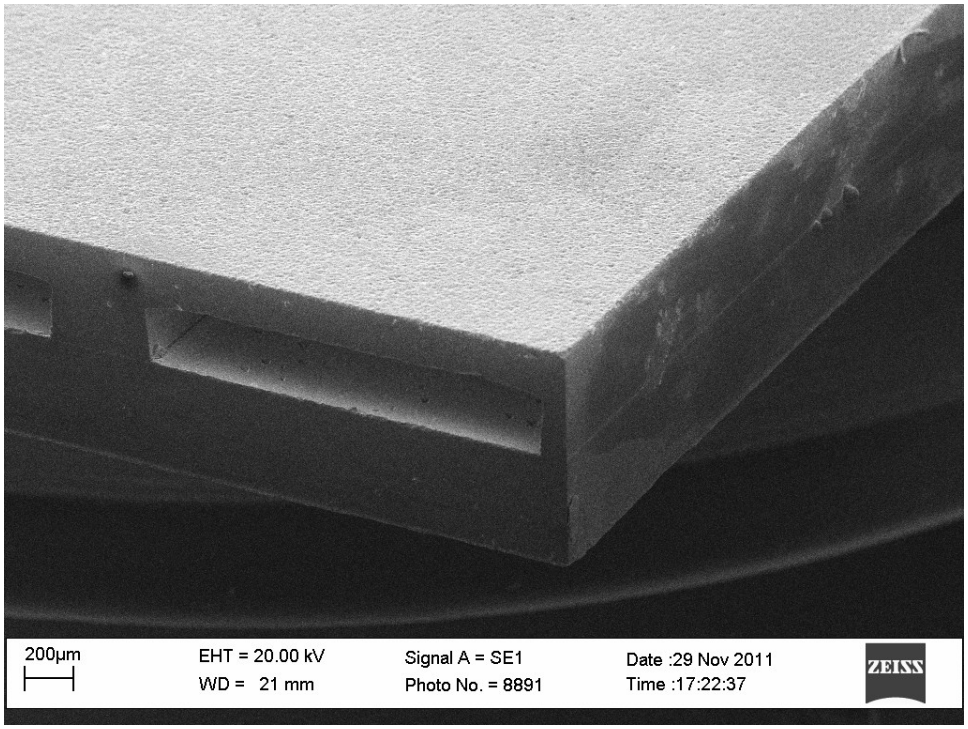
200µm
EHT = 20.00 kV
WD = 21 mm
Signal A = SE1
Photo No. = 8891
Date :29 Nov 2011
Time :17:22:37
ZEISS

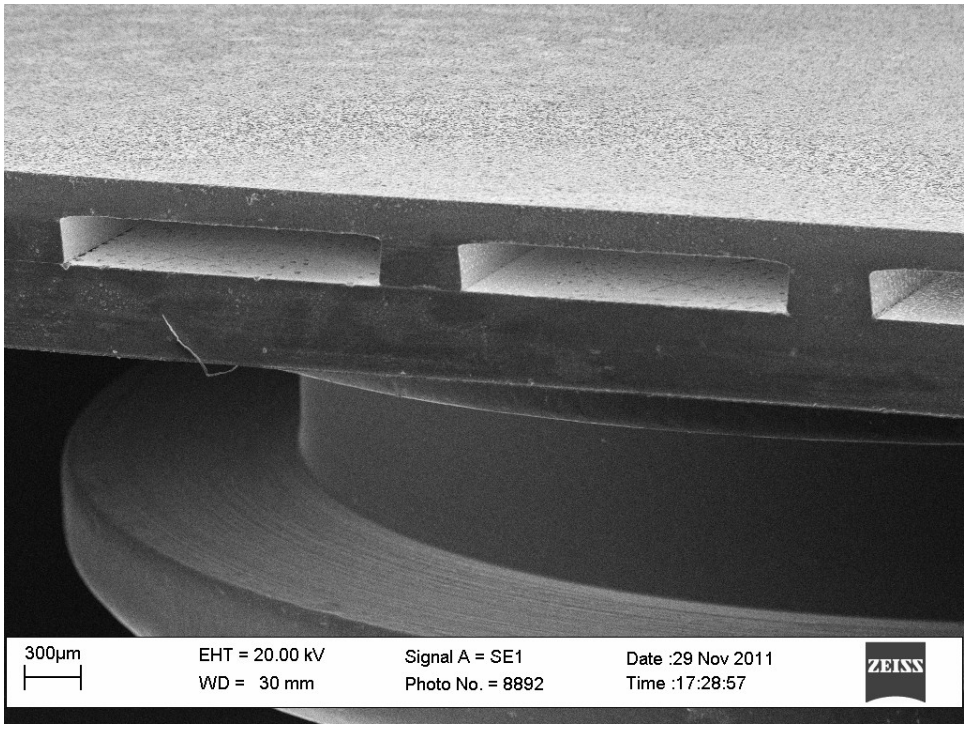
300µm
EHT = 20.00 kV
WD = 30 mm
Signal A = SE1
Photo No. = 8892
Date :29 Nov 2011
Time :17:28:57
ZEISS

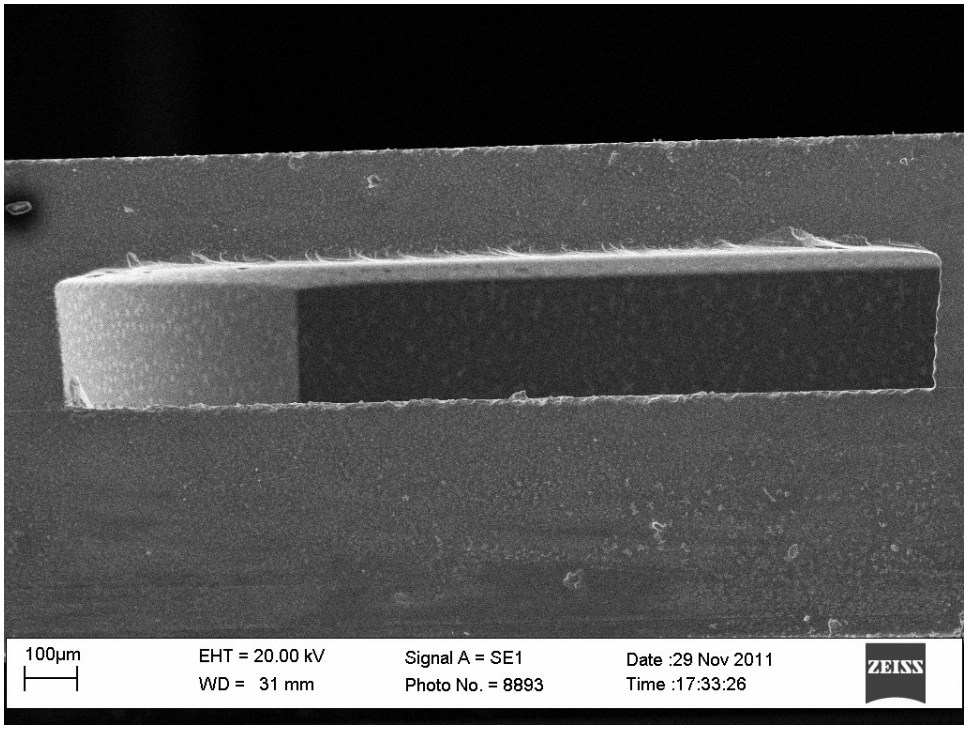
100µm
EHT = 20.00 kV
WD = 31 mm
Signal A = SE1
Photo No. = 8893
Date :29 Nov 2011
Time :17:33:26
ZEISS

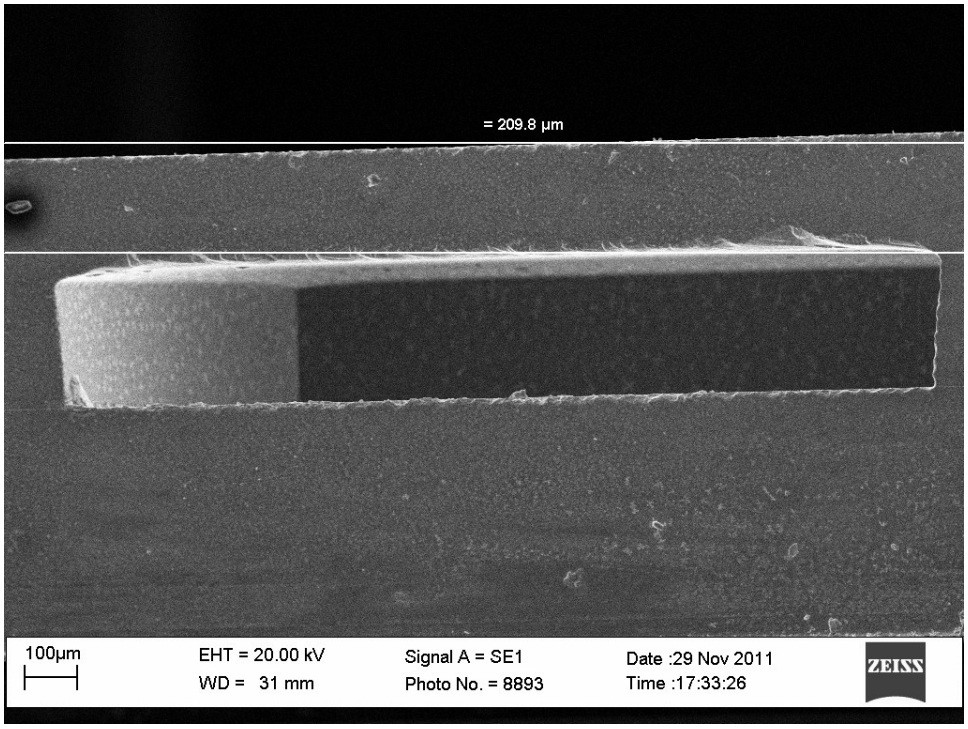
= 209.8 µm
100µm
EHT = 20.00 kV
WD = 31 mm
Signal A = SE1
Photo No. = 8893
Date :29 Nov 2011
Time :17:33:26
ZEISS

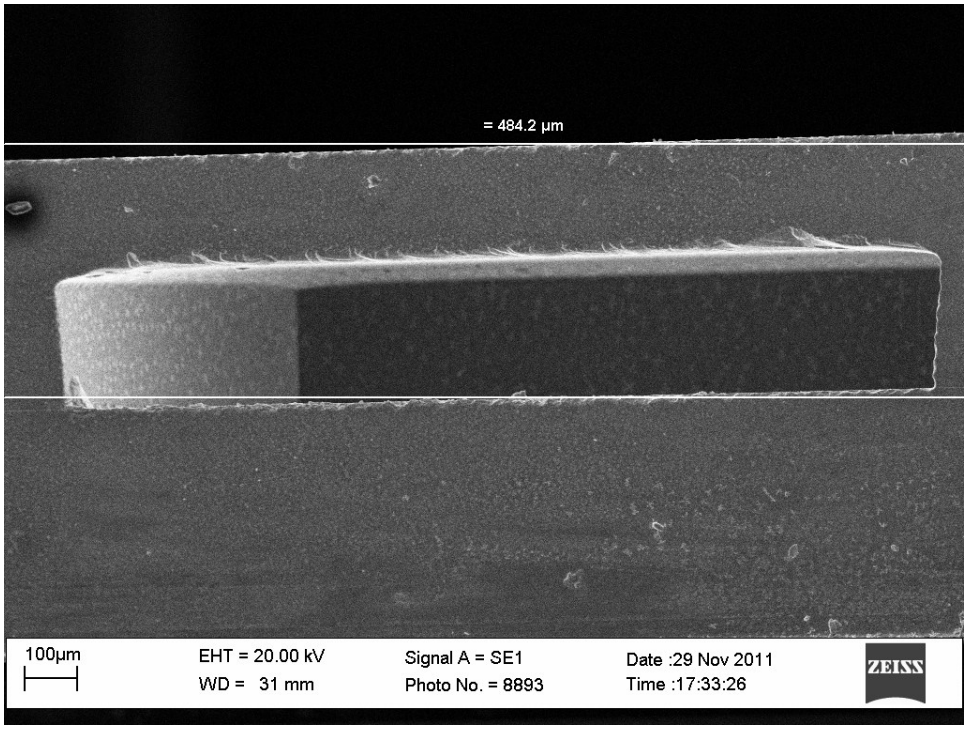
= 484.2 µm
100µm
EHT = 20.00 kV
WD = 31 mm
Signal A = SE1
Photo No. = 8893
Date :29 Nov 2011
Time :17:33:26
ZEISS

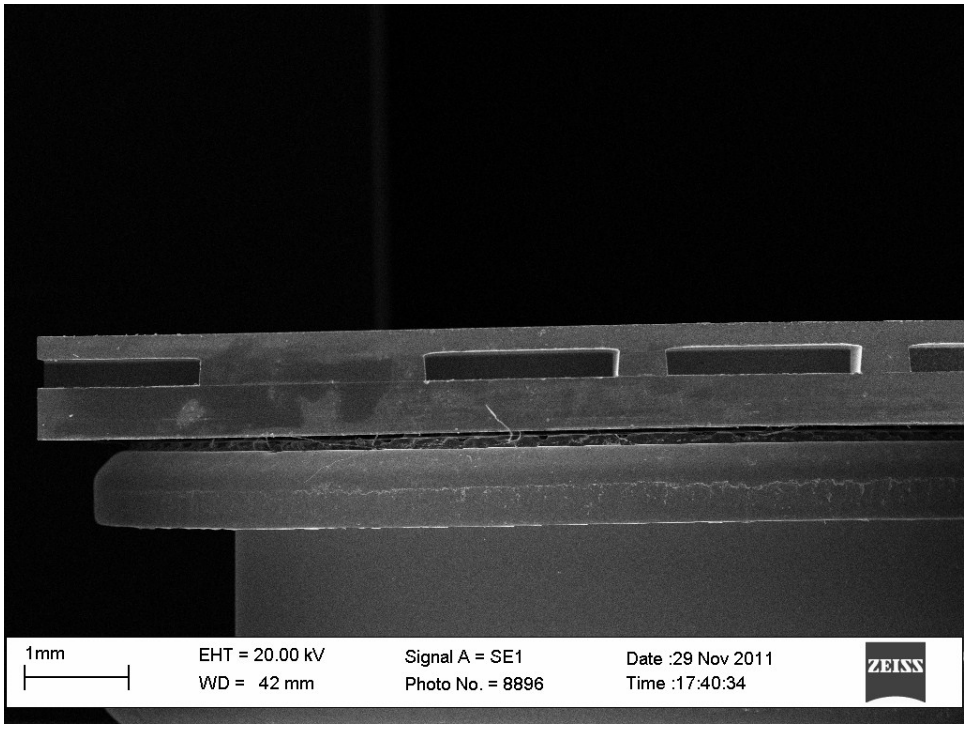
1mm
EHT = 20.00 kV
WD = 42 mm
Signal A = SE1
Photo No. = 8896
Date :29 Nov 2011
Time :17:40:34
ZEISS

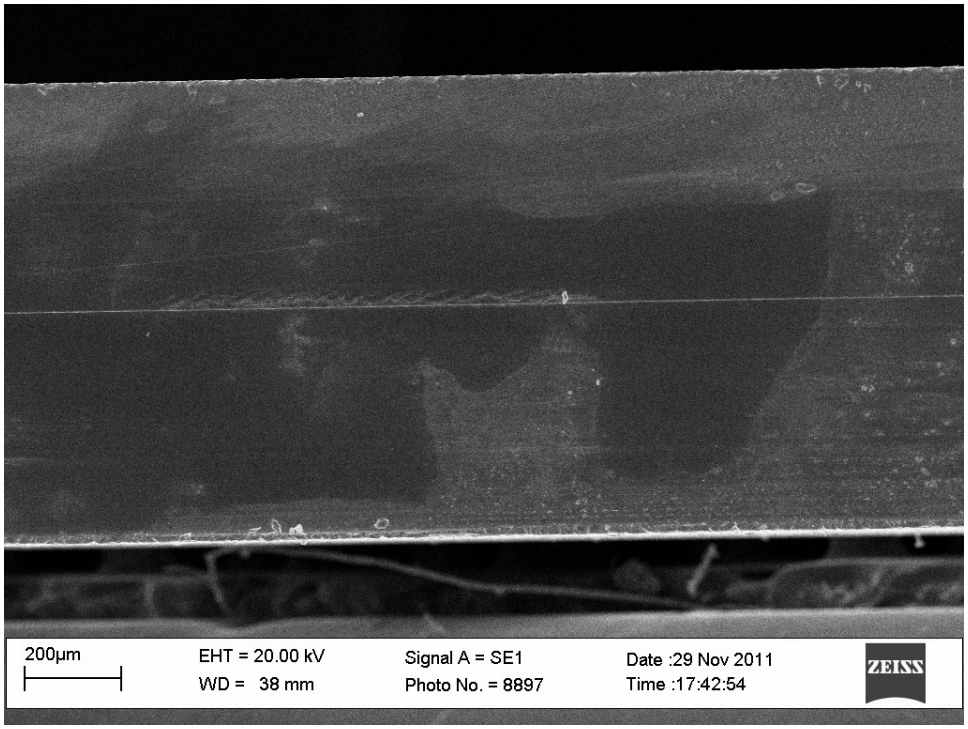
200µm
EHT = 20.00 kV
WD = 38 mm
Signal A = SE1
Photo No. = 8897
Date :29 Nov 2011
Time :17:42:54
ZEISS

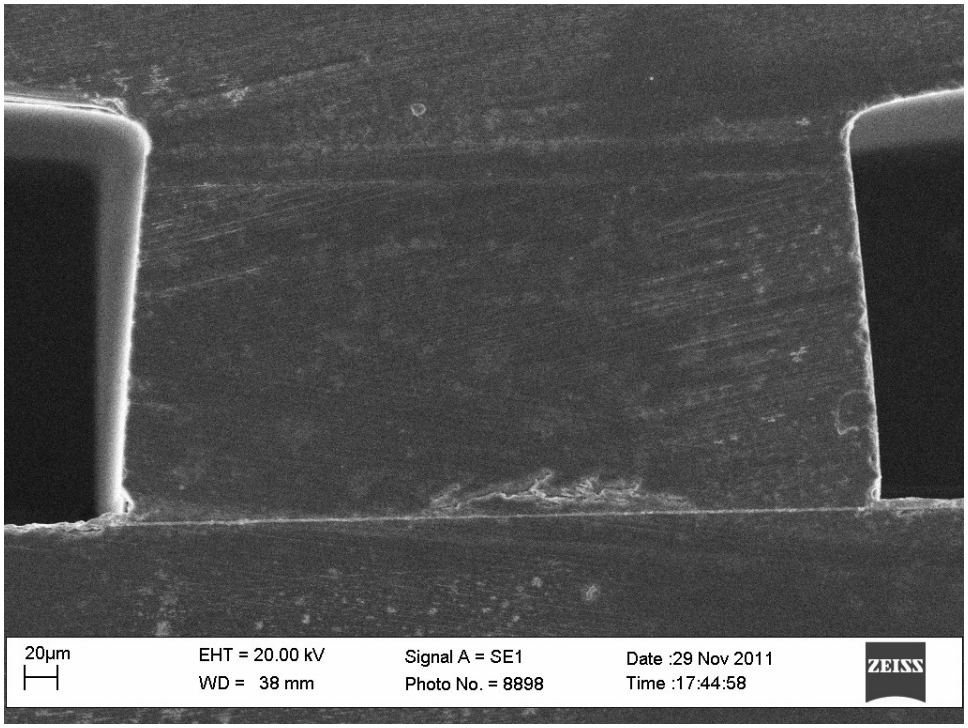
20µm
EHT = 20.00 kV
WD = 38 mm
Signal A = SE1
Photo No. = 8898
Date :29 Nov 2011
Time :17:44:58
ZEISS

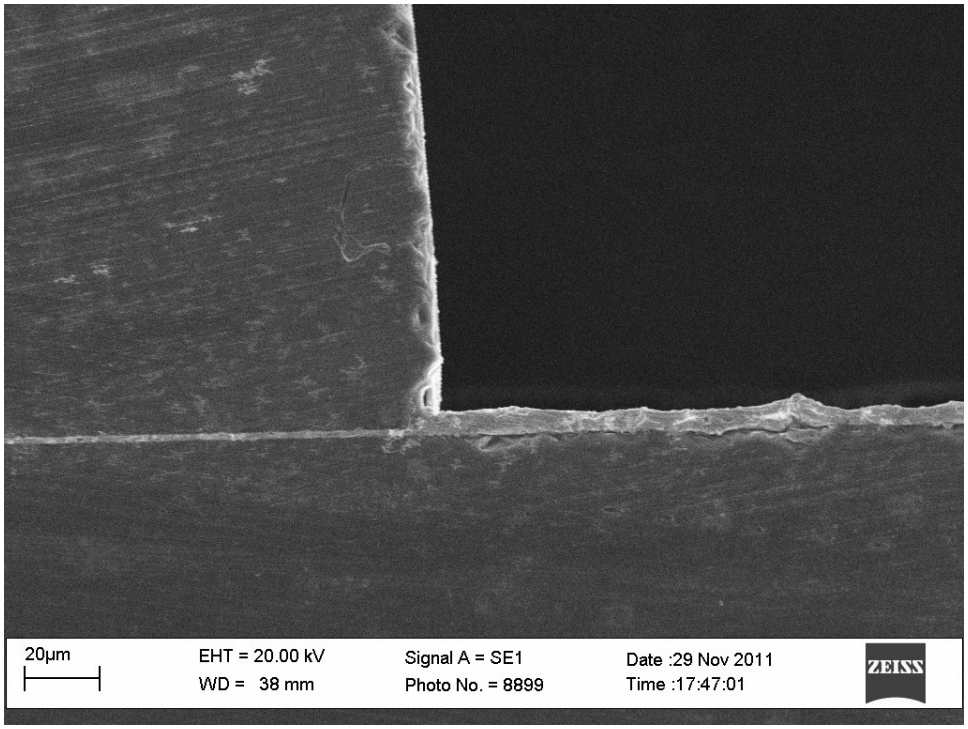
20µm
EHT = 20.00 kV
WD = 38 mm
Signal A = SE1
Photo No. = 8899
Date :29 Nov 2011
Time :17:47:01
ZEISS

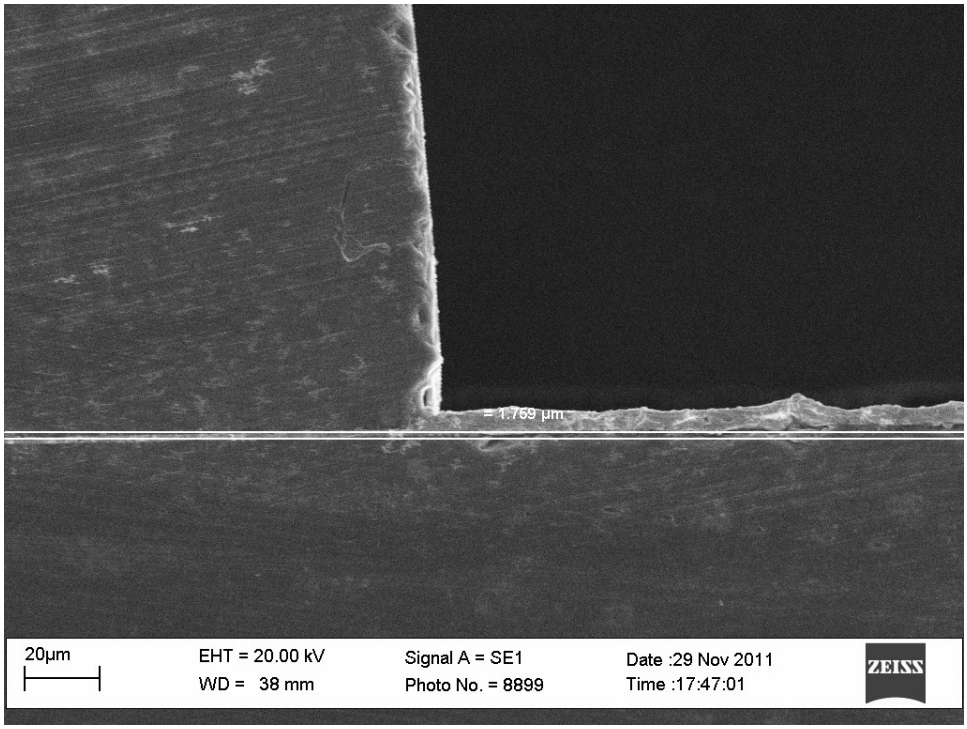
= 1.759 µm
20µm
EHT = 20.00 kV
WD = 38 mm
Signal A = SE1
Photo No. = 8899
Date :29 Nov 2011
Time :17:47:01
ZEISS

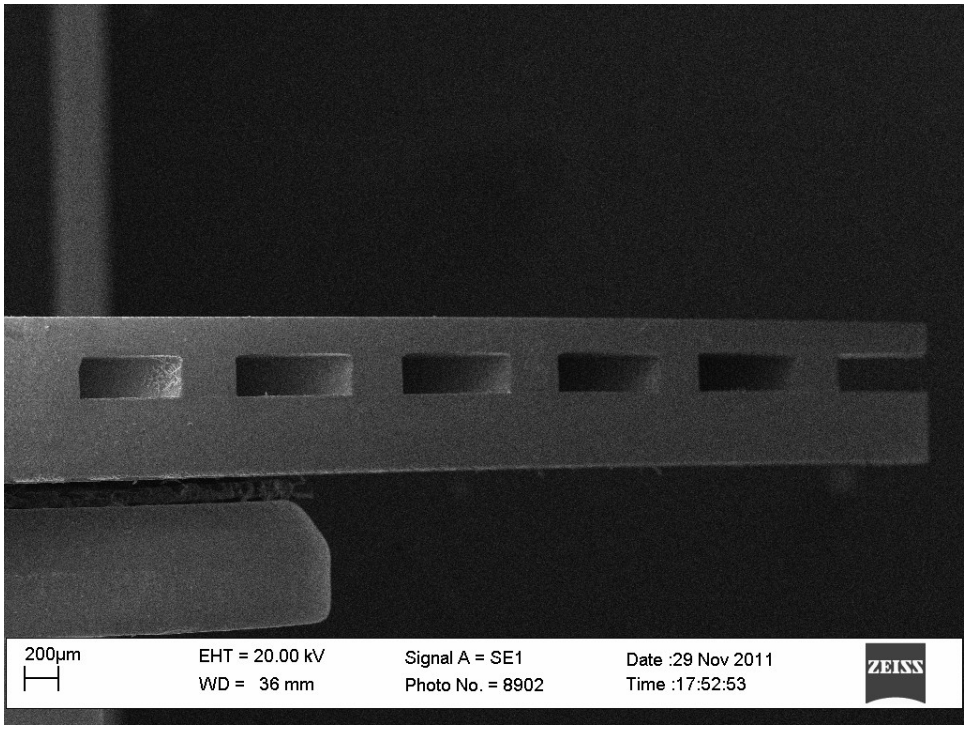
200µm
EHT = 20.00 kV
WD = 36 mm
Signal A = SE1
Photo No. = 8902
Date :29 Nov 2011
Time :17:52:53
ZEISS

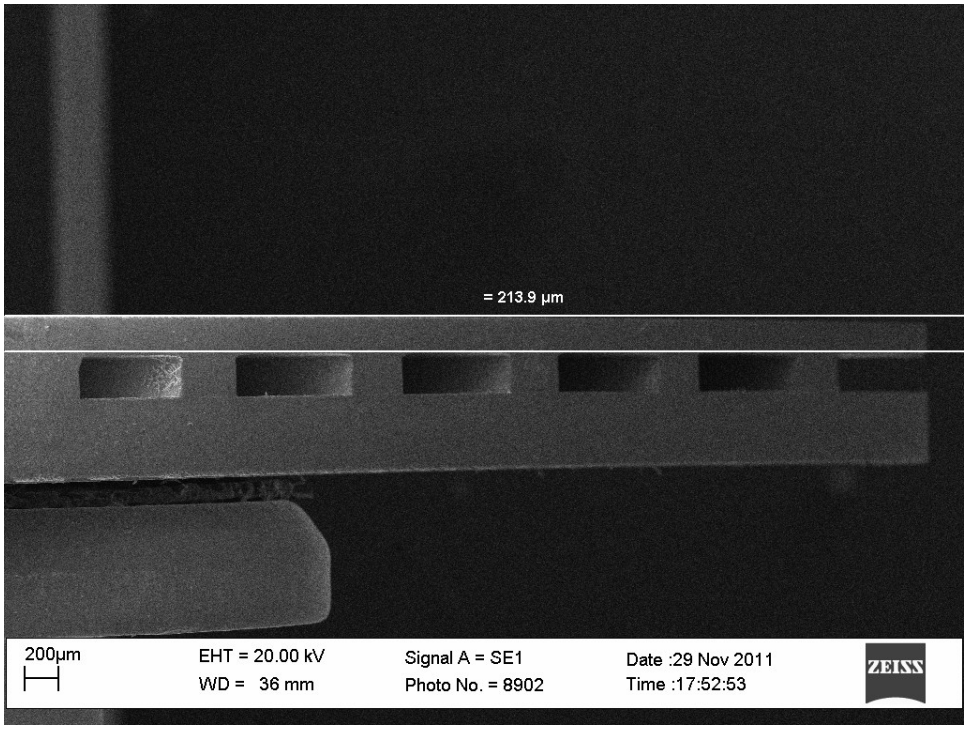
= 213.9 µm
200µm
EHT = 20.00 kV
WD = 36 mm
Signal A = SE1
Photo No. = 8902
Date :29 Nov 2011
Time :17:52:53
ZEISS

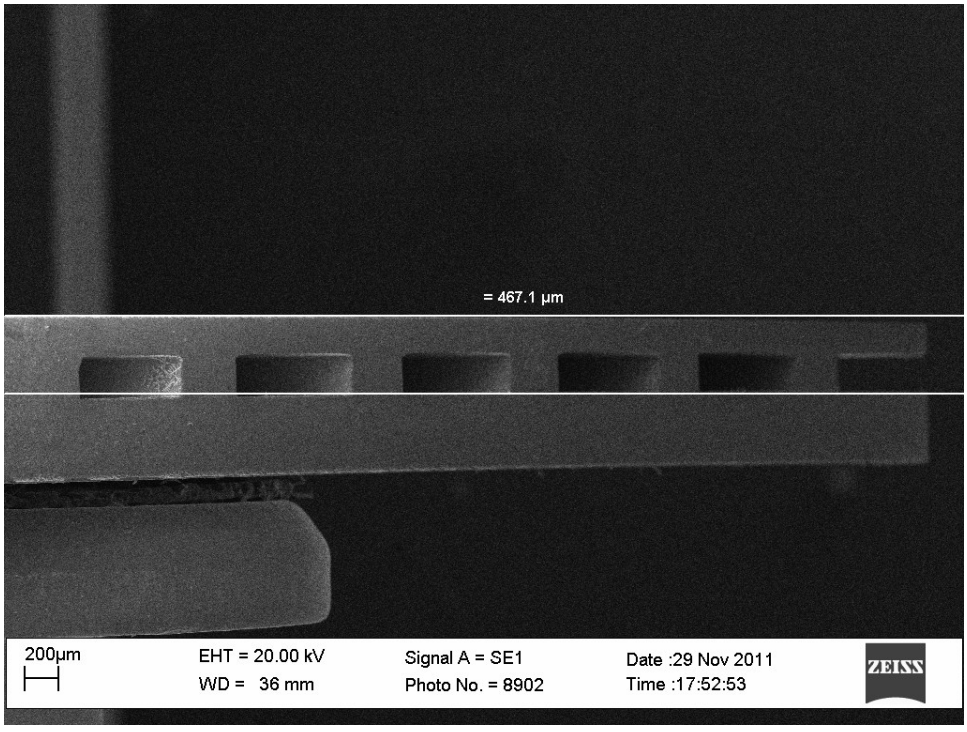
= 467.1 µm
200µm
EHT = 20.00 kV
WD = 36 mm
Signal A = SE1
Photo No. = 8902
Date :29 Nov 2011
Time :17:52:53
ZEISS

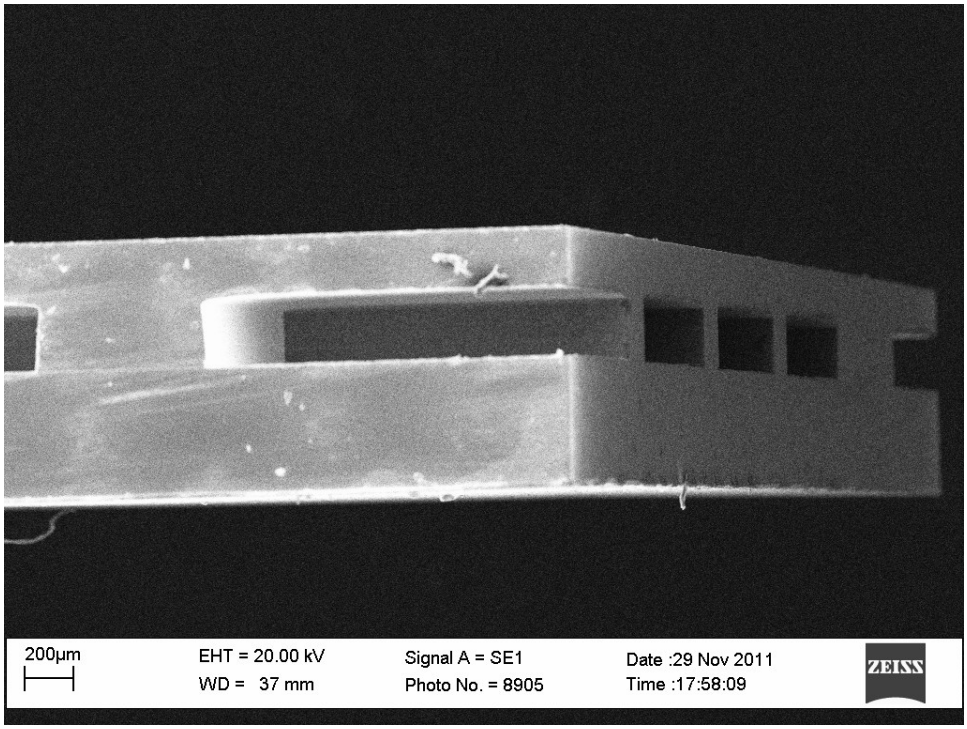
200µm
EHT = 20.00 kV
WD = 37 mm
Signal A = SE1
Photo No. = 8905
Date :29 Nov 2011
Time :17:58:09
ZEISS

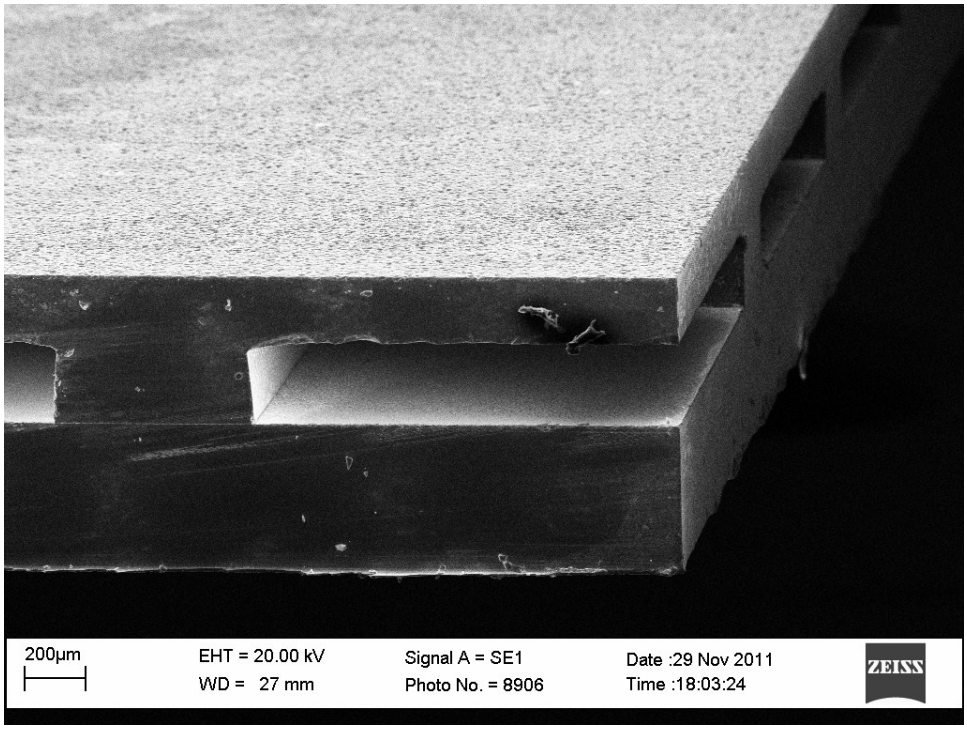
200µm
EHT = 20.00 kV
WD = 27 mm
Signal A = SE1
Photo No. = 8906
Date :29 Nov 2011
Time :18:03:24
ZEISS

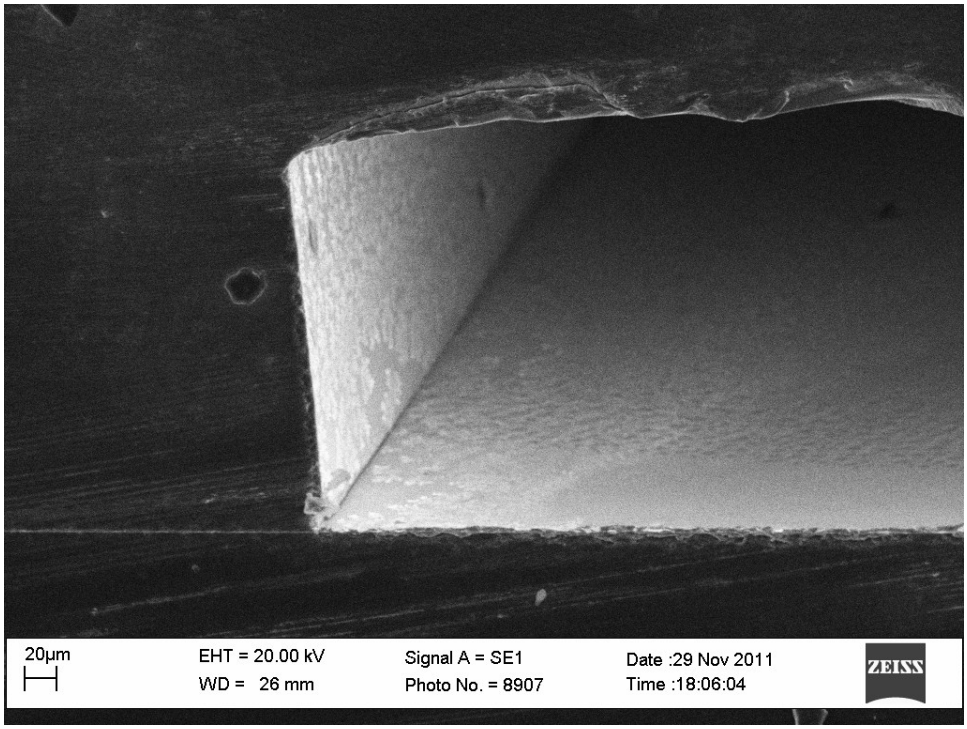
20µm
EHT = 20.00 kV
WD = 26 mm
Signal A = SE1
Photo No. = 8907
Date :29 Nov 2011
Time :18:06:04
ZEISS

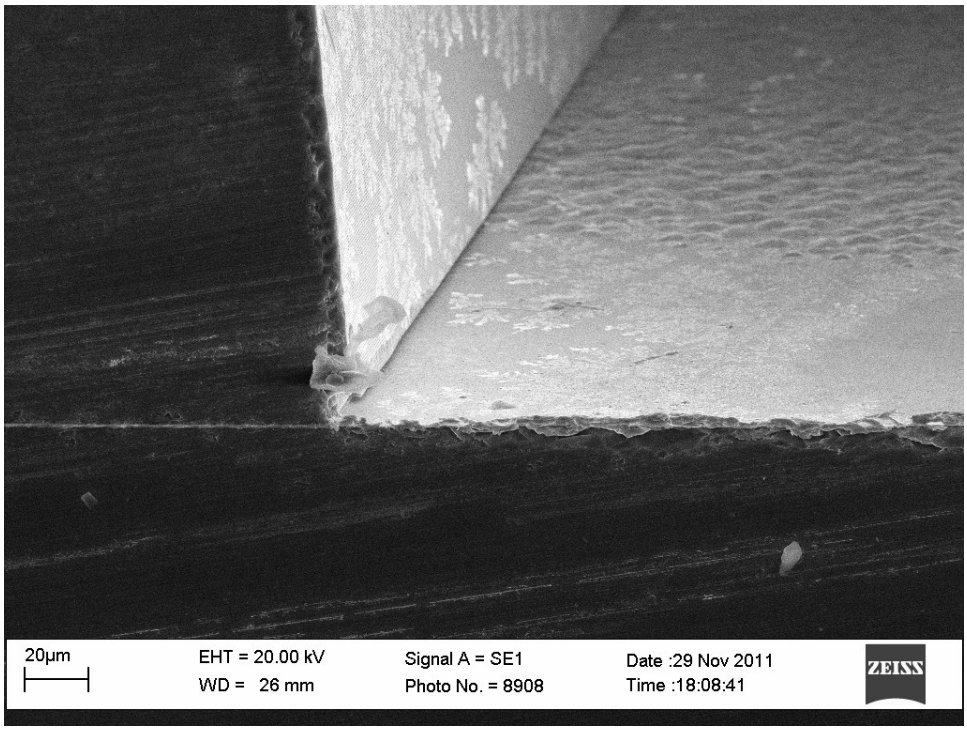
20µm
EHT = 20.00 kV
WD = 26 mm
Signal A = SE1
Photo No. = 8908
Date :29 Nov 2011
Time :18:08:41
ZEISS

REFERENCES

1. DeGroat B., "Major drop in traffic deaths: It's more than high gas prices", University of Michigan, Ann Arbor, MI, July 28, 2008.

2. Sivak M., “Is the U.S. on the path to the lowest motor vehicle fatalities in decades?” Report No. UMTRI-2008-39. Ann Arbor: The University of Michigan Transportation Research Institute, 2008.

3. Jain, S. Lochlann "’Dangerous Instrumentality’: The Bystander as Subject in Automobility” Cultural Anthropology 19:1 (February, 2004): 61-94.

4. Kopits E, Cropper M. Traffic fatalities and economic growth, Washington, DC, World Bank, (Policy Research Working Paper No. 3035, 2003.

5. R. Lachner, "Development Status of Next Generation Automotive Radar in EU – Infineon Radar Technology," presented at ITS Forum 2009, Tokyo (Japan), 2009.

6. D. Hoetzer, D. Freundt, “Driver Assist & Crash Avoidance Technologies: Radar and Video Systems”, Robert Bosch GmbH, presented at Telematics Detroit, Detroit, Ml, 2008.

7. Van Loon B.: ‘Radar 101: Celebrating 101 years of development’, Proc. IEEE, 93, (4), pp. 844–84, April 2005.

8. B.R. Norvell, R. J. Hancock, J. K. Smith, M.L. Pugh, S.W. Theis, and J. Kviatkofsky, “Micro Electro Mechanical Switch (MEMS) Technology Applied to Electronically Scanned Arrays for Space Based Radar,” IEEE Aerospace Conference Proceedings, vol. 3, pp.239– 247, 1999.

9. N. GHAFAR, “Design of a Compact Microstrip Antenna at 2.4 GHz,” M.S. Thesis, Dept. Elect. Eng., Universiti Teknologi Malaysia, November, 2005.

10. C. A. Balanis, “*Antenna Theory, Analysis and Design*,” John Wiley & Sons, New York, 1997.

11. M. Schneider, “Automotive Radar – Status and Trends,” Robert Bosch GmbH, Corporate Research, 2005.

12. J. Jermakian , “Crash Avoidance Potential of Four Passenger Vehicle Technologies”, *Insurance Institute of Highway safety*, http://www.iihs.org/research/topics/pdf/r1130.pdf, April, 2010.

13. “Cost Per Life Saved by the Federal Motor Vehicle Safety Standards,” by Charles J. Kahane. NHTSA Technical Report # DOT HS 809 835, December 2004.

14. G. Rollmann, “Frequency Regulations for Automotive Radar”, SARA, presented at Industrial Wireless Consortium (IWPC), Düsseldorf, Germany, 2009.

15. Sherif Sedky, Post-processing Techniques for Integrated MEMS, Artech House, Massachusetts, 2006.

16. Chang Liu, Foundation of MEMS, Illinois ECE Series, Pearson Prentice Hall, New Jersey, 2006.

17. (2007) The KOKON website. [Online]. Available: http://www.kokonproject.com/

18. K. Strohm, R. Schneider, J. Wenger, "KOKON – A Joint Project for the Development of 79 GHz Automotive Radar Sensors", International Radar

Symposium IRS 2005, Conference Proceedings, Berlin, Germany, pp. 97-101, September 06-08, 2005.

19. Toby Haynes, "A Primer on Digital Beamforming", March 26, 1998.

20. Brookner, E., "Phased array radar," *Scientific American*, Vol. 252, pp. 94-102, February 1985.

21. Haykin, S., ed., *Array Signal Processing*, Prentice Hall, Englewood Cliffs, New Jersey, 1985.

22. Munson, Jr., D.C., O'Brian, J.D. and Jenkins, W.K., "A tomography formulation of spot light mode synthetic aperture radar," *Proc. IEEE*, Vol. 71, pp. 917-925, August 1983.

23. Knight, W.C., Pridham, R.G. and Kay, S.M., "Digital signal processing for sonar," *Proc. IEEE*, Vol. 69, pp. 1451-1506, November 1981.

24. Owsley, N.L., in *Array signal Processing*, S. Haykin, ed., Prentice Hall, Englewood Cliffs, New Jersey, 1985.

25. Mayhan, J.T., "Nulling limitations for a multiple beam antenna," *IEEE Tran. On AP*, Vol. 24, pp. 769-779, November 1976.

26. Compton, Jr. R.T., "An adaptive array in a spread spectrum communication system," *Proc. IEEE*, Vol. 66, pp. 289-298, March 1978.

27. Adams, R.N., Horowitz, L.L. and Senne, K.D., "Adaptive main-beam nulling for narrow-beam antenna arrays," *IEEE Trans, on AES*, Vol. 19, pp. 509-519, July 1980.

28. Macovski, A., *Medical Imaging*, Prentice Hall, Englewood Cliffs, New Jersey, 1983

29. Pratt, W.K., *Digital Image Processing*, Wiley and Sons, New York, 1978

30. Kak, A.C., *Array Signal Processing*, S. Haykin, ed., Prentice Hall, Englewood Cliffs, New Jersey, 1985.

31. Justice, J.H., in Array Signal Processing, S. Haykin, ed., Prentice Hall, Englewood Cliffs, New Jersey, 1985.

32. Readhead, A., "Radio astronomy by very long baseline interferometery," Scientific American, Vol. 246, pp. 52-61, June 1982.

33. Yen, J.L., in *Array Signal Processing*, S. Haykin ed., Prentice Hall, Englewood Cliffs, New Jersey, 1985.

34. Widrow, B., Glover, Jr., J.R., McCool, J.M., Kaunitz, J., Williams, C.S., Hearn, R.H., Zeidler, J.R., Dong, Jr., E. And Goodlin, R.C. [1975], "Adaptive noise cancelling: principles and applications," Proc. IEEE, Vol. 63, pp. 1692-1716, December 1975.

35. Gee, W., Lee, S., Bong, N.K., Cain, C.A., Mitrra, R. And Magin, R.L., "Focused array hyperthermia applicator: theory and experiment," *IEEE Trans. On BME*, Vol. BME-31, pp. 38-45, January 1984.

36. Peterson, P.M., Durlach, N.I., Rabinowitz, W.M. and Zurek, P.M., "Multi-microphone adaptive beamforming for interference reduction in hearing aids," *Jour. of Rehab. R&D*, Vol. 24, Fall 1987.

37. T. Haynes. (1998, March 26). *A Primer on Digital Beamforming,* Spectrum Signal Processing. White paper [Online]. Available: http://www.spectrumsignal.com /publications/beamform_primer.pdf.

38. R. A. Mucci, “A Comparison of Efficient Beamforming Algorithms,” *IEEE Trans. Acoustics, Speech, and Signal Processing,* Vol. ASSP-32, No. 3, pp. 548-558, June 1984.

39. A. Kawakubo, S. Tokoro et al., “Electronically-Scanning Millimeter-Wave RADAR for Forward Objects detection,” *SAE Congress 2004*, pp. 127-134, Detroit, 2004.

40. Hall L., Hansen H., Abbott D., "Rotman lens for mm-wavelengths", Proceeding of SPIE, Vol. 4935, 2002.

41. Ruze, J., “Wide Angle Metal Plate Optics,” *Proc. IRE*, vol. 38, pp. 53-59, January 1950.

42. V. Jain *et al.*, “A 22–29-GHz UWB pulse-radar receiver front-end in 0.18 μm CMOS” *IEEE Trans. Microw. Theory Tech.*, vol. 57, pp. 1903–1914, August 2009.

43. R. Kulke *et al.*, “24 GHz radar sensor integrates patch antenna and frontend module in single multilayer LTCC substrate,” *Proc. Eur. Microelectronics and Packaging Conf.*, pp. 239–242, June 2005.

44. T. H. Ho *et al.*, “A compact 24 GHz radar sensor for vehicle sideway looking applications,” in *Proc. Eur. Microwave Conf.*, pp.351–354, October 2005.

45. Naoyuki Shino, Hiroshi Uchimura, and Kentaro Miyazato “77 GHz band Antenna Array Substrate for Short Range Car Radar”, 2005.

46. V.K. Singh, “Ka-band micromachined microstrip patch antenna”, defense Electronics Applications Laboratory, Dehradun 248001, India, 2010.

47. Jurgen Hasch, Tahereh Haghighi, Claus Schollhorn, Erich Kasper, “Patch Antenna on Micromachined Silicon” Robert Bosch GmbH, Central Research and Development, Germany Institut f¨ur Halbleitertechnik, University at Stuttgart, Germany, 2005.

48. M. Töns, “Evaluation of individual radar sensors as well as radar network”, Project funded by the European Community under the "Information Society Technology" Program (1998-2002).

49. P. Herrero, J.Schoebel, “Planar Antenna Array at D-Band Fed By Rectangular Waveguide for Future Automotive Radar Systems”, Institute for High Frequency Technology, TU-Braunschweig, Amsterdam, The Netherlands, October 2008.

50. Yi-An Li, Meng-Hsiung Hung, and Shih-Jou Huang, “A Fully-Integrated 77-GHz FMCW Radar Transceiver in 65-nm CMOS Technology”, IEEE JOURNAL OF SOLID-STATE CIRCUITS, Vol. 45, No. 12, December 2010.

51. R. Bancroft, “Rectangular microstrip antennas,” in *Microstrip and Printed Antenna Design*, pp. 37–48, Noble, Atlanta, Ga, USA, 2004.

52. C.A. Winterhalter, J. Teverovsky, P. Wilson, J. Slade, W. Horowitz, E. Tierney and V. Sharma, “Development of electronic textiles to support networks, communications, and medical applications in future U.S. Military protective clothing systems,” *IEEE Trans. Information Technology in Biomedicine*, vol. 9, pp. 402-406, 2005.

53. D. M. Pozar and D. H. Schaubert, Microstrip antennas, the analysis and design of Microstrip antennas and arrays, New York: IEEE press, 1995.

54. Lo, Y.T., Solomon D. and Richards, W.F. "Theory and Experiment on Microstrip Antennas," *IEEE Transactions on Antennas and Propagation,* AP-27, 1979 pp. 137-149.

55. F. E. Gardiol, “Broadband Patch Antennas,” Artech House.

56. A.G Derneryd, "A theoretical investigation of rectangular microstrip antenna element," IEEE Transactions Antennas and Propagation, Vol. AP-26, No. 4, pp. 232-535

57. W. F. Richards, "Microstrip Antennas", Chapter 10 in Antenna Handbook: Theory, Applications s and Design (Y.T.Lo and S.W.Lee.eds.), Van Norstrand Reinhold Co., New York, 1988.

58. E. Hammerstad and Ø. Jensen, ``Accurate Models for Microstrip Computer-Aided Design," *Symposium on Microwave Theory and Techniques*, pp. 407-409, June 1980.

59. J.K. Smith, F.W. Hopwood, and K.A. Leahy, “MEM Switch Technology in Radar,” IEEE 2000 Radar Conference, Nov. 2000.

60. Papapolymerou, Student Member, IEEE, Rhonda Franklin Drayton, Member, IEEE, and Linda P. B. Katehi, Fellow, IEEE, “Micromachined Patch Antennas”, IEEE Transactions Antennas and Propagation, Vol. 46, No. 2, Feb 1998.

61. http://www.memscap.com/aboutmems.html

62. J. R. James and P. S. Hall, eds, Handbook of Microstrip Antennas, Peter Peregrinus Ltd., London, 1989. Comprehensive two-volume work describing just about every possible variation of microstrip antenna

63. J. Papapolymerou, C. Schwartzlow, G Ponchak, "A Folded-Slot Antenna on Low Resisitivity Si Substrate with a Polyimide Interface Layer For Wireless Circuit," Silicon Monolithic Integrated Circuits in RF Systems, 2001, pp. 215 –218

64. G.Gauthier, J.-P.Raskin, L.P.B.Katehi and G.M.Rebeiz, "A 94-GHz Aperture-Coupled Micromachined Microstrip Antenna", IEEE Trans. On Antennas and Propagation, Vol.47, No.12, pp.1761-1766, Dec.1999.

65. G.P.Gauthier, A.Courtay and G.M.Rebeiz, "Microstrip Antennas on synthesized low dielectric-constant substrates", IEEE Trans. Antennas and Propagation, vol.45, pp.1310-1314, Aug.1997.

66. F. Yang and Y. Rahmat-Samii, "Mutual coupling reduction of microstrip antennas using electromagnetic band-gap structure," in *Proc. IEEE AP-S Dig.*, vol. 2, July 2001, pp. 478–481.

67. S. Sharma and L. Shafai, "Enhanced performance of an aperture-coupled rectangular microstrip antenna on a simplified unipolar compact photonic bandgap (UCPBG) structure," in *Proc. IEEE AP-S Dig.*, vol. 2, July 2001, pp. 498–501.

VITA AUCTORIS

Ismail Hamieh was born in 1978 in Kuwait City, Kuwait. He completed his B.Sc. in engineering (Hons.) in Computer Engineering in 2003 and his Master's degree in Electrical Engineering in 2007 from the University of Michigan, during which he took a job in the automotive industry at Chrysler. His research interests include Digital Controls, Digital Signal Processing on FPGAs, Antenna design, and Microelectromechanical Systems (MEMS). At the time of writing this thesis Ismail is a member of the MEMS Lab, and a candidate for the degree of M. A. Sc. in Electrical and Computer Engineering, at the University of Windsor (Ontario, Canada).